Dark Matter Bound State Formation for Pseudo-Scalar Mediators

by

Ask Juhl Markestad

Thesis for the degree of
Master of Science in Theoretical Physics

Faculty of Mathematics and Natural Sciences
Department of Physics
University of Oslo

May 2017

Abstract

Self-interacting dark matter is a popular and active field of research, it produces a rich phenomenology, and gives unique signals that we can search for. This thesis is devoted to the topic of dark matter bound state formation with emphasis on a pseudo-scalar mediator in the non-relativistic regime. Using the Bethe-Salpeter formalism we derive a method of finding two-particle fermion wavefunctions that reduce to solutions of the Schrödinger equation in the non-relativistic regime. We show the expressions for the bound state formation and annihilation cross-section. We find that the effective potential generated by a pseudo-scalar is dependent on the total angular momentum state of the particle configuration, $|J, S, P\rangle$ where J is total angular momentum, S is the total spin, and P is the parity are the quantum numbers of the configuration. Only one of such configuration leads to an attractive potential, and allows for a bound state solution. For this potential the Sommerfeld enhancement for the annihilation and bound state formation cross-section is found to be negligible. We find that the bound state formation process scales as momentum to leading order. During the bound state formation process a pseudo-scalar is released. Due to pseudo-scalars being CP odd, the configuration of the two-particle state must change for CP conservation to hold. Since the final configuration must be the one that allows for bound state formation, the initial configuration must be one that gives a repulsive potential, and therefore suppresses the process.

Acknowledgements

I would like to thank my supervisor, Torsten Bringmann, for helping me find an interesting thesis and for a guiding hand throughout. A big thank you to my co-supervisor, Andrzej Jan Hryczuk, for always being available for a discussion and for giving me invaluable feedback.

A thank you to fellow students Kristian Stlevik Olsen and Sean B. S. Miller, for being at hand to listen to my thought processes, whether they concern physics, writing, or general life complaints. And to Vidar, Kine, and Henrik for asking the type of annoying questions that shows me exactly how little I yet understand.

Last, I would like to thank the Theoretical Physics section as a whole creating a fantastic working environment, and many a laugh.

Contents

Chapter 1

Introduction

Dark matter is one of the large unknowns in modern physics. We know very little about it, yet has a rich theoretical and experimental field of research. The effects of dark matter have been studied since Fritz Zwicky showed that there was not enough mass in luminous matter to explain the velocity distribution of galaxies in the Coma galaxy cluster in 1933. Since then many astrophysical and cosmological observations have been made that indicate another form of matter exists [1–9]. Yet all these observations are indirect in that we do not directly observe the dark matter, and can be used primarily to put constraints on possible models. This means that we have a large freedom in building models that fit the observations.

We therefore prefer models that have some form of independent motivation, and from particle physics we receive several candidates. The most popular candidates are sterile neutrinos, axions, and weakly interacting massive particles (WIMPs), all motivated by the need to explain observations and discrepancies in particle physics [10]. In this thesis we focus on WIMP like particles with a long-range interaction. The motivation for self-interacting dark matter stems from discrepancies between observations and simulations of structure formation for cold dark matter only [11–13]. Introducing a self-interaction can reconcile these discrepancies and explain the observations [14–18].

With a self-interacting model comes new signals and effects one can look for experimentally [19–22]. In this thesis we focus on the effects in the non-relativistic regime, such as the Sommerfeld effect [23] and the possibility for formation of bound states [24–26]. In the non-relativistic regime, the long-range effects of a potential have a larger impact on the particles. For an attractive potential this leads to an enhanced cross-section, while a repulsive one will lead to a suppression. This suppression or enhancement is called the Sommerfeld effect.

The Sommerfeld effect has been studied for quantum field theories by, among

others, Iengo [27] and Cassel [28] but in 2015 Petraki *et al.* [29] published a comprehensive guide to finding the cross-sections of both annihilation and bound state formation processes using the Bethe-Salpeter equations [30] for scalar dark matter with massless scalar and vector mediating particles. This paper was followed up in 2016 with a study of massive scalar and vector mediators [31].

The goal of this thesis is two-fold. We review the physics and the method of Petraki *et al.* by applying it to fermionic dark matter. Secondly we explore the physics of a massive pseudo-scalar mediator in the context of annihilation and bound state formation. A first step in exploring the possibilities of a self-interacting model with a pseudo-scalar mediator.

1.1 Outline

The outline if the thesis is as follows;

Chapter 2 consists of an overview of dark matter, leading up to self-interacting models. A historical overlook is given, highlighting some of the most significant observations of dark matter. We review some of the particle models for dark matter, with emphasis on WIMPs, and the discrepancies between observation and cold dark matter only simulations motivating the introduction of self-interacting dark matter. We discuss some of the effects that follows from a self-interacting theory, like the Sommerfeld effect and bound state formation.

In chapter 3 we define what a bound state is, and how it is described in quantum field theory using Feynman diagrams. The difficulties with the quantum field theory description are specified, and we show how in the non-relativistic regime, these difficulties become manageable. Along the way we specify the assumptions used throughout the thesis concerning the non-relativistic approximation.

The derivation of the Bethe-Salpeter equation for fermionic dark matter is shown in chapter 4. The general outline of the derivation follows the work done by Petraki *et al.* [29] for scalar dark matter. The derivation done in this thesis accounts for the additional spinor structure that accompanies working with fermions. Transitioning to the non-relativistic regime is generalized to fermions and is shown the section 4.2 of this thesis.

Chapter 5 deals with finding the cross-section for dissipative bound state formation and annihilation. The method for deriving these results again follow the structure of Petraki *et al.* [29], from pole structure analysis to the non-relativistic approximation. We here keep track of the spinor components through these steps to ensure that the ordering of terms is correct. In section 5.3 we look at the

Schrödinger equation and how to solve it numerically, allowing us to write the three-momentum of the radiated particle in the dissipative BSF process in terms of the eigenenergy of the Schrödinger equation and introduce the phase-space suppression factor.

In Chapter 6 we derive the effective potential generated by a pseudo-scalar mediator, following the method of Bellazzini *et al.* [32]. We find that for the pseudo-scalar mediator the effective potential generated is dependent on the specific two-particle state of the incoming and outgoing particles. Additionally we incorporate a discussion on the nature of singular potentials, and why we need to renormalize them.

The results of the calculations of the Schrödinger equation, annihilation cross-section, and the bound state formation cross-section with a pseudo-scalar mediator is shown in Chapter 7. The boundary condition for the relevant potential of the pseudo-scalar mediator is found and the resulting wavefunctions are shown in section 7.1. Section 7.2 shows the final steps needed to calculate the annihilation cross-section numerically. For the bound state formation cross-section, the first order diagram is computed to leading order. Additionally, we discuss the implications of CP conservation for the bound state formation process.

Chapter 2

Introduction to dark matter

The nature of dark matter is one of the great mysteries of modern physics, despite that its existence has been known about for more than half a century. All evidence for dark matter comes from astrophysical and cosmological observations and are all indirect. We can only measure the effects of there being an unknown component to our universe, but not the component itself. The first indication that there may be something beyond standard matter came in 1933 when Fritz Zwicky found a discrepancy between the calculated mass of a galaxy cluster and the inferred mass from luminosity measurements [1]. Zwicky came to the conclusion that there must be some matter present that does not produce light, which he dubbed *"Dunkle Materie"*, dark matter. However it was not until 1970 the theory of dark matter started getting traction in the community, when Vera C. Rubin and W. Kent Ford showed that the measured angular velocities of luminous materials in the Andromeda galaxy, were much faster than expected from the gravitational effects of its known luminous material content [2]. Since then there have been other observational evidence from different galaxies and galaxy clusters using the methods of Zwicky and Rubin. These measurements are what is considered the classical evidence of dark matter, in the sense that they were the observations opened the field of dark matter study. However, today this does not produce the best constrains on the nature of dark matter.

Perhaps the most important evidence for dark matter comes from measurements of the Cosmic Microwave Background (CMB) radiation and what it tells us about the history of our universe, mapped most recently by the Plank experiment [3]. Shortly after the big bang the universe was very hot and dense. As the universe expanded and cooled down, elementary particles started to combine to form baryons. Eventually we get to the Recombination era, where protons and electrons became bound, and photons became free to travel the universe, gradually cooling down and having their wavelengths stretched by the expanding universe. The CMB is this radiation that was freed when recombination happened. Therefore the CMB is a snapshot of how the universe looked at this

point in time. While incredibly uniform the CMB has tiny fluctuations which act as seeds for large scale structure formation. These fluctuations form from small over-densities in the early universe. The over-densities can either grow by pulling in other matter through gravity or are wiped out by the pressure from the other forces between the matter, and from the expansion of the universe. In a universe with no dark matter the larger over-densities survive while smaller ones do not. With a matter ratio containing dark matter, some of these smaller densities survive due to the dark matter creating deeper potential wells that captures them. Measuring the CMB is done by mapping the photons wavelength λ from different regions of the sky, associating the wavelength with the temperature of the CMB in that direction. To analyze the mapping we transform the map into spherical harmonics where the size of a fluctuation is related to the mode l of the corresponding basis function. We can then plot the intensity of each such mode in a power spectrum plot, see figure 2.1. If there was no dark matter the tail of the power spectrum would fall to zero, while oscillating about the falling line. In figure 2.1 we see that the third peak in the spectrum is larger than the second peak. The third peak represents the smaller fluctuations that survive due to dark matter. From the size of the third peak within the ΛCDM model we can determine that the universe has a dark matter relic density of $\Omega_\chi = 0.2589 \pm 0.0057$, while normal matter has a relic density of $\Omega_m = 0.04860 \pm 0.00051$ and dark energy $\Omega_\Lambda = 0.6911 \pm 0.0062$ [4]. Relic density refers to the ratio of todays observed density over the critical density, where the critical density is the density needed for a geometrically flat universe. Since we see a flat universe today we know that the sum of all relic densities must add up to one $\sum \Omega_i = 1$, and where Ω_i tells us how much of the energy in the universe today is due to each component.

Along with the classic evidence of Zwicky and Rubin, and the precision measurements of the CMB there has been a steady stream of complementary evidence in the form of gravitational lensing observations [5,6] mapping out the amount of dark matter using weak lensing effects and mapping out the densities of galaxy clusters using strong lensing effect. Measuring the hot gas in clusters and using hydrodynamics predictions to map out the density profile of dark matter [7]. Measurements of the Big Bang nucleosynsthesis [8], that is the production of the lightest elements in the early universe and comparing them to todays value puts constraints on dark matter models as they cannot interfere with this process. The final significant evidence for dark matter is the bullet cluster [9]. The bullet cluster observation is of the aftermath of two galaxy clusters colliding, see figure 2.2. The luminous material is observed through X-ray telescopes to be clumped together while images of the same region shows gravitational lensing effects to both sides of the luminous clump. This indicates that the dark matter surrounding each cluster passes through each other instead of colliding.

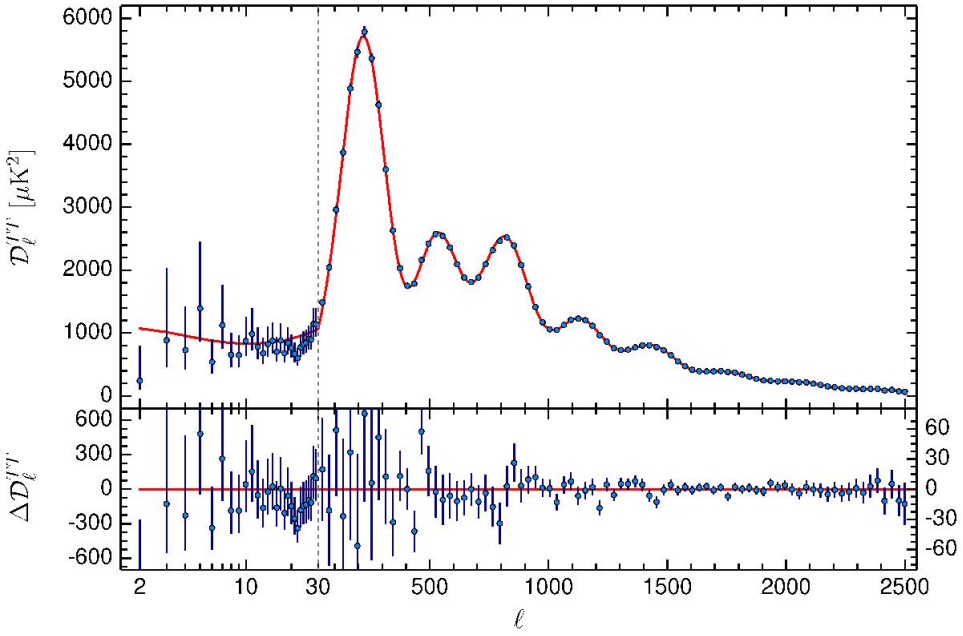

Figure 2.1: The thermal power spectrum from the 2015 Plank data. The solid line represents the ΛCDM model. The third peak in the power spectrum represents the fluctuations that survive due to the presence of dark matter. In a model with no dark matter the third peak would be lower than the second peak and the tail would decrease exponentially. With a dark matter content $\Omega_\chi = 0.268$ the third peak grows and as seen in the figure grows taller than the second peak. Image taken from [3]

One of the very first ideas for what produces effects, was that Newtonian dynamics where different of these large scales that previously thought, leading to the field of modified gravity theories [33]. Although it initially gathered interest to explain dark matter, its failure to predict all of the above observation simultaneously has lead to more focus on the idea of some form of unobserved matter. This could be many things, including primordial black holes, some unknown particle, etc. From an astrophysical point of view there is no a priori reason for choosing one over another, we can make all of them fit the parts, or all of the data. However, when considering particle physics, motivation for certain particle models emerges [10], three candidates emerge which are considered the most promising.

The first of which are sterile neutrinos. Sterile neutrino models are motivated as a possible explanation for neutrino oscillations. To explain the oscillation between neutrino species one needs to give the neutrinos mass. This can however not be done in the Standard Model as there are no right handed neutrinos present. Let us suppose we add right handed neutrinos. As so not to break the symme-

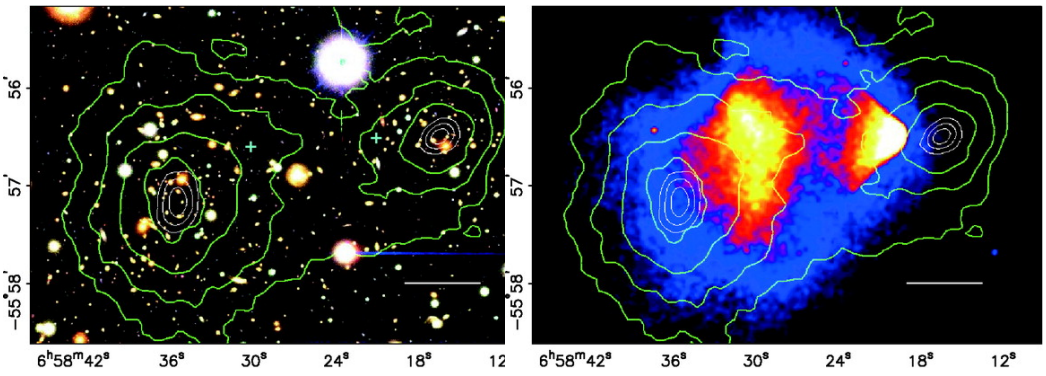

Figure 2.2: *Left:* Color image of the merging bullet cluster 1E 0657-558 with the mass density gradient overlapped in green measured using lensing effects. *Right:* X-ray image of the same merging event showing that the concentration of the luminous material does not overlap with the high mass density regions indicating that there exists and unknown component that is non-luminous. Image come from [9]

tries of the Lagrangian they cannot have any SM gauge interactions. The mass of the neutrinos are then determined by diagonalizing into mass eigenstates. By selecting the interaction strength to the higgs field to be of first order $\lambda \sim \mathcal{O}(1)$ you get three neutrinos with small masses $\sim \lambda^2/M$ and the rest of mass $\sim M$. This is called the seesaw mechanism, and for M of order $\sim 10^{14} GeV$ we get the correct mass range for the observed neutrinos but these sterile neutrinos are to heavy to be dark matter [10]. That is however only if we assume an interaction of order 1. With other interaction strengths we can produce lighter sterile neutrinos and still get out the correct neutrino mass.

Another possibility are axion models as explanation for the fine tuning of the CP violating terms in the strong sector of SM Lagrangian. This CP violating term is the one that would give the electric dipole moment to neutrons, which is measured to be very small. By adding a global $U(1)$ symmetry that is spontaneously broken a new pseudo-scalar field with a coupling that mimics the violating term emerges. One can make the degree of CP violation dynamically dependent on a new introduced mass scale. By tuning the value of this mass scale we can make the electric dipole moment of the neutron disappear and as a consequence a new very light particle arises that is naturally weakly interacting, fulfilling the criterion for a dark matter candidate.

The last of the prominent, and perhaps the most popular, candidates are WIMPs, to explain the hierarchy problem. The hierarchy problem refers to the need for a fine tuning of the Higgs mass. In classical mechanics the physical mass of an object is a parameter of the Lagrangian of the system, while in quantum

field theory the physical mass is given by the parameter from the Lagrangian plus quantum corrections,

$$m_H^2 = m_{H0}^2 + \Delta m_H^2, \text{ where } \Delta m_H^2 \sim \lambda^2 \Lambda^2, \tag{2.1}$$

where m_H is the physical higgs mass, m_{H0} is the Lagrangian parameter, Δm_H is the quantum correction to the mass, λ is an order $\mathcal{O}(1)$ coupling constant, and Λ is the energy scale at which the SM breaks down, which is of the order the Planck mass in the SM. So to produce the physical mass of $\sim$ 125 GeV there must be a cancellation of terms to the order of one part in 10^{36}, which is very unsettling. This fine tuning problem can be resolved by introducing new physics at a scale of 1 TeV implying new stable particles of mass $m \sim 10$ GeV-TeV with interaction strength of order weak interaction. Such particles are therefore called weakly interacting massive particle, or WIMPs.

WIMPs are further motivated by what is dubbed the "WIMP Miracle". From the CMB measurements we know that a large portion of the universe consists of dark matter, and this dark matter had to be produced somehow. A compelling mechanism is the thermal production. In the early universe, all particles that interact with the SM would be in thermal equilibrium. As the universe expands and cools heavier particles species would gradually fall out of equilibrium and their comoving number density would be fixed. This evolution of the number density is described by the Boltzmann equation

$$\frac{dn}{dt} + 3Hn = -\langle \sigma v \rangle \left(n^2 - n_{eq}^2 \right), \tag{2.2}$$

where n is the number density, n_{eq} is the number density at equilibrium, H is the Hubble parameter, and $\langle \sigma v \rangle$ is the thermally averaged annihilation cross section. This equation then balances how likely an interaction is with the expansion of the universe. If the expansion term was not there, the number density would drop nearly to zero as the universe cooled down and all the dark matter would have interacted away. Since the universe does expand, at some point the expansion would stop the interactions leading to what is referred to as freeze out, and giving the dark matter relic density seen today, see figure 2.3. We find that when freeze out happens the thermal relic density is given as

$$\Omega_\chi \sim \langle \sigma v \rangle^{-1} \simeq (3 \times 10^{-26} \text{cm}^3 \text{s}^{-1})^{-1} \tag{2.3}$$

[3]. To first order the thermally averaged annihilation cross section is

$$\Omega_\chi \sim \frac{m_\chi^2}{g_\chi^4}, \tag{2.4}$$

where m_χ is the mass of the particle in question and g_χ is its coupling constant. The "WIMP miracle" is that when using masses and couplings the correspond to

those of the weak scale needed to solve the hierarchy problem, the correct amount of dark matter is produced. Any other model that produces the correct thermally averaged annihilation cross section is just as valid, but given the motivation from particle physics, the WIMP has been one of the most studied models for dark matter. This analysis is done under the assumption of no unique interaction between the WIMPs themselves. Adding a self-interaction will produce corrections to the thermally averaged annihilation cross section, changing valid parameters slightly.

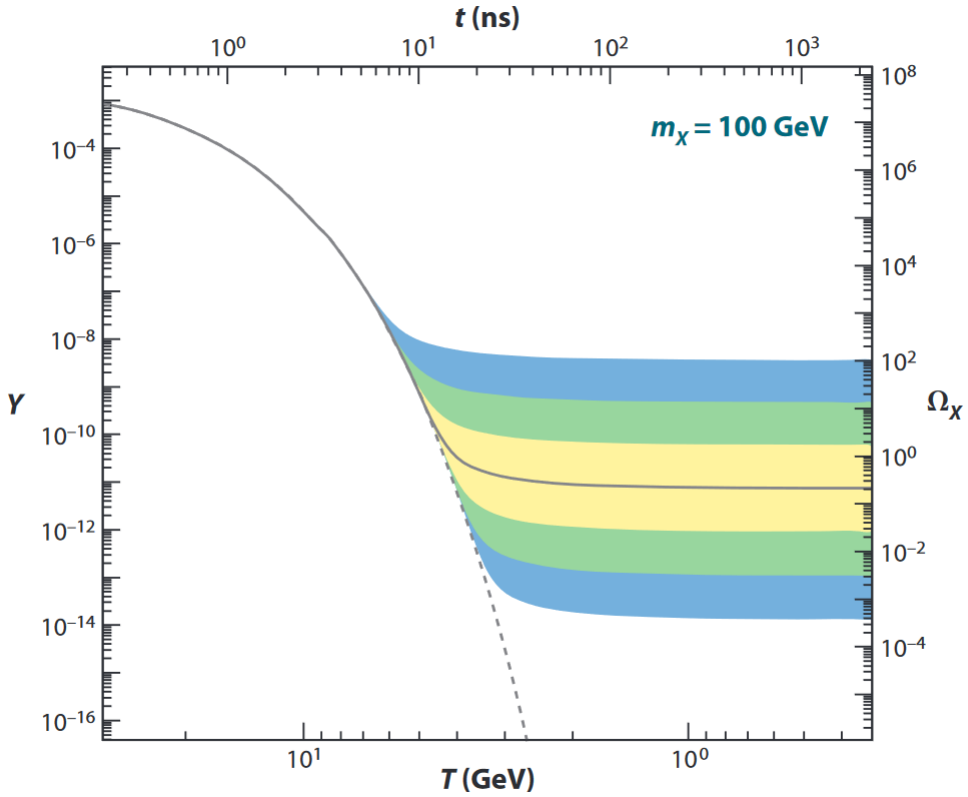

Figure 2.3: Figure of the evolution of the comoving number density Y according to equation 2.2 for a particle type of mass $100GeV$ at the lower end of the electroweak scale. The dotted gray line represents the evolution if the dark matter was always in equilibrium with the Standard Model plasma. The solid gray line represents the evolution to get the correct number density today for said particle type. The bands represents what changed when the cross section differs in value by a factor 10, 10^2, and 10^3 respectively. Image from [10]

With a WIMP model we can explain the phenomena attributed to dark matter. There are however some problems with structure formation. Using the CMB as an initial condition we can simulate the formation of large and small scale structure in the universe, assuming that dark matter is a non-interacting

cold component. Cold here meaning non-relativistic. The resulting simulations have three small scale discrepancies compared to observations of our universe today [11]. The cusp vs core problem where simulations show that the density profile of dark matter in galaxies go as $\sim 1/r$ whereas observations show that the profile is rounded towards the center [12]. The missing satellite problem states that simulations indicate that there should be significantly more sub halos/sub galaxies then what is observed. Simulations also show that the largest of these satellites should be significantly larger than observed, called the too large to fail problem. It should be noted that these simulations are done with only non-interacting cold dark matter, and does not include the effects from the difficult to simulate, baryonic physics. So these problems may very well be from the lack of proper treatment of baryonic effects [13], but they also can be explained by adding a self interaction to the dark matter [14–18]. There have also been claims to have experimentally observed unique effects of self interaction in the Abell 3827 galaxy cluster [19], but this is still in dispute.

The interest in self interacting dark matter theories and hidden sector models also stems from a lack of detection of dark matter, in particular WIMPs. The energy scale of WIMPs lies perfectly in the operating range of the LHC, indirect detection experiments like Fermi, PAMELA and AMS [20], and direct detection experiments such as DAMA/LIBRA, LUX, and IceCube [21], yet there is a lack of detection. Self interacting theories provides ways around the constraints that arise from the lack of detection, seemingly fixes discrepancies between simulation and observation regarding structure formation, and should provide unique detectable signals. However with a self-interacting theory comes their own restrictions, the most famous of which is the Bullet Cluster [22]. In the Bullet Cluster the two dark matter halos around each galaxy passes through each other to each side of the luminous material that clumps together, see figure 2.2. This is the exact behavior one would expect of the self interacting luminous matter and from non self-interacting dark matter. This then sets and upper bound on the self-interacting scattering cross section of $\sigma/m < 1.25\,\mathrm{cm}^2\mathrm{g}^{-1}$ and $\sigma/m < 0.7\,\mathrm{cm}^2\mathrm{g}^{-1}$ if one assumes an equal mass-to-light ratio of the clusters prior to the merger. The range to explain the discrepancies in the cold dark matter simulations versus observation are of the order $0.5 - 5\,\mathrm{cm}^2\mathrm{g}^{-1}$, restricting self-interacting dark matter models considerably.

To reconcile these restrictions with those from other observations we must consider some of the effects that come with a self-interacting theory. Two main effects that come into play with a self interacting theory are the Sommerfeld effect [23] and bound state formation. The idea behind the Sommerfeld effect is that two particles with a long range attractive force between them will be pulled together. If the particles are highly relativistic this effect is negligible but for

non-relativistic particles this effect can be significant. Therefore the cross section of a process, whether it is scattering, annihilation, or bound state formation, will be enhanced or suppressed for low relative velocities, see figure 2.4. While these effects allow the evasion of the bounds previously mentioned, they do lead to new signals from whom new bounds occur. In particular, the formation of bound states leads to new detectable signals for direct detection [21], indirect detection [24], production at the LHC [25], and it has an effect on the thermal production of dark matter [26].

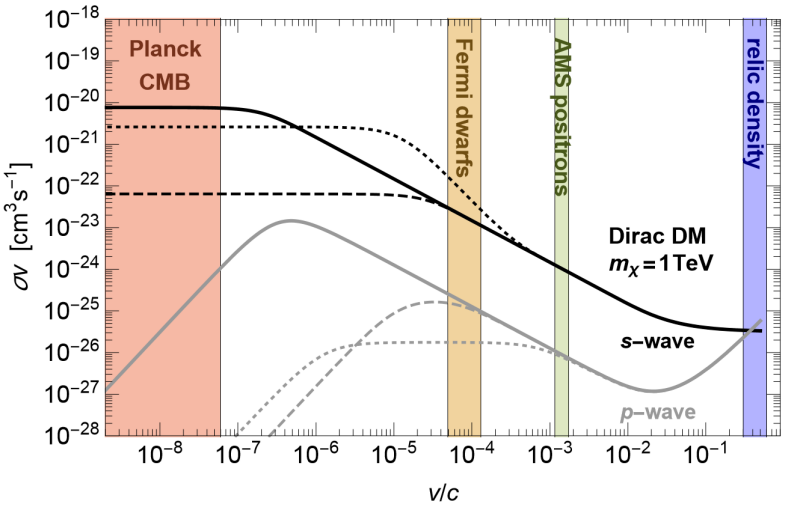

Figure 2.4: A plot of the annihilation cross sections for a vector mediator(s-wave) and a scalar mediator (p-wave) as a function of velocity for some selected combinations of the dark matter mass and the mediator mass. The highlighted regions show the velocities corresponding to regions probed by different observations. Relic density refers to restrictions from the thermal production of dark matter. The AMS positrons refers to the restrictions from galactic origin particle detection. Fermi dwarfs refers to measurements of dwarf galaxies, and Planck CMB refers to restrictions from the exact form of the CMB. Images from [34].

The state of dark matter research today is one of constraining, with hopes of detection. And we find that some of the most studied models are heavily constrained. Recent papers by Bringmann *et al.* [34] and Cirelli *et al.* [35] explore what regions of parameter space are left open for self interacting dark matter with a scalar or vector mediator that can both explain the three discrepancies in simulations and have consistent velocity scaling cross section to give the correct thermal relic density. The regions highlighted in figure 2.4 set different bounds on the cross-section. Being consistent with the bounds in one velocity regime will make it inconsistent with the bounds in another regime without these enhance-

ments or suppressions as a function of velocity. What they find is that there is no region of parameter space open that meets these conditions, with some caveats. If we still want to explain the simulation/observation discrepancy with self interacting dark matter we must turn to more complicated models. You can include connections to hidden sectors and sterile neutrinos that are still experimentally verifiable or, as is done in this thesis, we can turn to other mediators. A pseudo-scalar mediator is a viable next option. Interactions with pseudo-scalars can change spins of the interacting particles and gives a spin configuration dependent potential [32] which can change the cross sections, and their velocity dependents. This can allow us to possibly circumvent some of these constraints and it is not as well studied.

Chapter 3

Bound state mechanics

In this chapter we introduce the concept of a bound state as defined by a pole in a scattering amplitude, and the unique characteristics of a bound state. The main part of this chapter is the motivation for the Bethe-Salpeter equation. We see the occurrence of infinite sets of diagrams to each order in perturbation theory, and how the problem simplifies in the non-relativistic regime. We go on to study how to treat Dirac fermions in this non-relativistic regime of interest.

3.1 Defining a bound state

A natural starting point in a discussion of bound states is to ask what defines a bound state. The defining characteristic of a bound state is the concept of the rest mass being lower than the sum of individual masses $M = m_1 + m_2 + \mathcal{E} < m_1 + m_2$. In quantum mechanics we recognize the quantity $\mathcal{E}$ as the eigenvalue of the Hamilton operator. The eigenvalues form a discrete set of negative energies that are bounded from below. In quantum field theory we define the mass of a state as the poles in scattering amplitudes [36]. This is seen in the Källén-Lehmann spectral representation [37] of a two point correlation function

$$\langle\Omega|\, T\phi(x)\phi(y)\,|\Omega\rangle = \int_0^\infty \frac{dM^2}{2\pi}\rho(M^2)D_F(x-y;M^2) \tag{3.1}$$

here shown for a two point correlation function. The left hand side is the correlation between two time ordered fields ϕ in vacuum, $|\Omega\rangle$. The right hand side is an integral over mass squared, M^2, of a density function $\rho(M^2)$ and the energy dependent Feynman propagator $D_F(x-y;M^2)$. The variable M^2 in the propagator is the a generalized mass squared, such that the integral runs over all positive energies with a Lorentz invariant measure. The spectral density function $\rho(M^2)$ selects the physical masses/poles of states; be they single particle, a bound state, or a branch cut for multi particle state. This is derived by inserting a completeness relation of a physical state basis for the Hilbert space, generated

by the fields ϕ acting on a zero energy state $|0\rangle$, the zero element of the Hilbert space. The poles come with a corresponding field-strength renormalization factor that determines the contribution of each pole, and thus state, at a given energy scale.

Bound state formation consists of two incoming free and two outgoing but bounded particles. We will therefore consider four point correlation functions, $G^{(4)}$, rather than two point correlation function as in (3.1). For $G^{(4)}$ we will do a the decomposition in terms of bound and free states. The idea of this type of decomposition becomes important for the derivation of the Bethe-Salpeter equation [29, 30] as seen in chapter 4.1, when deriving the relevant cross-sections for bound state formation and annihilation chapter 5, and the derivation of the potential for a pseudo-scalar mediator [32] chapter 6.

In this thesis we will follow the notation of Petraki, Postma and Wiechers [29]. In this work, a center of mass frame will constantly be used. As such the definitions for reduced mass we use is given by

$$\mu \equiv \frac{m_1 m_2}{m}. \tag{3.2}$$

where

$$m \equiv m_1 + m_2, \tag{3.3}$$

A general bound state will be denoted by $|\mathcal{B}_{\mathbf{Q},n}\rangle$ with total momentum $\mathbf{Q}$ and energy $\omega_{\mathbf{Q},n} = \sqrt{\mathbf{Q}^2 + M_n^2}$, where n is a general placeholder for all relevant quantum numbers and $M_n < m$. There will similarly be use for a general notation for an unbounded, free two-particle state $|\mathcal{U}_{\mathbf{Q},\mathbf{q}}\rangle$ where the discrete quantum number is replaced by the relative momentum defined by $v_{\text{rel}} = \mathbf{q}/\mu$ and correspondingly $\omega_{\mathbf{Q},\mathbf{q}} \geq m$. The states $|\mathcal{B}_{\mathbf{Q},n}\rangle$ and $|\mathcal{U}_{\mathbf{Q},\mathbf{q}}\rangle$ can be constructed with fermions, in which case these states will represent a specific spin state. The coordinates will be split up into relative coordinates denoted by a lower case letter, and center of mass coordinates denoted by upper case letters as follows,

$$x \equiv x_1 - x_2, \quad X \equiv \eta_1 x_1 + \eta_2 x_2, \tag{3.4}$$

$$x_1 \equiv X + \eta_2 x, \quad x_2 \equiv X - \eta_1 x, \tag{3.5}$$

$$Q \equiv p_1 - p_2, \quad p \equiv \eta_2 p_1 - \eta_1 p_2, \tag{3.6}$$

$$p_1 \equiv \eta_1 Q + p, \quad p_2 \equiv \eta_2 Q - p, \tag{3.7}$$

with

$$\eta_{1,2} = \frac{m_{1,2}}{m}, \text{ such that } \eta_1 + \eta_2 = 1, \tag{3.8}$$

such that the Jacobian under this coordinate transformation is 1. x, X are position coordinates and p, Q are momentum coordinates.

3.2 Instantaneous approximation and the non-relativistic expansion

The Källén-Lehmann decomposition, eqs. (3.1), tells us that the pole of a bound state will be at its mass, $M = m_1 + m_2 + \mathcal{E} < m_1 + m_2$ where the binding energy will be dependent on the potential depth regulated by the coupling constant, such that $\mathcal{E} \sim \alpha$. Therefore the pole in the correlation function is dependent on the coupling constant. In Feynman diagrams the coupling constant is introduced in the vertex factors, as part of the numerator. To have the coupling to appear in the denominator there needs to be a resummation of diagrams of all orders. Therefore a pole in α cannot appear for any Feynman diagram of finite order n [36]. This means that the perturbative expansion has to diverge for any such four point correlation function G, irregardless of how small the coupling constant may be. So to calculate BSF (bound state formation) one can no longer rely on the familiar perturbative methods in the traditional sense and one needs to find a way to handle such an infinite set of diagrams.

The Bethe-Salpeter [30], formulates the problem of finding the correlation function in terms of an integro-differential equation for the exact correlation function in terms of irreducible kernels, rather than individual diagrams. It is this aspect of the formalism that makes the problem solvable in the non-relativistic regime. We will talk about two aspects of the non-relativistic regime separately; the instantaneous approximation for the momentum and energy of the mediating particle and the non-relativistic approximation for the momentum and energy of the dark matter particles.

The instantaneous approximation states that the momentum exchange of two particles is instant, i.e. does not depend on time. This implies a non-relativistic regime where energy can be written in terms of the three-momenta scaling as; $|\mathbf{q}| \sim \mu v_{rel}$ for unbounded particles and $|\mathbf{q}| \sim \mu\alpha$ for bounded particles [29] (i.e. order of the Bohr momenta [36]). The energy transfer will then be of order momenta squared, $q^0 \sim \mathbf{q}^2/2\mu = \frac{1}{2}\alpha^2$, $\frac{1}{2}v_{\text{rel}}^2\mu \ll |\mathbf{q}|$ which is very small for $\alpha, v_{rel} \ll 1$. This means that both fermion, scalar, and photon propagators contribute of order $\sim 1/\mathbf{q}^2 \sim 1/\alpha^2$ and loop integrals will contribute $\int dk^0 d\mathbf{k} \sim \alpha^2\alpha^3 = \alpha^5$. Diagrams which in the relativistic case would be of different orders can then be of the same order in the instantaneous approximation, as shown in figure 3.1. The two diagrams in figure 3.1 are examples of ladder diagrams, where there is an energy exchange through a mediator in a t-channel. The dependence on the coupling α is shown in figure 3.1 and when multiplying the factors together we see that both diagrams are of overall order $1/\alpha$. In fact any ladder diagram will be of order $1/\alpha$ while other types of diagrams will give higher orders in α. We still has an infinite set of diagrams to the lowest perturbative

order but only one one particle irreducible (1PI) kernel. In the regular perturbative method of finding correlation function we would still have to calculate an infinite set of diagram but the 1PI kernel consists only of one diagram and we get around the problem of having to calculate an infinite amount with the Bethe-Salpeter formalism. To be exact one would still need to include all possible 1PI kernels, but to first order we only need to include the ladder 1PI. Including only the ladder 1PI kernel is called the ladder approximation. This approximation has been an integral part of the Bethe-Salpeter equation and its viability since its start [30, 38], but was initially met with distrust. The Bethe-Salpeter formalism allows us to do calculations with an infinite set of diagrams built up by the 1PI diagrams. Relativistically this seems very strange as it automatically includes higher order ladder diagrams but ignores the higher order diagrams from other 1PI kernels, and for the first couple of years after the Bethe-Salpeter equations conception was a major criticism [38]. However, in the instantaneous approximation; as described above, one can see that the sums in the non-relativistic limit is consistent. This is why the instantaneous approximation is significant in giving a consistent way to solve the Bethe-Salpeter equation, as now all orders of ladder diagrams are of the same order in perturbation and the ladder approximation is now consistent.

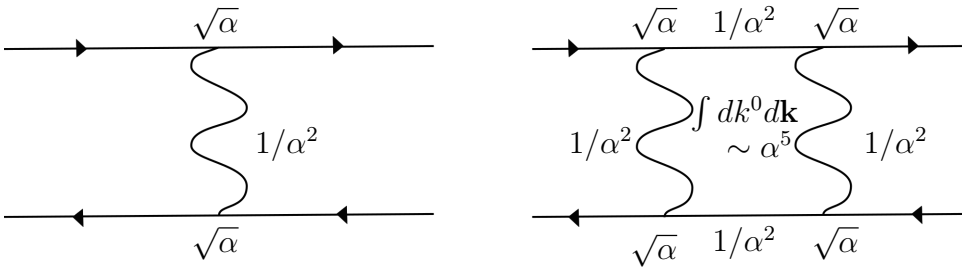

Figure 3.1: In the instantaneous approximation the momentum transfer for mediating particles in a bound state is of order $|\mathbf{q}| \sim \mu\alpha$ which means that the two diagrams shown above are of the same order in α due to the loop integral. The lowest order in perturbation theory gives an infinite sum of diagrams built up of the 1PI diagram. *Left*: One particle irreducible part of a ladder diagram, with corresponding order of α contribution from vertex and propagator in the instantaneous approximation. *Right*: The second possible ladder diagram consisting of two 1PI, with the corresponding order of α contribution from the vertex, both propagators, and loop integral in the instantaneous approximation.

Before we set about giving an overview of the derivation of the Bethe-Salpeter equation, we will finish discussion of the non-relativistic regime by summarizing what we called the non-relativistic approximation from Petraki *et al.* [29] and

show how to treat fermion and more specifically spinors in such an approximation.

From appendix C of Petraki *et al.* [29] we have the non-rel. approximation summarized; $\mathbf{P}, \mathbf{p} \ll P^0, m_1, m_2$ which leads to:

$$E_1(\mathbf{p}, \mathbf{P}) = \sqrt{\mathbf{p_1}^2 + m_1^2} \simeq \eta_1 \left(m + \frac{\mathbf{P}^2}{2m} \right) + \frac{\mathbf{P} \cdot \mathbf{p}}{m} + \frac{\mathbf{p}^2}{2m_1}, \tag{3.9}$$

$$E_2(\mathbf{p}, \mathbf{P}) = \sqrt{\mathbf{p_2}^2 + m_2^2} \simeq \eta_2 \left(m + \frac{\mathbf{P}^2}{2m} \right) - \frac{\mathbf{P} \cdot \mathbf{p}}{m} + \frac{\mathbf{p}^2}{2m_2}, \tag{3.10}$$

$$E_1(\mathbf{p}, \mathbf{P}) + E_2(\mathbf{p}, \mathbf{P}) \simeq m + \frac{\mathbf{P}^2}{2m} + \frac{\mathbf{p}^2}{2\mu}. \tag{3.11}$$

With these quantities established working with scalars is straight forward but does require quite a bit of algebra. However, we will be concerned with fermionic dark matter and as such we need to know how spinors and spin structure changes when going to the non-relativistic regime. The answer is found in the large and small component decomposition of a spinor[1]. The following derivation is taken from "Quantum Field Theory" by Itzykson and Zuber, for QED covariant derivative of U(1) symmetry but the emergence of a large and a small component is in general independent of the symmetry, and is due to the βm term in the Dirac equation

$$i\frac{\partial \psi}{\partial t} = (\boldsymbol{\alpha} \cdot \mathbf{p} + \beta m)\, \psi + \left(-e\boldsymbol{\alpha} \cdot \mathbf{A} + eA^0 \right) \psi, \tag{3.12}$$

where A^0 and $\mathbf{A}$ are the zeroth and three vector components of the vector potential, i.e. the gauge boson. Writing the spinors out in terms of distinct upper and lower components; $\psi = \begin{pmatrix} \phi \\ \chi \end{pmatrix}$ and in the aforementioned Dirac representation we have $\beta = \begin{pmatrix} \mathbf{I} & 0 \\ 0 & -\mathbf{I} \end{pmatrix}$, $\boldsymbol{\alpha} = \begin{pmatrix} 0 & \boldsymbol{\sigma} \\ \boldsymbol{\sigma} & 0 \end{pmatrix}$ we see that the β matrix has different signs for its diagonal components. Writing the equations in component form the mass term has a different sign in the two equations

$$i\frac{\partial \phi}{\partial t} = \boldsymbol{\sigma} \cdot \boldsymbol{\pi} \chi + eA^0 + m\phi, \tag{3.13}$$

$$i\frac{\partial \chi}{\partial t} = \boldsymbol{\sigma} \cdot \boldsymbol{\pi} \phi + eA^0 - m\chi, \tag{3.14}$$

where $\boldsymbol{\pi}$ is the gauge-invariant momentum defined by $\boldsymbol{\pi} \equiv \mathbf{p} - e\mathbf{A}$. Then in the non-relativistic regime the mass term dominates. We therefore introduce slowly

[1]Note that in this thesis we will be working in the Dirac representation of the gamma matrices.

varying functions

$$\phi = e^{-imt}\Phi, \tag{3.15}$$
$$\chi = e^{-imt}X, \tag{3.16}$$

which lead to the two equations

$$i\frac{\partial\Phi}{\partial t} = \boldsymbol{\sigma}\cdot\boldsymbol{\pi}X + eA^0\Phi, \tag{3.17}$$
$$i\frac{\partial X}{\partial t} = \boldsymbol{\sigma}\cdot\boldsymbol{\pi}\Phi + eA^0X - 2mX. \tag{3.18}$$

The second equation gives us, for $eA^0 \ll 2m$

$$X \simeq \frac{\boldsymbol{\sigma}\cdot\boldsymbol{\pi}}{2m}\Phi \ll \Phi. \tag{3.19}$$

Inserting this (3.12) gives the out the familiar Pauli equation, the spin half dependent version of the Schrödinger equation. And since the lower component χ is then much smaller than the upper component ϕ in the non-relativistic limit, they are respectively called the small and large component. We have a way to handle spinors in the non-relativistic regime, where the large component gives zeroth order terms while the small components give higher order terms. This also allows us to see the effect of gamma matrices on spinors in the limit, as in the Dirac representation the $\gamma^0 \simeq 1$ since it does not mix terms, while both the $\boldsymbol{\gamma}$ and γ^5 mix small and large components. Therefore $\boldsymbol{\gamma}$ and γ^5 can induce higher correction in momentum separately but combinations can give leading order terms. The above discussion can be generalized also to other interactions than U(1).

We now have the motivation for using the Bethe-Salpeter equation and the tools necessary to handle going from the fully relativistic theory to the non-relativistic regime. Let us now look at the derivation of the Bethe-Salpeter equation and how to get to the non-relativistic version of it.

Chapter 4

Bethe-Salpeter equation

The Bethe-Salpeter(B-S) equation was derived in 1951 [30] using the diagrammatic approach of Feynman to tackle bound state formation, though several other authors proposed similar methods around the same time [38]. The different methods follow the same general principles and the formalism of Bethe and Salpeter solidified as the go to approach. The idea is that the amplitude of BSF, or any two body process, is exactly described by the four point correlation function

$$G^{(4)}(x_1, x_2, y_1, y_2)_{ab;cd} = \langle \Omega | \, T\chi_{1,a}(x_1)\bar{\chi}_{2,b}(x_2)\chi_{1,c}(y_1)\bar{\chi}_{2,d}(y_2) \, | \Omega \rangle \, , \tag{4.1}$$

where $\chi_{1,a}$, $\chi_{2,b}$ are the fermion fields of particle type 1 and 2, with indices a, b in spinor space running from 1 to 4. Repeated indices will be summed over. This correlation function can be written out as an infinite sum of diagram[1], both fully connected and disconnected, through the Dyson-Schwinger equation [29,39]. The disconnected diagrams together constitute the first right hand side term in figure 4.1. The connected diagrams consists of products of 1PI kernels W. This then repeats to infinity, and we recognize that this infinite sum contains the four point function itself, in expanded form. We therefore write the correlation function as a non-scattering amplitude plus the product of the 1PI kernel and the four point function making a differential equation, figure 4.1. Based on this expansion we can do a decomposition of the four point function $G^{(4)}$ similar to the Källén-Lehmann spectral decomposition but in terms of two-particle wavefunctions. By analyzing the pole structure of this decomposition and comparing it to the general form of the solution to the Dyson-Schwinger equation one arrives at the Bethe-Salpeter equation. In this chapter we go through the derivation as done by Petraki *et al.* [29], along the way showing the differences when dealing with fermions, instead of scalars. In the last section we apply the instantaneous and non-relativistic assumptions presented in chapter 3.2 and show that the Bethe-Salpeter reduces to the Schrödinger equation.

[1]Note that unlike what I will present here, Itzykson and Zuber derive the integro-differential equation that leads to the B-S equation though Legandre transformation of the Dyson-Schwinger equation but leads to the answer as the diagrammatic approach that follows.

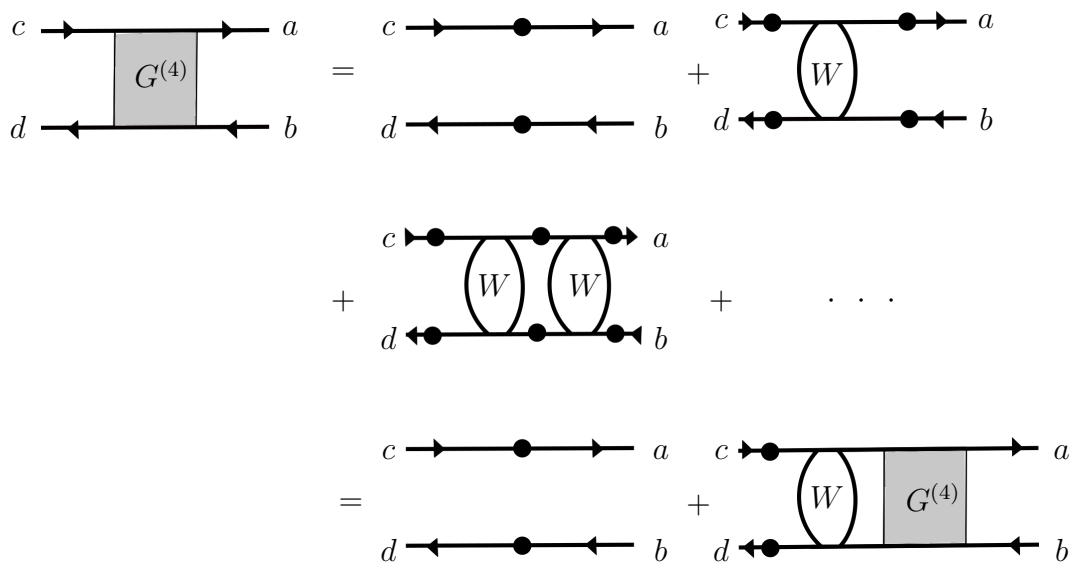

Figure 4.1: The diagrammatic expansion of the four point correlation function $G^{(4)}$. The first term gives the non connected diagrams, where there is no interactions between the two particles. The remaining terms are the fully connected scattering diagrams in terms of 1PI kernels W. Using the properties of infinite sums we can rewrite the sum on the right hand side in terms of $G^{(4)}$ giving us an integro-differential equation describing the exact full four point correlation function. The a, b, c, d indices signify the spinor index each external fermion line has.

4.1 Derivation of the Bethe-Salpeter equation

As with the Källén-Lehmann decomposition we want to have a complete set of states to decompose the correlation function into. For this we use the bound and free states introduced in chapter 3.1 to create the completeness relation

$$\mathbf{1} = \sum_n \int \frac{d^3Q}{(2\pi)^3 2\omega_{\mathbf{q},n}} \left|\mathcal{B}_{\mathbf{Q},n}\right\rangle \left\langle\mathcal{B}_{\mathbf{Q},n}\right| + \int \frac{d^3q}{(2\pi)^3}\frac{d^3Q}{(2\pi)^3}\frac{1}{2\omega_{\mathbf{Q},\mathbf{q}}2\varepsilon_{\mathbf{Q},\mathbf{q}}} \left|\mathcal{U}_{\mathbf{Q},\mathbf{q}}\right\rangle \left\langle\mathcal{U}_{\mathbf{Q},\mathbf{q}}\right|, \tag{4.2}$$

with the relativistic normalization $\langle\mathbf{p}|\mathbf{k}\rangle = 2E_{\mathbf{p}}(2\pi)^3\delta^3(\mathbf{p}-\mathbf{k})$ where $E_{\mathbf{p}}$ is the energy of the one particle state $|\mathbf{p}\rangle$. The ε is just to indicate that it is connected to the normalization of the second continuous variable but is otherwise identical to ω. For fermions, these states represent a specific spinor states. The normalizations give to lowest order

$$2\omega_{\mathbf{Q},\mathbf{q}}2\varepsilon_{\mathbf{Q},\mathbf{q}} \simeq 2E_1(\mathbf{q};\mathbf{Q})2E_2(\mathbf{q};\mathbf{Q}). \tag{4.3}$$

to be consistent in the non-relativistic limit.

We therefore define two-particle wavefunctions as two point correlation functions between the vacuum and some final physical state

$$\Psi_{\mathbf{Q},n,ab}(x_1,x_2) \equiv \langle\Omega|\, T\chi_{1,a}(x_1)\bar{\chi}_{2,b}(x_2)\,|\mathcal{B}_{\mathbf{Q},n}\rangle\,, \tag{4.4}$$
$$\Psi^{\star}_{\mathbf{Q},n,ab}(x_1,x_2) \equiv \langle\mathcal{B}_{\mathbf{Q},n}|\, T\chi_{1,a}(x_1)\bar{\chi}_{2,b}(x_2)\,|\Omega\rangle\,, \tag{4.5}$$
$$\Phi_{\mathbf{Q},\mathbf{q},ab}(x_1,x_2) \equiv \langle\Omega|\, T\chi_{1,a}(x_1)\bar{\chi}_{2,b}(x_2)\,|\mathcal{U}_{\mathbf{Q},\mathbf{q}}\rangle\,, \tag{4.6}$$
$$\Phi^{\star}_{\mathbf{Q},\mathbf{q},ab}(x_1,x_2) \equiv \langle\mathcal{U}_{\mathbf{Q},\mathbf{q}}|\, T\chi_{1,a}(x_1)\bar{\chi}_{2,b}(x_2)\,|\Omega\rangle\,, \tag{4.7}$$

which are unknown quantities we want to solve for. The wavefunction for a bound state is described by its center of mass momentum and a discrete set of quantum numbers noted by n. The free wavefunction is described by the two continuous variables of CM and relative momentum.

With these wavefunctions it is straightforward to change into the relative coordinates (3.4)-(3.7) defined in chapter 3.1 by use of translation invariance. This leads to the wavefunctions with variables

$$\Psi_{\mathbf{Q},n,ab}(x) \equiv \langle\Omega|\, T\chi_{1,a}(\eta_2 x)\bar{\chi}_{2,b}(-\eta_1 x)\,|\mathcal{B}_{\mathbf{Q},n}\rangle\,, \tag{4.8}$$

in relative coordinates. In turn we can define the wavefunctions in momentum space as the Fourier transform with respect to the previously defined relative coordinates of x and p respectively. Having established the wavefunction we write out the Dyson-Schwinger equation in terms relative momentum coordinates

$$\begin{aligned}\tilde{G}^{(4)}_{ab;cd}(p,p';Q) =&(2\pi)^4\delta^4(p-p')S_{ab;cd}(p;Q)\\ &+ S_{ab;ef}(p;Q)\int\frac{d^4k}{(2\pi)^4}\tilde{W}_{ef;gh}(p,k;Q)\tilde{G}^{(4)}_{gh;cd}(k,p';Q),\end{aligned} \tag{4.9}$$

where

$$S_{ab;cd}(p;q) \equiv \tilde{S}_{1,a;c}(\eta_1 Q+p)\tilde{S}_{2,b;d}(\eta_2 Q-p), \tag{4.10}$$

is the product of the exact propagator of particle type 1 and 2, and the tilde indicates that it is in momentum space. The spinor indices are such that they are consistent with figure 4.1.

We now have all the tools necessary to start the derivation. By insertion of the completeness relation (4.2) we can then split up the four point function into contributions to bound states and scattering states

$$\tilde{G}^{(4)}_{ab;cd}(p,p';Q) = \sum_n \tilde{G}^{(4)}_{n,ab;cd}(p,p';Q) + \tilde{G}^{(4)}_{\mathcal{U},ab;cd}(p,p';Q). \tag{4.11}$$

This splitting allows us to analyze each contribution separately and distinguish the contributions from each part separately.

First a small interlude into the Heaviside step function needed to explicitly do the time ordering in each contribution. The integral representation of the function is

$$\theta(z) = \frac{i}{2\pi}\int_{-\infty}^{\infty} dk \frac{e^{-ikz}}{k+i\epsilon}, \tag{4.12}$$

and from [40] we have the relation

$$\theta[\min(x_1^0, x_2^0) - \max(y_1^0, y_2^0)] = \theta[X^0 - Y^0 + h_-(x^0) - h_+(y^0)], \tag{4.13}$$

with $h_\pm(x^0) \equiv \frac{1}{2}(\eta_2 - \eta_1)x^0 \pm \frac{1}{2}|x^0|$ for relative coordinates. The bound states contribution of (4.11) gives

$$\begin{aligned}
&G^{(4)}_{n,ab;cd}(x,y;X-Y) = \\
&\int \frac{d^3K}{(2\pi)^3}\frac{1}{2\omega_{\mathbf{K},n}} \langle\Omega|\, T\chi_{1,a}(x_1)\bar{\chi}_{2,b}(x_2)\,|\mathcal{B}_{\mathbf{K},n}\rangle\, \langle\mathcal{B}_{\mathbf{K},n}|\,\chi_{1,c}(y_1)\bar{\chi}_{2,d}(y_2)\,|\Omega\rangle \\
&\qquad\qquad \times \theta[\min(x_1^0, x_2^0) - \max(y_1^0, y_2^0)] \\
&= \int \frac{d^3K}{(2\pi)^3}\frac{1}{2\omega_{\mathbf{K},n}} \Psi_{\mathbf{K},n,ab}(x)\Psi^\star_{\mathbf{K},n,cd}(y) e^{-i\omega_{\mathbf{K},n}(X^0-Y^0)} e^{i\mathbf{K}\cdot(\mathbf{X}-\mathbf{Y})} \\
&\times \frac{i}{(2\pi)}\int_{-\infty}^{\infty} dK^0 \frac{e^{-i[K^0-\omega_{\mathbf{K},n}][X^0-Y^0+h_-(x^0)-h_+(y^0)]}}{K^0-\omega_{\mathbf{K},n}+i\epsilon} \\
&= i\int \frac{d^4K}{(2\pi)^4} e^{-iK(X-Y)} \Psi_{\mathbf{K},n,ab}(x)\Psi^\star_{\mathbf{K},n,cd}(y) \frac{e^{-i[K^0-\omega_{\mathbf{K},n}][X^0-Y^0+h_-(x^0)-h_+(y^0)]}}{\omega_{\mathbf{K},n}(K^0-\omega_{\mathbf{K},n}+i\epsilon)},
\end{aligned}$$

when applying the relations (4.13) in the first step and (4.12) in the second step integrating over K^0. We Fourier transform the above expression with respect to x, y, and $X-Y$

$$\begin{aligned}
\tilde{G}^{(4)}_{n,ab;cd}(p,p';Q) &= \int d^4x d^4y d^4(X-Y) e^{[px-p'y+Q(X-Y)]} G^{(4)}_n(x,y;X-Y) \\
&= i\int d^4x d^4y e^{[px-p'y]} \Psi_{\mathbf{Q},n,ab}(x)\Psi^\star_{\mathbf{Q},n,cd}(y) \frac{e^{-i[Q^0-\omega_{\mathbf{Q},n}][X^0-Y^0+h_-(x^0)-h_+(y^0)]}}{2\omega_{\mathbf{Q},n}(Q^0-\omega_{\mathbf{Q},n}+i\epsilon)},
\end{aligned} \tag{4.14}$$

to arrive at the pole structure in terms of the energy. At the pole $Q^0 \to \omega_{\mathbf{Q},n}$ we have

$$\tilde{G}^{(4)}_{n,ab;cd}(p,p';Q) \to \frac{\Psi_{\mathbf{Q},n,ab}(p)\Psi^\star_{\mathbf{Q},n,cd}(p')}{2\omega_{\mathbf{Q},n}(Q^0-\omega_{\mathbf{Q},n}+i\epsilon)}. \tag{4.15}$$

Following the same process for the scattering state contribution to the corre-

lation function leads to the expression

$$\tilde{G}^{(4)}_{\mathcal{U},ab;cd}(p,p';Q) = i\int\frac{d^3q}{(2\pi)^3}\int d^4x d^4y e^{[px-p'y]}\Phi_{\mathbf{Q},\mathbf{q},ab}(x)\Phi^{\star}_{\mathbf{Q},\mathbf{q},cd}(y) \times \frac{e^{-i[Q^0-\omega_{\mathbf{Q},\mathbf{q}}][X^0-Y^0+h_-(x^0)-h_+(y^0)]}}{2\omega_{\mathbf{Q},\mathbf{q}}2\varepsilon_{\mathbf{Q},\mathbf{q}}(Q^0-\omega_{\mathbf{Q},\mathbf{q}}+i\epsilon)}. \tag{4.16}$$

Note that unlike for the bound states, which have simple poles, the scattering states give rise to a branch cut. The cut arises due to the extra integral over the free variable $\mathbf{q}$.

With the pole structure having been established, we turn to solving the Dyson-Schwinger equation. By defining an operator

$$A(p,p';Q)_{ab;cd} \equiv (2\pi)^4\delta^4(p-p')S^{-1}_{ab;cd}(p;Q) - \tilde{W}_{ab;cd}(p,p';Q), \tag{4.17}$$

we can rewrite the Dyson-Schwinger equation into

$$\int\frac{d^4k}{(2\pi)^4}A_{ef;gh}(p,k;Q)\tilde{G}^{(4)}_{gh;cd}(k,p';Q) = I_{ef;cd}, \tag{4.18}$$

where $I = (2\pi)^4\delta^4(p-p')\delta_{ec}\delta_{fd}$. We check that relation (4.17) holds by inserting the definition (4.18) into (4.17)

$$S^{-1}_{ef;gh}(p;Q)\tilde{G}^{(4)}_{gh;cd}(p,p';Q) - \int\frac{d^4k}{(2\pi)^4}\tilde{W}_{ef;gh}(p,k;Q)\tilde{G}^{(4)}_{gh;cd}(k,p';Q) = I_{ef;cd}. \tag{4.19}$$

We then multiply from the left $S_{ab;ef}(p;Q) = \tilde{S}_{1,ae}\tilde{S}_{2,bf}$. The product of the propagators will then be

$$\begin{aligned} S_{ab;ef}(p;Q)S^{-1}_{ef;gh}(p;Q) &= \tilde{S}_{1,ae}(p;Q)\tilde{S}_{2,bf}(p;Q)\tilde{S}^{-1}_{2,fg}(p;Q)\tilde{S}^{-1}_{1,eh}(p;Q) \\ &= \tilde{S}_{1,ae}(p;Q)\delta_{bg}\tilde{S}^{-1}_{1,eh}(p;Q) = \delta_{ah}\delta_{bg} \end{aligned} \tag{4.20}$$

and with this equation (4.19) becomes

$$\begin{aligned} &\tilde{G}^{(4)}_{ab;cd}(p,p';Q) - S_{ab;ef}(p;Q)\int\frac{d^4k}{(2\pi)^4}\tilde{W}_{ef;gh}(p,k;Q)\tilde{G}^{(4)}_{gh;cd}(k,p';Q) \\ &= S_{ab;ef}(p;Q)I_{ef;cd}, \end{aligned} \tag{4.21}$$

therefore

$$\begin{aligned} \tilde{G}^{(4)}_{ab;cd}(p,p';Q) &= S_{ab;cd}(p;Q) \\ &\quad + S_{ab;ef}(p;Q)\int\frac{d^4k}{(2\pi)^4}\tilde{W}_{ef;gh}(p,k;Q)\tilde{G}^{(4)}_{gh;cd}(k,p';Q), \end{aligned} \tag{4.22}$$

which is the Dyson-Schwinger equation (4.9).

The solution to equation (4.18) is formally

$$\tilde{G}^{(4)}_{ab;cd}(p,p';Q) = \sum_n \frac{1}{c_n(Q)} C_{n,ab}(p;Q)\bar{C}_{n,cd}(p';Q) + \int \frac{ds}{f_s(Q)} F_{s,ab}(p;Q)\bar{F}_{s,cd}(p';Q), \tag{4.23}$$

given in terms of functions $C_{n,a,b}(p;Q)$ and $F_{s,a,b}(p;Q)$, where n, as before, represent a general collection of discrete quantum numbers and s a continuous one. These function are eigenfunctions of the operator $A_{a,b;e,f}(p,p';Q)$

$$\int \frac{d^4k}{(2\pi)^4} A_{ab;ef}(p,k;Q)C_{n,ef}(k;Q) = c_n(Q)C_{n,ab}(p;Q), \tag{4.24}$$

$$\int \frac{d^4k}{(2\pi)^4} A_{ab;ef}(p,k;Q)F_{s,ef}(k;Q) = f_s(Q)F_{s,ab}(p;Q), \tag{4.25}$$

for the discrete and continuous spectrum respectively with corresponding eigenvalues $c_n(Q)$ and $f_s(Q)$. With the eigenfunctions are normalized such that

$$\sum_n C_{n,ab}(p;Q)\bar{C}_{n,cd}(p';Q) + \int ds F_{s,ab}(p;Q)\bar{F}_{s,cd}(p';Q) = (2\pi)^4\delta^4(p-p')\delta_{ac}\delta_{bd}. \tag{4.26}$$

Given the same form of eq. (4.11) and eq. (4.23), we can use equations (4.14) and (4.16) to read of the eigenfunction, up to a proportionality

$$C_{n,ab}(p;Q) \propto \int d^4x \Psi_{\mathbf{Q},n,ab}(p) e^{ipx} e^{-i[Q^0-\omega_{\mathbf{Q},n}]h_-(x^0)}, \tag{4.27}$$

$$\bar{C}_{n,cd}(p';Q) \propto \int d^4x \Psi^\star_{\mathbf{Q},n,cd}(p) e^{-ip'y} e^{-i[Q^0-\omega_{\mathbf{Q},n}]h_+(y^0)}, \tag{4.28}$$

$$c_n(Q) \propto 1 - \frac{\omega_{\mathbf{Q},n}}{Q^0}, \tag{4.29}$$

and

$$F_{s,ab}(p;Q) \propto \int d^4x \Phi_{\mathbf{Q},\mathbf{q},ab}(p) e^{ipx} e^{-i[Q^0-\omega_{\mathbf{Q},\mathbf{q}}]h_-(x^0)}, \tag{4.30}$$

$$\bar{F}_{s,cd}(p';Q) \propto \int d^4x \Phi^\star_{\mathbf{Q},\mathbf{q},cd}(p) e^{-ip'y} e^{-i[Q^0-\omega_{\mathbf{Q},\mathbf{q}}]h_+(y^0)}, \tag{4.31}$$

$$f_s(Q) \propto 1 - \frac{\omega_{\mathbf{Q},\mathbf{q}}}{Q^0}. \tag{4.32}$$

Here we have made sure that all dependence on p and p' is contained in the respective eigenfunction, while the eigenvalues are chosen such that the eigenfunctions themselves are not singular in the limit $Q^0 \to \omega$.

To summarize, we have now found an operator that allows us to rewrite the Dyson-Schwinger equation in a form that allows us to decompose the four point correlation function $\tilde{G}^{(4)}$ in terms of the functions $C_n(p;Q)$, $F_s(p;Q)$, $c_n(Q)$,and $f_s(Q)$. It also allows us to decompose the Dyson-Schwinger equation to two eigenvalue equations, eqs. (4.24) and (4.25). Then by a spectral decomposition we found the pole structure of $\tilde{G}^{(4)}$ in term of the two-particle wavefunction defined in eqs. (4.4)-(4.7). This was used to find the eigenfunctions $C_n(p;Q)$, $F_s(p;Q)$ and eigenvalues $c_n(Q)$, $f_s(Q)$. The last step now is to insert these functions into the decomposed Dyson-Schwinger equation (4.24) and (4.25) in the limit of $Q^0 \to \omega$ to arrive at the Bethe-Salpeter equations

$$\tilde{\Psi}_{\mathbf{Q},n,ab}(p) = S(p;Q)_{ab;ef} \int \frac{d^4k}{(2\pi)^4} \tilde{W}_{ef;gh}(p,k;Q)\tilde{\Psi}_{\mathbf{Q},n,gh}(k), \tag{4.33}$$

$$\tilde{\Phi}_{\mathbf{Q},\mathbf{q},ab}(p) = S(p;Q)_{ab;ef} \int \frac{d^4k}{(2\pi)^4} \tilde{W}_{ef;gh}(p,k;Q)\tilde{\Phi}_{\mathbf{Q},\mathbf{q},gh}(k), \tag{4.34}$$

for the bound and scattering wavefunctions respectively. Like the Schrödinger equation, these equations do not determine the normalizations of the wavefunctions. And since we can only determine the eigenvalues to a proportionality, we cannot use the normalization of the formal solutions to determine their normalizations. One therefore needs a new equation for the normalizations, which can be found using relations of the Dyson-Schwinger equation in operator form, eq.(4.18), and its derivative.

The ordering of equation (4.18) is such that it recreates the ordering of equation (4.9). However we could have just as easily factored the $G^{(4)}$ out on the left hand side of the last term in figure 4.1, see figure 4.2, in which case the corresponding operator equation would be with the A and $\tilde{G}^{(4)}$ switched in eq. (4.18). Therefore A and $\tilde{G}^{(4)}$ must commute and we have some freedom when manipulating these equations.

Symbolically figure 4.2 means that

$$A_{ab;ef}\tilde{G}^{(4)}_{ef;cd} = \tilde{G}^{(4)}_{ab;ef}A_{ef;cd} = I_{ab;cd}, \tag{4.35}$$

where $I = (2\pi)^4\delta^4(p-p')\delta_{ac}\delta_{bd}$ is defined as before. We can now differentiate the equation $A_{ab;ef}\tilde{G}^{(4)}_{ef;cd} = I_{ab;cd}$ with respect to Q^0. Through the product rule and using equation (4.35) we obtain

$$\tilde{G}^{(4)}_{ab;ef}\left(\frac{dA_{ef;gh}}{dQ^0}\right)\tilde{G}^{(4)}_{hg;cd} = -\left(\frac{d\tilde{G}^{(4)}_{ab;cd}}{dQ^0}\right), \tag{4.36}$$

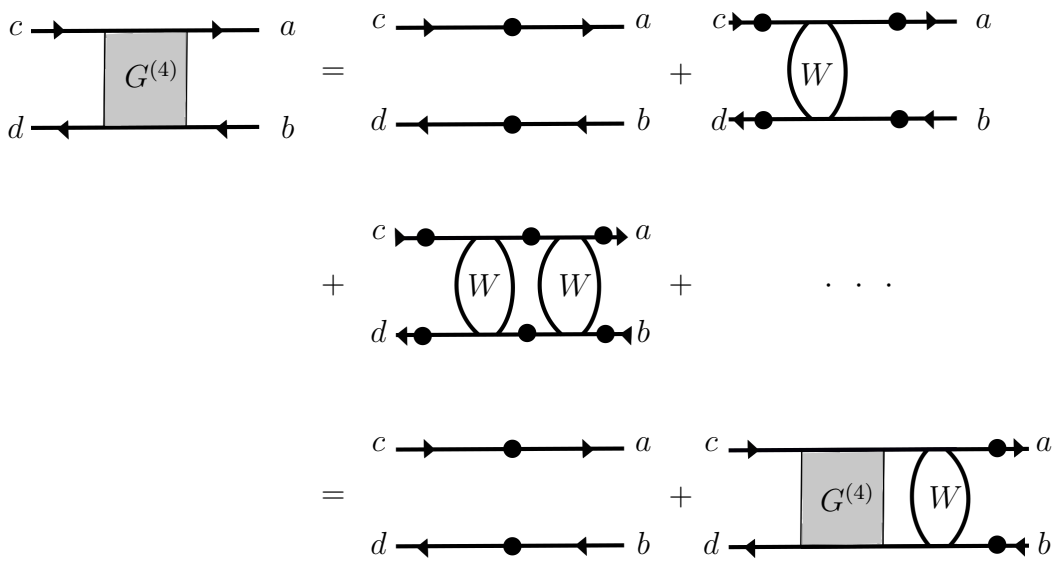

Figure 4.2: The diagrammatic expansion of the four point correlation function $G^{(4)}$ where we have factorized out the four point correlation function out on the left hand side rather than on the right hand side as in figure 4.1. This freedom is important in both determining the normalization and in keeping track of ordering of terms.

a normalization condition for the Bethe-Salpeter wave equations. For our ease we define two quantities

$$\tilde{N}_{n,ab;cd}(p,p';\mathbf{Q}) \equiv i\left[\frac{dA_{ab;cd}(p,p';Q)}{dQ^0}\right]_{Q^0=\omega_{\mathbf{Q},n}}, \tag{4.37}$$

$$\tilde{N}_{\mathbf{q},ab;cd}(p,p';\mathbf{Q}) \equiv i\left[\frac{dA_{ab;cd}(p,p';Q)}{dQ^0}\right]_{Q^0=\omega_{\mathbf{Q},\mathbf{q}}}, \tag{4.38}$$

as normalization operators. Notice that we defined these quantities in the limit $Q^0 \to \omega$ as that is the limit in which the Bethe-Salpeter equations (4.33) and (4.34) hold. In this limit we can insert equations (4.15) and the equivalent limit of (4.16) into the normalization condition (4.36) to obtain the two normalizations

$$\int \frac{d^4p}{(2\pi)^4}\frac{d^4p'}{(2\pi)^4}\tilde{\Psi}^{\star}_{\mathbf{Q},n,ab}\tilde{N}_{n,ab;cd}(p,p';\mathbf{Q})\tilde{\Psi}_{\mathbf{Q},n',cd} = 2\omega_{\mathbf{Q},n}\delta_{n,n'}, \tag{4.39}$$

$$\int \frac{d^4p}{(2\pi)^4}\frac{d^4p'}{(2\pi)^4}\tilde{\Phi}^{\star}_{\mathbf{Q},\mathbf{q},ab}\tilde{N}_{\mathbf{q},ab;cd}(p,p';\mathbf{Q})\tilde{\Phi}_{\mathbf{Q},\mathbf{q}',cd} = 2\omega_{\mathbf{Q},\mathbf{q}}2\varepsilon_{\mathbf{Q},\mathbf{q}}(2\pi)^3\delta^3(\mathbf{q}-\mathbf{q}'). \tag{4.40}$$

4.2 Non-relativistic limit

The Bethe-Salpeter equations, (4.33) and (4.34), are exceedingly difficult to solve and can only be done with approximations such as the non-relativistic approximation. We are interested in what the instantaneous approximation tells us about the 1PI kernel W. The instantaneous approximation stated that the interactions in this kernel happens instantly, implying that the energy exchanged by the mediating particle is given in terms of the three momenta $q^0 \sim \mathbf{q}^2/2\mu \ll |\mathbf{q}|$. This means that the zeroth momentum component of the kernel can be neglected, and we are left with only explicit three-momentum dependence. When considering ladder diagrams in relative coordinates, we note that exchanged momenta will only depend on the absolute difference of the relative momenta and is therefore independent of the center of mass momentum Q. We then have that

$$\tilde{W}_{ab;cd}(p,p';Q) \simeq \mathcal{W}_{ab;cd}(|\mathbf{p}-\mathbf{p}'|), \tag{4.41}$$

implying that the four momentum integral in eqs. (4.33) and (4.34) is reduced to an integral over three momentum. When multiplying both sides of eqs. (4.33) and (4.34) with the inverse of the propagator product we see that the right hand side does not depend on p^0. This motivates the definition of the p^0 independent quantities

$$S_{0,ab;cd}(\mathbf{p};Q) \equiv \int \frac{dp^0}{2\pi} S_{ab;cd}(p,Q), \tag{4.42}$$

$$\tilde{\psi}_{\mathbf{Q},n,ab}(\mathbf{p}) \equiv \sqrt{2\mathcal{N}_{\mathbf{Q}}(\mathbf{p})} S^{-1}_{ab;ef}(p;Q) S_{0,ef;gh}(\mathbf{p};Q) \tilde{\Psi}_{\mathbf{Q},n,gh}(p), \tag{4.43}$$

$$\tilde{\phi}_{\mathbf{Q},\mathbf{q},ab}(\mathbf{p}) \equiv \sqrt{\frac{2\mathcal{N}_{\mathbf{Q}}(\mathbf{p})}{2\varepsilon_{\mathbf{Q},\mathbf{q}}}} S^{-1}_{ab;ef}(p;Q) S_{0,ef;gh}(\mathbf{p};Q) \tilde{\Phi}_{\mathbf{Q},\mathbf{q},gh}(p), \tag{4.44}$$

$$\mathcal{N}_{\mathbf{Q}}(\mathbf{p}) \equiv \frac{E_1(\mathbf{p};\mathbf{Q}) E_2(\mathbf{p};\mathbf{Q})}{E_1(\mathbf{p};\mathbf{Q}) + E_2(\mathbf{p};\mathbf{Q})}, \tag{4.45}$$

which are chosen a posteriori such that they will allow us to reduce to the Schrödinger equation. The final equation is chosen such that it coincides with the normalization for the Bethe-Salpeter wavefunctions and in the non-relativistic limit gives the correct completeness relations one would expect for Schrödinger wavefunctions. Equations (4.43) and (4.44) can be further rewritten by multiplying both sides with $S(p,Q)$ and integrating over p^0

$$\tilde{\psi}_{\mathbf{Q},n,ab}(\mathbf{p}) = \sqrt{2\mathcal{N}_{\mathbf{Q}}(\mathbf{p})} \int \frac{dp^0}{2\pi} \tilde{\Psi}_{\mathbf{Q},n,ab}(p), \tag{4.46}$$

$$\tilde{\phi}_{\mathbf{Q},\mathbf{q},ab}(\mathbf{p}) = \sqrt{\frac{2\mathcal{N}_{\mathbf{Q}}(\mathbf{p})}{2\varepsilon_{\mathbf{Q},\mathbf{q}}}} \int \frac{dp^0}{2\pi} \tilde{\Phi}_{\mathbf{Q},\mathbf{q},ab}(p), \tag{4.47}$$

The time ordering in the definitions of the wavefunctions (4.4) and (4.6) becomes trivial and $\tilde{\psi}^{\star}_{\mathbf{Q},n}(\mathbf{p}) = \tilde{\psi}^{*}_{\mathbf{Q},n}(\mathbf{p})$. Rewriting equation (4.43) by multiplying both side by the combination of propagators $S^{-1}S_0^{-1}S$ and dividing by the normalization factor we see that

$$S^{-1}_{ab;ef}(p;Q)\tilde{\Psi}_{\mathbf{Q},n,ef}(p) = \frac{S^{-1}_{ab;ef}(p;Q)S^{-1}_{0,ef;gh}(\mathbf{p};Q)S_{gh;ij}(p;Q)\tilde{\psi}_{\mathbf{Q},n,ij}(p)}{\sqrt{2\mathcal{N}_{\mathbf{Q}}(\mathbf{p})}}. \quad (4.48)$$

Using this relation and (4.44) with (4.46) and (4.47) in conjunction with the assumption (4.41), we can then rewrite the Bethe-Salpeter equations (4.33) and (4.34) as

$$\frac{S^{-1}_{ab;ef}(p;Q)S^{-1}_{0,ef;gh}(\mathbf{p};Q)S_{gh;ij}(p;Q)\tilde{\psi}_{\mathbf{Q},n,ij}(p)}{\sqrt{2\mathcal{N}_{\mathbf{Q}}(\mathbf{p})}} = \int \frac{dk^3}{(2\pi)^3}\frac{\mathcal{W}_{ab;gh}(|\mathbf{p}-\mathbf{k}|)}{\sqrt{2\mathcal{N}_{\mathbf{Q}}(\mathbf{p})}}\tilde{\psi}_{\mathbf{Q},n,gh}(\mathbf{p}), \quad (4.49)$$

$$\frac{S^{-1}_{ab;ef}(p;Q)S^{-1}_{0,ef;gh}(\mathbf{p};Q)S_{gh;ij}(p;Q)\tilde{\phi}_{\mathbf{Q},\mathbf{q},ij}(p)}{\sqrt{2\mathcal{N}_{\mathbf{Q}}(\mathbf{p})}} = \int \frac{dk^3}{(2\pi)^3}\frac{\mathcal{W}_{ab;gh}(|\mathbf{p}-\mathbf{k}|)}{\sqrt{2\mathcal{N}_{\mathbf{Q}}(\mathbf{p})}}\tilde{\phi}_{\mathbf{Q},\mathbf{q},gh}(\mathbf{p}). \quad (4.50)$$

Going to the Schrödinger equation we will only keep leading order terms. This is due to our previous approximation of the interacting kernel. Higher order terms in the non-relativistic expansion would also imply higher order diagrams for the kernel. To leading order the normalization is given as $\mathcal{N}_{\mathbf{Q}}(\mathbf{p}) \simeq \mu$, and is independent of momenta and thus cancels out. When calculating $S_0(\mathbf{p};\mathbf{Q})$ for fermions we have to take into account the such things as the spin structure and large/small components as well as the pole along the p^0 axis.

We define a function $S(t;\mathbf{p};P) \equiv \int \frac{dp^0}{2\pi}\tilde{S}_1(\eta_1 P + p)\tilde{S}_2(\eta_2 P - p)e^{ip^0 t}$ as a generalization of $S(\mathbf{p};P)$, such that we can calculate $S_0(\mathbf{p},\mathbf{P})$ by closing the contour parameterized by the variable t, without adding a contribution to $S_0(\mathbf{p},\mathbf{P}) = S(0;\mathbf{p};P)$ from the contour. To explicitly handle the spin structure of the fermion propagator we use an alternative way of writing the propagator from Itzykson & Zuber [39],

$$\frac{\not{p}_1 + m_1}{p_1^2 - m_1^2 + i\epsilon} = \left[\frac{\Lambda^+(\mathbf{p_1})}{p_1^0 - E_1 + i\epsilon} + \frac{\Lambda^-(\mathbf{p_1})}{p_1^0 + E_1 - i\epsilon}\right]\gamma_1^0, \quad (4.51)$$

where $\Lambda^{\pm}(\mathbf{p}_1) = \frac{E_1 \pm H(\mathbf{p}_1)}{2E_1}$ with $H(\mathbf{p}_1) = \gamma_1^0\boldsymbol{\gamma}_1\cdot\mathbf{p}_1 + \gamma_1^0 m_1$. The index 1 and 2 on the Dirac matrices represent the particle that they act on. Since the two

particles never interact we must keep track of which particles spinor space the matrices are a basis for. The Λ^+ and Λ^- can be thought of as operator that project over positive and negative energy states, and as such have respectively poles at positive and negative energies. We write out the integral

$$S(t;\mathbf{p};P) = -\int \frac{dp^0}{2\pi}\left[\frac{\Lambda_1^+}{\eta_1 P^0 + p^0 - E_1 + i\epsilon} + \frac{\Lambda_1^-}{\eta_1 P^0 + p^0 + E_1 - i\epsilon}\right]\gamma_1^0 \times \left[\frac{\Lambda_2^+}{\eta_2 P^0 - p^0 - E_1 + i\epsilon} + \frac{\Lambda_2^-}{\eta_2 P^0 - p^0 + E_1 - i\epsilon}\right]\gamma_1^0 e^{ip^0 t}, \tag{4.52}$$

in terms of the expansion (4.51). We have here used the shorthand notation of $\Lambda_1^+ = \Lambda^\pm(\mathbf{p}_1)$. We identify the poles for each their respective Λ factor

$$\begin{aligned} t>0:\ \Lambda_1^-:\ p^0 &= -\eta_1 P^0 - E_1 + i\epsilon = -\sigma_1, \quad & \Lambda_2^+:\ p^0 &= \eta_2 P^0 - E_2 + i\epsilon = \rho_2, \\ t<0:\ \Lambda_1^+:\ p^0 &= -\eta_1 P^0 + E_1 - i\epsilon = -\rho_1, \quad & \Lambda_2^-:\ p^0 &= \eta_2 P^0 + E_2 - i\epsilon = \sigma_2, \end{aligned} \tag{4.53}$$

allowing for easy identification of poles. When doing the integral we get

$$S(t;\mathbf{p};P) = -i\begin{cases} \frac{-\Lambda_1^+\gamma_1^0\Lambda_2^+\gamma_2^0 e^{i\rho_2 t}}{P^0-E_1-E_2} + \frac{\Lambda_1^-\gamma_1^0\Lambda_2^+\gamma_2^0 e^{-i\sigma_1 t}}{P^0+E_1-E_2} \\ -\frac{\Lambda_1^-\gamma_1^0\Lambda_2^+\gamma_2^0 e^{i\rho_2 t}}{P^0+E_1-E_2} + \frac{\Lambda_1^-\gamma_1^0\Lambda_2^-\gamma_2^0 e^{-i\sigma_1 t}}{P^0+E_1+E_2} & \text{if } t>0 \\ \\ \frac{-\Lambda_1^+\gamma_1^0\Lambda_2^+\gamma_2^0 e^{-i\rho_1 t}}{P^0-E_1-E_2} - \frac{\Lambda_1^+\gamma_1^0\Lambda_2^-\gamma_2^0 e^{-i\rho_1 t}}{P^0-E_1+E_2} \\ +\frac{\Lambda_1^+\gamma_1^0\Lambda_2^-\gamma_2^0 e^{i\sigma_2 t}}{P^0-E_1+E_2} + \frac{\Lambda_1^-\gamma_1^0\Lambda_2^-\gamma_2^0 e^{-i\sigma_2 t}}{P^0+E_1+E_2} & \text{if } t<0 \end{cases}, \tag{4.54}$$

for closing the contour in the lower and upper half plane respectively. We get out both the explicit pole structure and the spin structure

$$S_0(\mathbf{p};P) = i\left(\frac{\Lambda_1^+\gamma_1^0\Lambda_2^+\gamma_2^0}{P^0 - E_1 - E_2} - \frac{\Lambda_1^-\gamma_1^0\Lambda_2^-\gamma_2^0}{P^0 + E_1 + E_2}\right), \tag{4.55}$$

of the reduced propagator in the fully relativistic regime. Going to the non-relativistic regime we look closer at the combinations of Λ in terms of momentum

following the analysis of Iengo [27],

$$\Lambda_1^{\mp}\gamma_1^0\Lambda_2^{\mp}\gamma_2^0 = \frac{(E_1 \mp \gamma_1^0\boldsymbol{\gamma}_1\cdot(\eta_1\mathbf{P}+\mathbf{p}) \mp \gamma_1^0 m_1)\gamma_1^0(E_2 \mp \gamma_2^0\boldsymbol{\gamma}_2\cdot(\eta_2\mathbf{P}-\mathbf{p}) \mp \gamma_2^0 m_2)\gamma_2^0}{4E_1E_2}$$

$$= 1/4\Bigg[\gamma_1^0\gamma_2^0 + \frac{m_1m_2}{E_1E_2} \pm \left(\frac{\gamma_1^0 m_2}{E_2} + \frac{m_1\gamma_2^0}{E_1}\right)$$

$$\mp \left(\frac{\boldsymbol{\gamma}_1\cdot(\eta_1\mathbf{P}+\mathbf{p})\gamma_2^0}{E_1} - \frac{\gamma_1^0\boldsymbol{\gamma}_2\cdot(\eta_2\mathbf{P}-\mathbf{p})}{E_2}\right)$$

$$- \left(\frac{\boldsymbol{\gamma}_1\cdot(\eta_1\mathbf{P}+\mathbf{p})m_2}{E_1E_2} + \frac{\boldsymbol{\gamma}_2\cdot(\eta_2\mathbf{P}-\mathbf{p})m_1}{E_1E_2}\right)$$

$$+ \frac{\boldsymbol{\gamma}_1\cdot(\eta_1\mathbf{P}+\mathbf{p})\boldsymbol{\gamma}_2\cdot(\eta_2\mathbf{P}-\mathbf{p})}{E_1E_2}\Bigg].$$

Terms with a single $\boldsymbol{\gamma}$ will mix small and large component and thus create a higher order term, while γ^0 will neither mix nor change the components and is therefore effectively of order $\sim \mathbb{1}$. To lowest order the energy is the mass of the particle which is why we get

$$\Lambda_1^{\mp}\gamma^0\Lambda_2^{\mp}\gamma^0 \sim \begin{cases} 1 & \text{if} ++ \\ 0 & \text{else} \end{cases}, \tag{4.56}$$

where we include the result for other possible combinations of Λ as well. Since the small component is of higher order in momentum we effectively cut away the half of the matrix γ^0 that acts on the small component, hence $\gamma^0 \sim \mathbb{1}$. This means that we are here finding the equation for the large component in the non-relativistic limit. Since $\gamma^0 \sim \mathbb{1}$, S_0 is diagonal and then commutes with other matrices such as S. Using this commutation in equations (4.49) and (4.50) to commute the S_0^{-1} with S allows us to cancel S with S^{-1} on the left hand side.

In the non-relativistic limit the dominant component of S_0 has the momentum dependence

$$S_0(\mathbf{p}, P) \simeq \frac{-1}{i(P^0 - E_1 - E_2)} = \frac{-1}{i(\mathcal{E} - \frac{\mathbf{p}^2}{2\mu})}, \tag{4.57}$$

where $\mathcal{E}$ is either the energy, for bound or free states respectively as in

$$P^0 = m + \frac{\mathbf{P}^2}{2m} + \mathcal{E}. \tag{4.58}$$

This means that the equations (4.49) and (4.50) now become

$$\left(-\frac{\mathbf{p}^2}{2\mu}+\mathcal{E}_n\right)_{ab;ef}\tilde{\psi}_{n,ef}(\mathbf{p})=\frac{-1}{i}\int\frac{d^3k}{(2\pi)^3}\mathcal{W}_{ab;ef}(|\mathbf{p}-\mathbf{k}|)\tilde{\psi}_{n,ef}(\mathbf{p}), \tag{4.59}$$

$$\left(-\frac{\mathbf{p}^2}{2\mu}+\mathcal{E}_\mathbf{q}\right)_{ab;ef}\tilde{\phi}_{\mathbf{q},ef}(\mathbf{p})=\frac{-1}{i}\int\frac{d^3k}{(2\pi)^3}\mathcal{W}_{ab;ef}(|\mathbf{p}-\mathbf{k}|)\tilde{\phi}_{\mathbf{q},ef}(\mathbf{p}), \tag{4.60}$$

where we have written the factor in front of the integral as $-1/i$ for simple comparison with the factor of equations (2.78) and (2.79) of [29], $-1/i4m\mu^2$. By doing the derivation for fermion fields rather than scalar fields as done by Petraki *et al.* [29] the only difference is this $-1/i$ factor in front of the integral in (4.59) and (4.60). Pertaki *et al.* arrives at a different factor due to the difference in units of a scalar field compared to a fermion field, and a four factor from the difference in degrees of freedom. This difference in degrees of freedom is seen in equation (4.2) of [31] as a factor 4 difference when comparing the coupling constant between fermionic and scalar dark matter for a scalar mediator. We have arrived at the Schrödinger equation, with constant factors corresponding to fermions, in momentum space. By a Fourier transform we get the familiar equation

$$\left[-\frac{\boldsymbol{\Delta}^2}{2\mu}+V(\mathbf{r})\right]\psi_n(\mathbf{r})=\mathcal{E}_n\psi_n(\mathbf{r}), \tag{4.61}$$

$$\left[-\frac{\boldsymbol{\Delta}^2}{2\mu}+V(\mathbf{r})\right]\phi_\mathbf{q}(\mathbf{r})=\mathcal{E}_\mathbf{q}\phi_\mathbf{q}(\mathbf{r}), \tag{4.62}$$

with the potential defined as

$$V(\mathbf{r})\equiv\frac{-1}{i}\int\frac{d^3k}{(2\pi)^3}\mathcal{W}(\mathbf{k})e^{i\mathbf{k}\cdot\mathbf{r}}. \tag{4.63}$$

Through eqs. (4.42)-(4.45) we have been able to relate the relativistic quantities of the Bethe-Salpeter wavefunctions with the Schrödinger wavefunctions in the non-relativistic limit. This is important, as we now have the tools to solve more complicated amplitudes by first decomposing them to the B-S wavefunctions and then be able to consistently solve in the non-relativistic limit. This is the approach we will use to derive cross sections for bound state formation and annihilation processes.

Finally one could to look at the normalizations of the wavefunctions in the non-relativistic limit. As the details of the analysis of the limit on these normalizations hold no significance for the further calculations, we will omit them

[2]Note that we here drop the subscript **Q** as there is no longer any explicit dependence on it.

here but the details can be found in section 2.7 of [29]. The result is that the Schrödinger wavefunctions are normalized exactly as one would expect from quantum mechanics. This would have had to have been the case for the Schrödinger wavefunctions, but it is nice to see that the method is consistent in deriving conditions from the Dyson-Schwinger equation (4.9).

Chapter 5

General cross-section calculation

Having established a connection between relativistic and non-relativistic two-particle wavefunctions through the Bethe-Salpeter equation we will now turn towards calculating cross sections. The goal is to decompose the more intricate diagrammatic processes of bound state formation and annihilation in term of the four point correlation function (4.1) and thereby into the relativistic two-particle wavefunctions. This will allow us to calculate the cross section in the non-relativistic limit through the relations (4.42)-(4.45) and the Schrödinger equations (4.61) and (4.62). The method of deriving the cross sections is that of Petraki *et al.* [29] with careful note of the changes when considering fermionic dark matter.

5.1 Bound state formation

The radiative bound state formation happens through a five point correlation function

$$G^{(5)}_{ab;cd}(X_\varphi, x_1, x_2; y_1, y_2) \equiv \langle \Omega | T\varphi(X_\varphi)\chi_{1,a}(x_1)\bar{\chi}_{2,b}(x_2)\chi_{1,c}(y_1)\bar{\chi}_{2,d}(y_2)|\Omega\rangle \,, \quad (5.1)$$

where the field φ gives the mediating particle of the interaction. A bound state is defined by its mass $M = m_1 + m_2 + \mathcal{E} < m_1 + m_2$, and to go from two free particle into a bound state it therefore must emit some energy through a radiative process, hence $G^{(5)}$. Our goal is then to find the **S**-matrix element of the process

$$_{\text{out}}\left\langle \mathcal{B}_{\mathbf{P},n}; \varphi_{\mathbf{P}_\varphi} | \mathcal{U}_{\mathbf{K},\mathbf{k}} \right\rangle_{\text{in}} = \left\langle \mathcal{B}_{\mathbf{P},n}; \varphi_{\mathbf{P}_\varphi} | \mathbf{S} | \mathcal{U}_{\mathbf{K},\mathbf{k}} \right\rangle . \quad (5.2)$$

Attaining the **S**-matrix element will be done through an LSZ reduction and by the decomposition into four point correlation functions, $G^{(4)}$. We can diagrammatically decompose the five point function (5.1) into a fully amputated hard scattering part $\mathcal{A}^{(5)}$, the four point correlation function $G^{(4)}$ and the full propagator for the force mediator as shown in figure 5.1.

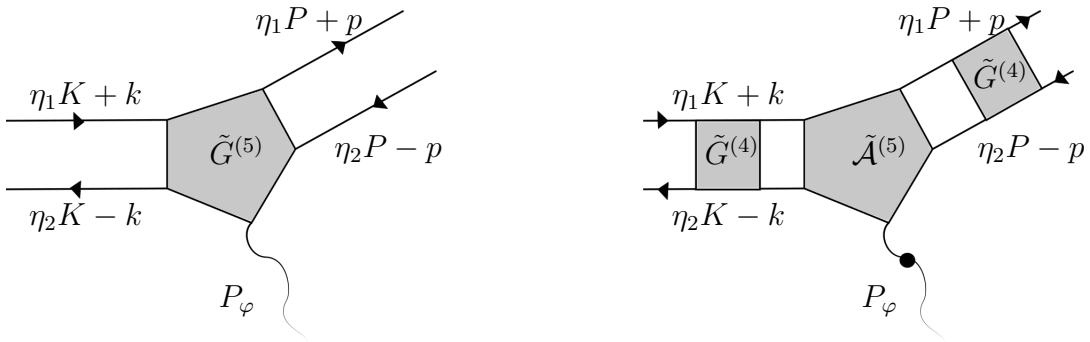

Figure 5.1: The expansion of the five point correlation function $\tilde{G}^{(5)}$ in terms of four point correlation functions $\tilde{G}^{(4)}$, the full propagator of the force mediator, and a fully amputated, hard scattering five point function $\tilde{\mathcal{A}}^{(5)}$.

Using the established relative coordinates (3.5)-(3.6) and the decomposition in figure 5.1, the five point correlation function in momentum space can be written

$$\begin{aligned}\tilde{G}^{(5)}_{ab;cd}(P_\varphi, \eta_1 P + p, \eta_2 P - p; \eta_1 K + k, \eta_2 K - k) = \\ \tilde{S}_\varphi(P_\varphi) \int \frac{d^4p'}{(2\pi)^4} \frac{d^4k'}{(2\pi)^4} \tilde{G}^{(4)}_{ab;ef}(p, p'; P)(2\pi)^4 \delta^4(K - P - P_\varphi) i \\ \times \mathcal{A}^{(5)}_{ef;gh}(P_\varphi, \eta_1 P + p', \eta_2 P - p'; \eta_1 K + k', \eta_2 K - k') \tilde{G}^{(4)}_{gh;cd}(k', k; K) \quad (5.3)\end{aligned}$$

where

$$\tilde{S}_\varphi(P_\varphi) = \frac{i Z_\varphi}{P_\varphi^2 - m_\varphi^2 + i\epsilon} \quad (5.4)$$

is the φ field propagator with Z_φ being the field strength renormalization factor for φ. Extracting the **S**-matrix element in the limit

$$P^0_\varphi \to \omega_\varphi(\mathbf{P}_\varphi), \quad P^0 \to \omega_{\mathbf{P},n}, \quad K^0 \to \omega_{\mathbf{K},\mathbf{k}}, \quad (5.5)$$

using the LSZ reduction formula for the left hand side of (5.3) we get

$$\begin{aligned}\int d^4X_\varphi d^4X d^4Y d^4x d^4y e^{i(P_\varphi X_\varphi + PX - KY)} e^{i(px - qy)} \\ \times G^{(5)}_{ab;cd}(X_\varphi, X + \eta_2 x, X - \eta_1 x; Y + \eta_2 y, Y - \eta_1 y) \\ \sim \left[\frac{i\sqrt{Z_\varphi(\mathbf{P}_\varphi)}}{2\omega_\varphi(\mathbf{P}_\varphi)(P^0_\varphi - \omega_\varphi(\mathbf{P}_\varphi) + i\epsilon)}\right] \left[\frac{i\tilde{\Psi}_{\mathbf{P},n,ab}(p)}{2\omega_{\mathbf{P},n}(P^0 - \omega_{\mathbf{P},n} + i\epsilon)}\right] \times \\ \left\langle \mathcal{B}_{\mathbf{P},n}; \varphi_{\mathbf{P}_\varphi} | \mathbf{S} | \mathcal{U}_{\mathbf{K},\mathbf{k}} \right\rangle \int \frac{d^3k'}{(2\pi)^3 2\varepsilon_{\mathbf{K}.\mathbf{k}}} \frac{i\tilde{\Phi}^\star_{\mathbf{K}.\mathbf{k}',cd}(q)}{2\omega_{\mathbf{K}.\mathbf{k}'}(K^0 - \omega_{\mathbf{K}.\mathbf{k}'} + i\epsilon)}, \quad (5.6)\end{aligned}$$

where we have used the definitions of the relativistic two-particle wavefunction (4.4) and (4.7). The LSZ reduction formula is based on the same expansion as

the Källén-Lehmann spectral representation (3.1). The LSZ reduction into one particle states leaves the **S**-matrix element as a scalar, while the two-particle states have a matrix structure. Taking the same limits for equations (4.14) and (4.16) and inserting them into the right hand side of (5.3) we get

$$\begin{aligned}\tilde{G}^{(5)}_{ab;cd}&(P_\varphi,\eta_1 P+p,\eta_2 P-p;\eta_1 K+q,\eta_2 K-q)\sim\\ &\frac{iZ_\varphi(\mathbf{P}_\varphi)}{P_\varphi^2-m_\varphi^2+i\epsilon}\int\frac{d^4p'}{(2\pi)^4}\frac{d^4q'}{(2\pi)^4}\frac{i\Psi_{\mathbf{P},n,ab}(p)\Psi^\star_{\mathbf{P},n,ef}(p')}{2\omega_{\mathbf{P},n}(P^0-\omega_{\mathbf{P},n}+i\epsilon)}\\ &\times(2\pi)^4\delta^4(K-P-P_\varphi)i\mathcal{A}^{(5)}_{ef;gh}(P_\varphi,\eta_1 P+p',\eta_2 P-p';\eta_1 K+q',\eta_2 K-q')\\ &\times\int\frac{d^3k'}{(2\pi)^3}\frac{i\Phi_{\mathbf{K},\mathbf{k}',gh}(q')\Phi^\star_{\mathbf{K},\mathbf{k}',cd}(q)}{2\omega_{\mathbf{K},\mathbf{k}'}2\varepsilon_{\mathbf{K},\mathbf{k}'}(K^0-\omega_{\mathbf{K},\mathbf{k}'}+i\epsilon)},\end{aligned}\tag{5.7}$$

where the ordering becomes fixed by the decomposition done as shown in figure 5.1. Equations (5.7) and (5.6) are now equal at the poles (5.5). The mediator particle pole and renormalization factor we can easily cancel, and to cancel the $\Psi_{\mathbf{P},n,a,b}(p)$ factor we notice that by multiplying both sides by $\Psi^{-1}_{\mathbf{P},n,ab}(p)$ from the left hand side we have no problems with commutations. Since the Ψs have spin structure that is independent of the surrounding products we can exactly cancel the terms on both sides. This gives us the equation

$$\begin{aligned}&\sqrt{Z_\varphi(\mathbf{P}_\varphi)}\int\frac{d^4p'}{(2\pi)^4}\frac{d^4q'}{(2\pi)^4}\Psi^\star_{\mathbf{P},n,ef}(p')(2\pi)^4\delta^4(K-P-P_\varphi)\\ &\quad\times i\mathcal{A}^{(5)}_{ef;gh}(P_\varphi,\eta_1 P+p',\eta_2 P-p';\eta_1 K+q',\eta_2 K-q')\\ &\quad\times\int\frac{d^3k'}{(2\pi)^3}\frac{\Phi_{\mathbf{K},\mathbf{k}',gh}(q')\Phi^\star_{\mathbf{K},\mathbf{k}',cd}(q)}{2\omega_{\mathbf{K},\mathbf{k}',c,d}2\varepsilon_{\mathbf{K},\mathbf{k}'}(K^0-\omega_{\mathbf{K},\mathbf{k}'}+i\epsilon)}\\ &\sim\left\langle\mathcal{B}_{\mathbf{P},n};\varphi_{\mathbf{P}_\varphi}|\mathbf{S}|\mathcal{U}_{\mathbf{K},\mathbf{k}}\right\rangle\int\frac{d^3k'}{(2\pi)^3 2\varepsilon_{\mathbf{K}.\mathbf{k}}}\frac{i\tilde{\Phi}^\star_{\mathbf{K},\mathbf{k}',cd}(q)}{2\omega_{\mathbf{K}.\mathbf{k}'}(K^0-\omega_{\mathbf{K}.\mathbf{k}'}+i\epsilon)},\end{aligned}\tag{5.8}$$

where we are left with the $\Phi^\star_{\mathbf{K},\mathbf{k}',c,d}(q)$ term to cancel. Because of the integrals over k' on both sides being independent of each other we cannot simply cancel them by multiplying with an inverse. Instead we make use of the normalization relation (4.40). By multiplying both sides of (5.8) from the right by $\tilde{N}_{\mathbf{k},cd;ij}(q,q'';\mathbf{K})\tilde{\Phi}_{\mathbf{K},\mathbf{k},ij}(q'')$ and integrating over q and q'', letting the normalization fix $\mathbf{k}'$ to obtain

$$\begin{aligned}\left\langle\mathcal{B}_{\mathbf{P},n};\varphi_{\mathbf{P}_\varphi}|\mathbf{S}|\mathcal{U}_{\mathbf{K},\mathbf{k}}\right\rangle&=\sqrt{Z_\varphi(\mathbf{P}_\varphi)}\int\frac{d^4p}{(2\pi)^4}\frac{d^4q}{(2\pi)^4}\Psi^\star_{\mathbf{P},n,ef}(p)(2\pi)^4\delta^4(K-P-P_\varphi)\\ &\times i\mathcal{A}^{(5)}_{ef;gh}(P_\varphi,\eta_1 P+p,\eta_2 P-p;\eta_1 K+q,\eta_2 K-q)\Phi_{\mathbf{K},\mathbf{k},gh}(q).\end{aligned}\tag{5.9}$$

We can then write the **S**-matrix element in term of an amplitude

$$\left\langle\mathcal{B}_{\mathbf{P},n};\varphi_{\mathbf{P}_\varphi}|\mathbf{S}|\mathcal{U}_{\mathbf{K},\mathbf{k}}\right\rangle=(2\pi)^4\delta^4(K-P-P_\varphi)i\mathcal{M}_{\mathbf{k}\to n},\tag{5.10}$$

where

$$\mathcal{M}_{\mathbf{k}\to n} = \sqrt{Z_\varphi(\mathbf{P}_\varphi)} \int \frac{d^4p}{(2\pi)^4}\frac{d^4q}{(2\pi)^4}\Psi^\star_{\mathbf{P},n,ef}(p) \times \mathcal{A}^{(5)}_{ef;gh}(P_\varphi, \eta_1 P + p, \eta_2 P - p; \eta_1 K + q, \eta_2 K - q)\Phi_{\mathbf{K},\mathbf{k},gh}(q). \tag{5.11}$$

Next we look closer at the hard scattering five point function $\mathcal{A}^{(5)}$. $\mathcal{A}^{(5)}$ is the sum of all connected diagrams and is fully amputated such that

$$i\mathcal{C}^{(5)}_{ab;cd}(P_\varphi, p_1, p_2; k_1, k_2) = \tilde{S}_{1,ae}(k_1)\tilde{S}_{2,bf}(k_1) i\mathcal{A}^{(5)}_{ef;gh}(P_\varphi, p_1, p_2; k_1, k_2)\tilde{S}_\varphi(P_\varphi)\tilde{S}_{1,gc}(p_1)\tilde{S}_{2,hd}(p_2), \tag{5.12}$$

where $\mathcal{C}^{(5)}$ is the sum of all connected diagrams. This then excludes all vacuum

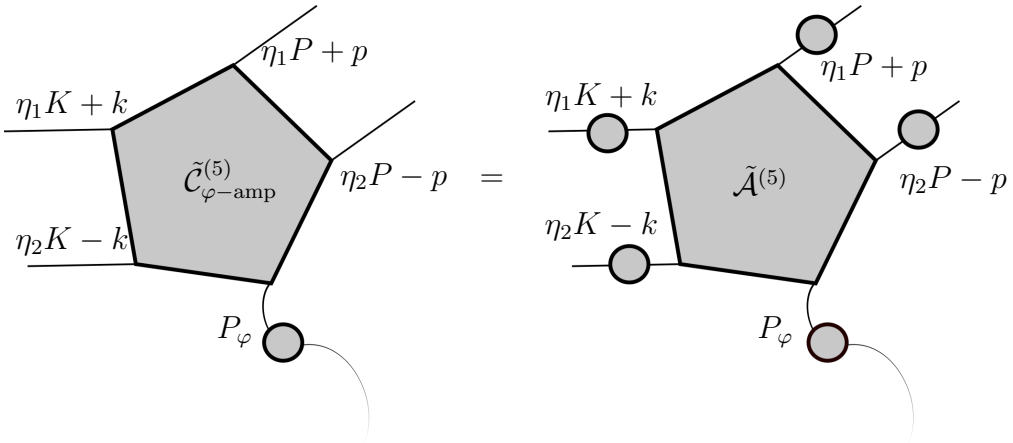

Figure 5.2: Showing diagrammatically the relation between the fully amputated, connected, hard scattering five point correlation function $\tilde{\mathcal{A}}^{(5)}$ and the only φ amputated, connected, hard scattering five point correlation function $\tilde{\mathcal{C}}^{(5)}_{\varphi-\text{amp}}$ relation of equation (5.13).

bubble diagrams but includes non fully connected diagrams as is the convention for the LSZ reduction formalism. We can also define a middle ground between these with only the force carrier amputated

$$i\mathcal{C}^{(5)}_{ab;cd}(P_\varphi, p_1, p_2; k_1, k_2) = i\mathcal{C}^{(5)}_{\varphi-\text{amp},ab;cd}(P_\varphi, p_1, p_2; k_1, k_2)\tilde{S}_\varphi(P_\varphi), \tag{5.13}$$

with the ordering as according to figure 5.2. This allows us to rewrite the hard scattering five point correlation function in terms of this semi-amputated correlation function

$$i\mathcal{A}^{(5)}_{ab;cd}(P_\varphi, p_1, p_2; k_1, k_2) = iS^{-1}_{ab;ef}(p; P)\mathcal{C}^{(5)}_{\varphi-\text{amp},ef;gh}(P_\varphi, p_1, p_2; k_1, k_2)S^{-1}_{gh;cd}(k; K) \tag{5.14}$$

where $S(p;P)$ and $S(k;K)$ are defined by (4.10). By substituting eq. (5.14) into the amplitude (5.11) we get

$$\mathcal{M}_{\mathbf{k}\to n} = \sqrt{Z_\varphi(\mathbf{P}_\varphi)} \int \frac{d^4p}{(2\pi)^4}\frac{d^4q}{(2\pi)^4}\Psi^\star_{\mathbf{P},n,ab}(p)S^{-1}_{ab;cd}(p;P) \\ \times \mathcal{C}^{(5)}_{\varphi-\mathrm{amp},cd;ef}(P_\varphi,\eta_1 P+p,\eta_2 P-p;\eta_1 K+q,\eta_2 K-q)S^{-1}_{ef;gh}(q;K)\Phi_{\mathbf{K},\mathbf{k},gh}(q). \tag{5.15}$$

where the right most product of wavefunction and propagator is well known in the non-relativistic limit from (4.48). The left most combination however, has the wrong ordering according to (4.48). Remember that there is an freedom in the ordering of terms in the Dyson-Schwinger equation (4.35), see figure 4.2. This means that there is also an freedom in the ordering of term in the eigenvalue equations (4.24) and (4.25), i.e. one can also write

$$\int \frac{d^4k}{(2\pi)^4} C_{n,ab}(k;Q)A_{ab;cd}(k,p;Q) = c_n(Q)C_{n,cd}(p;Q), \tag{5.16}$$

and the Bethe-Salpeter equation will become

$$\tilde{\Psi}_{\mathbf{Q},n,cd}(p) = \int \frac{d^4k}{(2\pi)^4}\tilde{\Psi}_{\mathbf{Q},n,ab}(k)\tilde{W}_{ab;ef}(k,p;Q) \quad S_{ef;cd}(p;Q), \tag{5.17}$$

$$\tilde{\Phi}_{\mathbf{Q},\mathbf{q},cd}(p) = \int \frac{d^4k}{(2\pi)^4}\tilde{\Phi}_{\mathbf{Q},\mathbf{q},ab}(k)\tilde{W}_{ab;ef}(k,p;Q) \quad S_{ef;cd}(p;Q). \tag{5.18}$$

To reduce to the Schrödinger equation we define the non-relativistic wavefunction with a different ordering of terms

$$\tilde{\psi}_{\mathbf{Q},n,cd}(\mathbf{p}) \equiv \sqrt{2\mathcal{N}_{\mathbf{Q}}(\mathbf{p})}\tilde{\Psi}_{\mathbf{Q},n,ab}(p)S_{0,ab;ef}(\mathbf{p};Q)S^{-1}_{ef;cd}(p;Q), \tag{5.19}$$

$$\tilde{\phi}_{\mathbf{Q},\mathbf{q},cd}(\mathbf{p}) \equiv \sqrt{\frac{2\mathcal{N}_{\mathbf{Q}}(\mathbf{p})}{2\varepsilon_{\mathbf{Q},\mathbf{q}}}}\tilde{\Phi}_{\mathbf{Q},\mathbf{q},ab}(p)S_{0,ab;ef}(\mathbf{p};Q)S^{-1}_{ef;cd}(p;Q), \tag{5.20}$$

which means that the equation (4.48) changes its ordering

$$\tilde{\Psi}_{\mathbf{Q},\mathbf{q},ab}(p)S^{-1}_{ab;cd}(p;Q) = \frac{\tilde{\psi}_{\mathbf{Q},n,ab}(\mathbf{p})S_{ab;ef}(p;Q)S^{-1}_{0,ef;gh}(\mathbf{p};Q)S^{-1}_{gh;cd}(p;Q)}{\sqrt{2\mathcal{N}_{\mathbf{Q}}(\mathbf{p})}}, \tag{5.21}$$

such that it matches the left most term in equation (5.15). We have established that S_0 is diagonal to leading order and therefore commutes with S meaning we can simplify the expression

$$\tilde{\Psi}_{\mathbf{Q},\mathbf{q},ab}(p)S^{-1}_{ab;cd}(p;Q) = \frac{\tilde{\psi}_{\mathbf{Q},n,ab}(\mathbf{p})S^{-1}_{0,ab;cd}(\mathbf{p};Q)}{\sqrt{2\mathcal{N}_{\mathbf{Q}}(\mathbf{p})}}. \tag{5.22}$$

Because of the freedom in factorization of the last term in the Dyson-Schwinger equation we get two equations to solve the for the same quantity Ψ. Further, these two equivalent equations reduce to the same non-relativistic Schrödinger equation, through slightly different definitions of the Schrödinger wavefunctions. They are however solutions to the same equation so they must be the same function. We can therefore insert both (4.48) and (5.21) into (5.15) to obtain

$$\mathcal{M}_{\mathbf{k}\to n} \simeq \sqrt{2\varepsilon_{\mathbf{K},\mathbf{k}}} \int \frac{d^3p}{(2\pi)^3}\frac{d^3q}{(2\pi)^3}\frac{\tilde{\psi}_{n,ab}(\mathbf{p})\mathcal{M}_{\mathrm{trans},ab;cd}(\mathbf{q};\mathbf{p})\tilde{\phi}_{\mathbf{k},cd}(\mathbf{q})}{\sqrt{2\mathcal{N}_{\mathbf{P}}(\mathbf{p})}\sqrt{2\mathcal{N}_{\mathbf{K}}(\mathbf{q})}}, \tag{5.23}$$

with

$$\begin{aligned}\mathcal{M}_{\mathrm{trans},ab;cd}(\mathbf{q};\mathbf{p}) \equiv \int \frac{dp^0}{2\pi}\frac{dq^0}{2\pi} S^{-1}_{0,ab;ef}(\mathbf{p};Q) \\ \times \mathcal{C}^{(5)}_{\varphi-\mathrm{amp},ef;gh}(P_\varphi, \eta_1 P + p, \eta_2 P - p; \eta_1 K + q, \eta_2 K - q) S^{-1}_{0,gh;cd}(\mathbf{q};K)\end{aligned} \tag{5.24}$$

defined for later convenience. We have also here set an energy scale such that $Z_\varphi(\mathbf{P}_\varphi) \simeq 1$ to lowest order.

With the amplitude of the process derived all that remains is to insert it into the differential cross-section for the $2-2$ process

$$v_{\mathrm{rel}}\frac{d\sigma^{nlm}_{\mathrm{BSF}}}{d\Omega} = \frac{|\mathbf{P}_\varphi|}{64\pi^2 m^2 \mu}|\mathcal{M}_{\mathbf{k}\to nlm}|^2. \tag{5.25}$$

5.2 Annihilation

Like with the bound state formation cross section, we want to decompose the annihilation amplitude into the constituents of a four point correlation function $G^{(4)}$ and a hard scattering amplitude, see figure 5.3. The process in figure 5.3 describes what is called the Sommerfeld effect [23]. For relativistic particles the zeroth order term of $\tilde{G}^{(4)}$ is a no vertex diagram and does not contribute. In the non-relativistic regime however we get an infinite number of vertices as discussed in chapter 3. The physics interpretation is that when two particles are non-relativistic they are susceptible to the weaker long range effects of the effective potential, and they will either be slowly attracted together or repulsed apart. This means an effective enlargement or suppression of the cross-section in this regime.

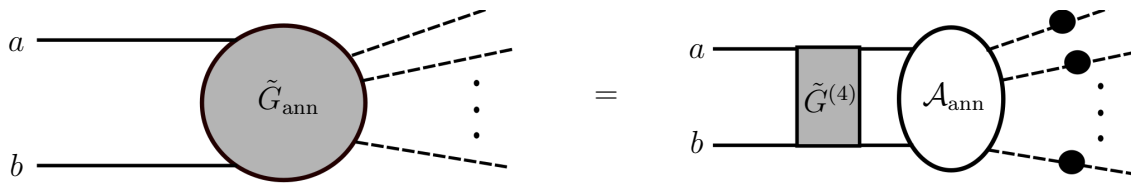

Figure 5.3: Diagrammatic representation of an annihilation amplitude into final state particles that is decomposed into a four point correlation function in momentum space $\tilde{G}^{(4)}$ and a hard scattering amplitude $\mathcal{A}_{\rm ann}$. This decomposition is what constitutes the Sommerfeld effect [23].

The amplitude $\tilde{G}_{\rm ann}$ in figure 5.3 describes a $2 \to N$ process where two dark matter particles annihilate into final state particles. This $N+2$ correlation function is then

$$\tilde{G}^{\rm ann}_{ab}(p_1,...,p_N;k_1,k_2) = \prod_{j=1}^{N}\int d^4x_j e^{ip_jx_j}\int d^4y_1 d^4y_2 e^{-i(k_1y_1+k_2y_2)} \times \langle\Omega|Tf(x_1)...f(x_N)\bar{\chi}_{1,a}(y_1)\chi_{2,b}(y_2)|\Omega\rangle\,, \tag{5.26}$$

where $f(x_j)$ is the field of the final state particle, here assumed to be non-fermionic. Given the decomposition shown in figure 5.3 we can also write the annihilation amplitude as

$$\tilde{G}^{\rm ann}_{ab}(p_1,...,p_N;\eta_1K+k,\eta_2K-k) = \prod_{j=1}^{N}\tilde{S}_{f_j}(p_j)(2\pi)^4\delta^4\left(K-\sum_{j=1}^{N}p_j\right) \int\frac{d^4k'}{(2\pi)^4}i\mathcal{A}^{\rm ann}_{ef}(p_1,...,p_N;\eta_1K+k',\eta_2K-k')\tilde{G}^{(4)}_{ef;ab}(k',k;K), \tag{5.27}$$

where $\mathcal{A}^{\rm ann}$ is the sum of all connected and amputated diagrams contributing to the annihilation process, and $\tilde{S}_{f_j}(p_j)$ is the propagator of the final state particles in momentum space. Unlike the amplitude $\mathcal{A}^{(5)}$ that appears in the bound state formation calculation of last chapter, figure 5.1, this amplitude has to be fully connected for it to be an annihilation process.

We want to extract the **S**-matrix element of the process

$$_{\rm out}\langle f_1f_2...f_N|\mathcal{U}_{\mathbf{K},\mathbf{k}}\rangle_{\rm in} = \langle f_1f_2...f_N|\mathbf{S}|\mathcal{U}_{\mathbf{K},\mathbf{k}}\rangle\,, \tag{5.28}$$

and will do so as for the bound state formation. Analyzing the pole structure of

(5.26) in the limits $p_j^0 \to \omega_j(\mathbf{p}_j)$ and $K^0 \to \omega_{\mathbf{K},\mathbf{k}}$ we derive

$$\tilde{G}^{\rm ann}_{ab} \sim \prod_{j=1}^{N}\left(\frac{i\sqrt{Z_j(\mathbf{p}_j)}}{2\omega_j(\mathbf{p}_j)\left(p_j^0-\omega_j(\mathbf{p}_j)+i\epsilon\right)}\right) \langle f_1 f_2 ... f_N|\mathbf{S}|\mathcal{U}_{\mathbf{K},\mathbf{k}}\rangle \int \frac{d^3k'}{(2\pi)^3 2\varepsilon_{\mathbf{K}.\mathbf{k}}} \frac{i\tilde{\Phi}^{\star}_{\mathbf{K},\mathbf{k}',ab}(q)}{2\omega_{\mathbf{K}.\mathbf{k}'}(K^0-\omega_{\mathbf{K}.\mathbf{k}'}+i\epsilon)}, \quad (5.29)$$

where $\sqrt{Z_j(\mathbf{p}_j)} = \langle\Omega|f(0)|f_j\rangle$ is the renormalization factor for the fields f_j. In the same limits we can also analyze the pole structure of (5.27) by inserting the found pole structure of $G^{(4)}_{\mathcal{U}}$ (4.16)

$$\tilde{G}^{\rm ann}_{ab} \sim \prod_{j=1}^{N}\frac{iZ_j(\mathbf{p}_j)}{p_j^2-m_j^2+i\epsilon}\int\frac{d^4q'}{(2\pi)^4}\,(2\pi)^4\delta^4\left(K-\sum_{j=1}^{N}p_j\right) i\mathcal{A}^{\rm ann}_{ef}(p_1,...,p_N;\eta_1K+q',\eta_2K-q')\int\frac{d^3k'}{(2\pi)^3}\frac{i\Phi_{\mathbf{K},\mathbf{k}',ef}(q')\Phi^{\star}_{\mathbf{K},\mathbf{k}',ab}(q)}{2\omega_{\mathbf{K},\mathbf{k}'}2\varepsilon_{\mathbf{K},\mathbf{k}'}(K^0-\omega_{\mathbf{K},\mathbf{k}'}+i\epsilon)}. \quad (5.30)$$

As before we cancel terms and multiply both sides of (5.8) from the right by $\tilde{N}_{\mathbf{k},ab;ij}(q,q'';\mathbf{K})\tilde{\Phi}_{\mathbf{K},\mathbf{k},ij}(q'')$ and integrate over q and q'' to use the normalization condition (4.40)

$$\langle f_1 f_2 ... f_N|\mathbf{S}|\mathcal{U}_{\mathbf{K},\mathbf{k}}\rangle = \prod_{j=1}^{N}\sqrt{Z_j(\mathbf{p}_j)}\int\frac{d^4q}{(2\pi)^4}\,(2\pi)^4\delta^4\left(K-\sum_{j=1}^{N}p_j\right) \times i\mathcal{A}^{\rm ann}_{ab}(p_1,...,p_N;\eta_1K+q,\eta_2K-q)\Phi_{\mathbf{K},\mathbf{k},ab}(q). \quad (5.31)$$

The **S**-matrix element is related to the amplitude of the process through

$$\langle f_1 f_2 ... f_N|\mathbf{S}|\mathcal{U}_{\mathbf{K},\mathbf{k}}\rangle = (2\pi)^4\delta^4\left(K-\sum_{j=1}^{N}p_j\right) i\mathcal{M}_{\rm ann} \quad (5.32)$$

with

$$\mathcal{M}^{\rm ann} = \prod_{j=1}^{N}\sqrt{Z_j(\mathbf{p}_j)}\int\frac{d^4q}{(2\pi)^4}\mathcal{A}^{\rm ann}_{ab}(p_1,...,p_N;\eta_1K+q,\eta_2K-q)\Phi_{\mathbf{K},\mathbf{k},ab}(q). \quad (5.33)$$

By setting the momentum scale such that $\sqrt{Z_j(\mathbf{p}_j)} = 1$ and using the relation

(4.44) we can derive the amplitude in the non-relativistic limit

$$\mathcal{M}^{\text{ann}} \simeq \sqrt{2\varepsilon_{\mathbf{K},\mathbf{k}}} \int \frac{d^3q}{(2\pi)^2} \frac{1}{\sqrt{2\mathcal{N}_{\mathbf{Q}}(\mathbf{p})}} \times \int \frac{dq^0}{2\pi} \mathcal{A}^{\text{ann}}_{ab}(p_1, ..., p_N; \eta_1 K + q, \eta_2 K - q) S^{-1}_{0,ab;ef}(\mathbf{q}; K) S_{ef;gh}(q; K) \tilde{\phi}_{\mathbf{k},gh}(\mathbf{q}). \tag{5.34}$$

Unlike for bound state formation, the hard process is here fully connected. For a non-fully connected diagram, at least one leg will be off-shell, while for fully connected diagrams all legs will be on-shell. Since this process is fully connected we can use the on-shell approximation. If $\mathcal{A}_{\text{ann}}$ does not have any singularities in q^0 then the propagator $S(q; K)$ forces the evaluation of $\mathcal{A}_{\text{ann}}$ at its poles under the integration over q^0. As seen in the relation (4.53) the propagator has two poles; one in the upper and one in the lower q^0 complex plane. Of these two poles there is one physical pole that is on-shell and one unphysical pole where the other particles energy becomes negative. In the non-relativistic regime we expect the particles to be on-shell and so, by closing the contour in the lower half plane we select the physical pole

$$q^0 = -\eta_1 K^0 + E_1(\mathbf{q}; \mathbf{K}) - i\epsilon. \tag{5.35}$$

By fixing this value the energies of the particles χ_1, χ_2 becomes a function of $\mathbf{q}$, $\mathbf{K}$, and the quantum number $\mathbf{k}$. Inserting equations (3.9), (3.10), and (4.58) into (5.35) and using the fact that we have required the limit $K^0 = \omega_{\mathbf{K},\mathbf{k}}$ to derive

$$q_1^0 = E_1(\mathbf{q}; \mathbf{K}), \qquad q_2^0 = \omega_{\mathbf{K},\mathbf{k}} - E_1(\mathbf{q}; \mathbf{K}) \simeq E_2(\mathbf{q}; \mathbf{K}) + \mathcal{E}_{\mathbf{k}} - \frac{\mathbf{q}^2}{2\mu}. \tag{5.36}$$

What we find is that the χ_2 particle is off-shell by a factor $\mathcal{E}_{\mathbf{k}} - \frac{\mathbf{q}^2}{2\mu}$. However, in the non-relativistic limit the energy $\mathcal{E}_{\mathbf{k}} \approx \frac{\langle \mathbf{q}^2 \rangle}{2\mu}$ is the average kinetic energy. Therefore the amplitude $\mathcal{A}_{\text{ann}}$ may be evaluated on-shell.

This means that when doing the integral over q^0 we impose the on-shell condition on $\mathcal{A}_{\text{ann}}$ and $S \to S_0$. With this the amplitude for the annihilation process becomes

$$\mathcal{M}^{\text{ann}} \simeq \int \frac{d^3q}{(2\pi)^3} \mathcal{A}^{\text{ann}}_{ab}(\mathbf{p}_1, ..., \mathbf{p}_N; \eta_1 \mathbf{K} + \mathbf{q}, \eta_2 \mathbf{K} - \mathbf{q}) \tilde{\phi}_{\mathbf{k},ab}(\mathbf{q}), \tag{5.37}$$

where we have used the zeroth order approximations $\mathcal{N} \simeq \mu$ and $\varepsilon \simeq \mu$ to stay consistent with the on-shell approximation.

It is often useful to expand the amplitude into partial waves, i.e. Legendre polynomials

$$\mathcal{M}(\Omega) = \sum_l \left(\frac{2l+1}{4\pi}\right) \mathcal{M}_l P_l(\cos\theta), \tag{5.38}$$

where $d\Omega = \sin\theta\, d\theta d\varphi$ is the solid angle, $P_l(\cos\theta)$ are the Legendre polynomials, and

$$\mathcal{M}_l = \int d\Omega P_l(\cos\theta)\mathcal{M}(\Omega). \tag{5.39}$$

With this expansion we can then decompose the cross-section into partial waves as well

$$\sigma = \sum_l \sigma_l, \tag{5.40}$$

where

$$\sigma_l \sim \frac{2l+1}{4\pi}|\mathcal{M}_l|^2, \tag{5.41}$$

is the l dependence of the cross-section originating from (5.38). This decomposition allows us to put a bound on the different partial wave contributions through unitarity for the inelastic cross-section [41]

$$\sigma_{\text{inel},l} \leq \frac{(2l+1)\pi}{\mu^2 v_{\text{rel}}^2}. \tag{5.42}$$

For massless scalar and vector boson models, this can be used to set an upper bound on the coupling $\alpha_{\text{upper}} \approx 0.54$ [29] and similar restrictions from further analysis congruent with thermal production [26].

For annihilation into two final-state particles in the CM frame, $\mathbf{K} = 0$, the momenta of the final-state particles will be $|\mathbf{p}_1| = |\mathbf{p}_2| = |\mathbf{p}|$ where $|\mathbf{p}| \simeq K^0/2 = (m + \mathcal{E}_{\mathbf{k}})/2 \simeq m/2$ to zeroth order. This means we can define the angles in (5.38) and (5.39) in terms of the momenta $\mathbf{p}$

$$\Omega \to \Omega_{\mathbf{p}} \text{ and } \theta \to \theta_{\mathbf{p}}. \tag{5.43}$$

The annihilation cross-section times the relative velocity are then

$$\sigma_{\text{ann}} v_{\text{rel}} = \frac{f_s}{128\pi^2 m\mu} \int |\mathcal{M}_{\text{ann}}(\Omega_{\mathbf{p}})|^2 d\Omega_{\mathbf{p}} = \frac{f_s}{128\pi^2 m\mu} \sum_l \frac{2l+1}{4\pi} |\mathcal{M}_{\text{ann},l}|^2 \tag{5.44}$$

where f_s is a multiplicity factor that is $1/2$ for identical final state particles and 1 for non-identical. Next we want to express the annihilation amplitude $\mathcal{A}_{\text{ann}}$ in partial waves as follows

$$\mathcal{A}_{\text{ann}}(\mathbf{q}, -\mathbf{q}; \mathbf{p}, -\mathbf{p}) = \sum_{l=0}^{\infty} \frac{\tilde{a}_l}{(m\mu)^l} |\mathbf{p}|^l |\mathbf{q}|^l P_l(\cos\theta_{\mathbf{q},\mathbf{p}}) \tag{5.45}$$

where $\theta_{\mathbf{q},\mathbf{p}}$ refers to the angle between the vector $\mathbf{q}$ and $\mathbf{p}$. The expansion coefficient $\tilde{a}_l$ can depend on $\mathbf{q}$ and can be expanded in the non-relativistic regime as

$$\tilde{a}_l(\mathbf{q}) \simeq a_l + \mathcal{F}_l(\mathbf{q}^2, \boldsymbol{\epsilon}_A \cdot \mathbf{q}), \tag{5.46}$$

with $\boldsymbol{\epsilon}_A$ being the polarization vectors if the final-states are vector bosons, and $\mathcal{F}_l$ is a polynomial function that vanishes at $\mathbf{q} = 0$. This general form of the expansion coefficient comes from the fact that any lower wave will have corrections to the higher wave. An s-wave has the characteristic that in the limit $v_{\text{rel}} \to 0$ then the amplitude will be a constant. For a p-wave the amplitude will go as $\sim v_{\text{rel}}^2$ and generally a $l - mode$ wave will scale as $\sim v_{\text{rel}}^{2l}$ to leading order. This does not however mean that the s-wave is generally independent of the relative velocity, it is just independent to the leading order. So a p-wave will contribute as the relative velocity squared to the expansion (5.45) but there will also be a contribution from the s-wave process and so on. For the rest of this thesis we will only take into account the a_l contribution to $\tilde{a}_l$. Including higher order terms would mean including corrections in both the normalizations $\mathcal{N}$, ε, and off-shell corrections to the on-shell approximation.

To express the amplitude of the process and the cross-section, we need the relation

$$\int d\Omega_{\mathbf{p}} P_{l'}(\cos\theta_{\mathbf{p}}) \int \frac{d^3q}{(2\pi)^3} \tilde{\phi}_{\mathbf{k}}(\mathbf{q}) |\mathbf{q}|^l P_l(\cos\theta_{\mathbf{q},\mathbf{p}}) = \delta_{ll'} \frac{(2l+1)!!}{i^l (2l+1) l!} \left[\frac{d^l}{dr^l} \int d\Omega_{\mathbf{r}} P_l(\cos\theta_{\mathbf{r}}) \phi_{\mathbf{k}}(\mathbf{r}) \right]_{\mathbf{r}=0}, \tag{5.47}$$

which is proven in appendix D of [29]. Using this relation we can calculate the l mode amplitude (5.39) to be

$$\mathcal{M}_{\text{ann},l} \simeq \frac{a_l |\mathbf{p}|^l}{(m\mu)^l} \frac{(2l+1)!!}{i^l (2l+1) l!} \left[\frac{d^l}{dr^l} \int d\Omega_{\mathbf{r}} P_l(\cos\theta_{\mathbf{r}}) \phi_{\mathbf{k}}(\mathbf{r}) \right]_{\mathbf{r}=0}. \tag{5.48}$$

Using this relation and inserting it into the cross-section (5.44) we can find the l partial wave

$$(\sigma_{\text{ann}} v_{\text{rel}})_l = \sigma_l S_{l,\text{ann}}, \tag{5.49}$$

with

$$\sigma_l = \frac{[l!/(2l)!!]^2}{2l+1} \frac{f_s |a_l|^2}{32\pi m\mu}, \tag{5.50}$$

and where

$$S_{l,\text{ann}} = \frac{[(2l+1)!/(l!)^2]^2}{4^{l+2}\pi^2\mu^{2l}} \left| \frac{d^l}{dr^l} \int d\Omega_{\mathbf{r}} P_l(\cos\theta_{\mathbf{r}}) \phi_{\mathbf{k}}(\mathbf{r}) \right|_{\mathbf{r}=0}, \tag{5.51}$$

is the Sommerfeld enhancement factor.

5.3 The Schrödinger equation and phase-space suppression

Having expressed the cross-sections of both bound state formation (5.25) and annihilation (5.49) in the non-relativistic limit through solutions of the Schrödinger equation we next look at solving the equation. The two equations for a bound and free system are

$$\left[-\frac{\boldsymbol{\Delta}^2}{2\mu} + V(\mathbf{r})\right]\psi_{nlm}(\mathbf{r}) = \mathcal{E}_{nl}\psi_{nlm}(\mathbf{r}), \tag{5.52}$$

$$\left[-\frac{\boldsymbol{\Delta}^2}{2\mu} + V(\mathbf{r})\right]\phi_{\mathbf{k}}(\mathbf{r}) = \mathcal{E}_{\mathbf{k}}\psi_{\mathbf{k}}(\mathbf{r}), \tag{5.53}$$

where the wavefunctions have the standard normalizations

$$\int d^3r\psi^*_{nlm}(\mathbf{r})\psi_{nlm}(\mathbf{r}) = 1, \tag{5.54}$$

$$\int d^3r\phi^*_{\mathbf{k}}(\mathbf{r})\phi_{\mathbf{k}'}(\mathbf{r}) = (2\pi)^3\delta^3(\mathbf{k}-\mathbf{k}'). \tag{5.55}$$

In this thesis we will only work with spherically symmetric potentials and we can then preform the separation of variables

$$\psi_{nlm}(\mathbf{r}) = \kappa^{3/2}\left[\frac{\chi_{nl}(\kappa r)}{\kappa r}\right]Y_{lm}(\Omega_{\mathbf{r}}), \tag{5.56}$$

$$\phi_{\mathbf{k}}(\mathbf{r}) = \sum_{l=0}^{\infty}(2l+1)\left[\frac{\chi_{|\mathbf{k}|,l}(\kappa r)}{\kappa r}\right]P_l(\hat{\mathbf{k}}\cdot\hat{\mathbf{r}}), \tag{5.57}$$

where $\kappa = \mu\alpha$. We will use $\alpha = \frac{\lambda^2}{4\pi}$, where λ is the coupling constant of the interaction. This is equivalent to that of a Yukawa potential with fermion matter particles[1]. Using $x = \kappa r$, we have set

$$R(x) = \left[\frac{\chi(x)}{x}\right], \tag{5.58}$$

as the radial part of the wavefunction. Defining the unitless parameter

$$\gamma \equiv \sqrt{-2\mu\mathcal{E}}/\kappa, \tag{5.59}$$

for the eigenvalue, the radial equation becomes

$$\chi''(x) + \left[\frac{-l(l+1)}{x^2} - \frac{2\mu}{\kappa^2}V(x) - \gamma^2\right]\chi(x) = 0. \tag{5.60}$$

[1]In the next chapter we will see that the Yukawa potential shows up as a factor in the potentials for pseudo-scalar mediators, eqs. (6.23)-(6.26)

The boundary condition for $x \to 0$ depends on the form of the potential and not whether the energy $\mathcal{E}$ is negative or positive and will be treated on an individual basis for each potential. On the other hand, the condition for $x \to \infty$ does depend on the sign of the eigenenergy. For a bounded system, $\mathcal{E} < 0$, we require that the wavefunctions vanish at infinity $\lim_{x\to\infty} \chi(x) = 0$ to fulfill the normalization condition (5.54) and preserve unitarity. For a bounded system we can then write the energy in terms of (5.59) as

$$\mathcal{E} = \mathcal{E}_{nl} \equiv -\gamma_{nl}^2 \times \frac{\kappa^2}{2\mu} \tag{5.61}$$

where γ_{nl}^2 needs to be determined numerically for the potentials we will use.

For the scattering system the energy will be positive,$\mathcal{E} > 0$, and is in the non-relativistic regime

$$\mathcal{E} = \mathcal{E}_{\mathbf{k}} = \frac{\mathbf{k}^2}{2\mu} = \frac{1}{2}\mu v_{\text{rel}}^2, \tag{5.62}$$

which, from (5.59) gives

$$\gamma^2 = -\frac{1}{\zeta^2}, \tag{5.63}$$

where $\zeta = \frac{\alpha}{v_{\text{rel}}}$. The asymptotic behavior of the scattering solution is known

$$\chi_{|\mathbf{k}|,l}(x) \xrightarrow[x\to\infty]{} C\frac{\zeta}{2i}\left[e^{i(x/\zeta+\delta_l)} - e^{-i(x/\zeta-l\pi)}\right], \tag{5.64}$$

up to a normalization C, where the only unknown parameter is the phase shift δ_l. This implies the condition

$$\left|\chi_{|\mathbf{k}|,l}(x)\right|^2 + \left|\chi_{|\mathbf{k}|,l}(x - \pi\zeta/2)\right|^2 = C^2\zeta^2. \tag{5.65}$$

This means that to solve for the scattering solution we can use a shooting method to produce a solution that we then normalize using (5.65) to determine C. Since the solution shows up in the form of absolute squares in the cross-sections, the phase does not have physical meaning.

In terms of the variables defined in (5.61) and (5.62) we can express the absolute three-momenta of the mediator, $|\mathbf{P}_\varphi|$, from the bound state formation cross-section (5.25). In the CM frame, the energy that is released in the bound state formation is the difference between the kinetic energy of the scattered states and the binding energy of the bound state, assuming the bound state at rest. Since the force carrier is on-shell we have that

$$\sqrt{|\mathbf{P}_\varphi|^2 + m_\varphi^2} = \mathcal{E}_{\mathbf{k}} - \mathcal{E}_{nl} = \frac{\mathbf{k}^2}{2\mu} + \frac{\kappa^2}{2\mu}\gamma_{nl}^2. \tag{5.66}$$

Using the relations $\kappa = \mu\alpha$ and $\mathbf{k} = \mu v_{\text{rel}}$ can rewrite this into the form

$$\frac{|\mathbf{P}_\varphi|}{\kappa} = \frac{\alpha}{2}\left[\frac{1+\zeta^2\gamma_{nl}^2}{\zeta^2}\right] \times pss_{nl}^{1/2}, \tag{5.67}$$

where

$$pss_{nl} = 1 - \frac{4\zeta^4}{\alpha^2\xi^2[1+\zeta^2\gamma_{nl}^2]}, \tag{5.68}$$

with $\xi = \frac{\kappa}{m_\varphi}$. pss_{nl} is the phase space suppression factor. With the emitted particle being on-shell and massive, the phase space of its momenta becomes restricted by four-momentum conservation. The more restricted the phase space is the less freedom there is for the interaction to happen and the cross-section for the process diminishes. This suppression is dependent on the mass of the forces carrying particle. When the mass $m_\varphi \to 0$ the factor $\xi \to \infty$ and $pss_{nl} \to 1$, as this opens up the phase space maximally. As the mass increases the pss_{nl} factor becomes smaller, as the phase space is restricted until bound state formation is no longer kinematically allowed as $m_\varphi < \mathcal{E}_{\mathbf{k}} - \mathcal{E}_{nl}$. Finally, we can write the differential cross-section for bound state formation as

$$v_{\text{rel}}\frac{d\sigma_{\text{BSF}}^{nlm}}{d\Omega} = \frac{\alpha^2}{2^7\pi^2m^2}pss_{nl}^{1/2}\left(\frac{1+\zeta^2\gamma_{nl}^2}{\zeta^2}\right)|\mathcal{M}_{\mathbf{k}\to nlm}|^2. \tag{5.69}$$

Chapter 6

The pseudo-scalar mediating potential and its renormalization

To solve the Schrödinger equation we must specify what the potential is. In this thesis we will look at a pseudo-scalar interaction. We start this chapter by introducing a more general method of deriving the potential associated with a mediator than that presented in chapter 4.2. The potential for the pseudo-scalar is presented along with a discussion about what it means for the initial and final states. We end the chapter by discussing the singularity problem that arises from the pseudo-scalar potential and how to renormalize this potential. The method used to derive the results of this chapter is taken from "*The effective theory of self-interacting dark matter*" by Bellazzini *et al.* [32] with additional discussions on the nature of singular potentials.

For a rotationally invariant, non-relativistic, self-interacting theory the elastic scattering amplitude of a two particle interaction is a scalar function that depends on the spins $\mathbf{s}_i$ of the particles, exchanged momentum $\mathbf{q}$ by the mediator, and relative velocity $\mathbf{v}$ of the particles. This amplitude is given by

$$\mathcal{M} = -\int_0^\infty dM^2 \frac{\rho(M^2)}{\mathbf{q}^2 + M^2} \sum_i g_i(\mathbf{q}^2/\Lambda^2, \mathbf{v}_\perp^2)\mathcal{O}_i(\mathbf{v}_i \cdot i\mathbf{q}/\Lambda, \mathbf{s}_i \cdot \mathbf{v}_\perp, \mathbf{s}_1 \cdot \mathbf{s}_2), \quad (6.1)$$

where $\mathbf{v}_\perp$ is the component of the relative velocity that is orthogonal to the momentum transfer $\mathbf{q}$, Λ is the scale of the dark sector, $g_i(\mathbf{q}^2/\Lambda^2, \mathbf{v}_\perp^2)$ are the coupling constants dependent on the energy and scale at which we work, and $\mathcal{O}_i(\mathbf{v}_i \cdot i\mathbf{q}/\Lambda, \mathbf{s}_i \cdot \mathbf{v}_\perp, \mathbf{s}_1 \cdot \mathbf{s}_2)$ are the operators which are allowed under the symmetries of the system. We have here used the general form of a two point correlation function known as the Källén-Lehmann spectral representation, eq. (3.1) in integral form, where M^2 is a parameter of units mass squared that together with the density function of physical states $\rho(M^2)$ selects to relevant poles at the corresponding scale as discusses in section 3.1 of this thesis. We wish to assume

a non-relativistic regime, and therefore we only keep leading order terms in exchanged momenta $\mathbf{q}/\Lambda$ and in the velocity. These assumptions imply simplifications for the couplings: the couplings are scale dependent and we can replace the momentum dependence in $g_i(\mathbf{q}^2/\Lambda^2, \mathbf{v}_\perp^2)$ with the scale factor $g_i(-M^2/\Lambda^2, \mathbf{v}_\perp^2)$ when neglecting short-range interactions. Furthermore, we are primarily interested in relatively light mediators compared to the matter particles such that $M^2 \ll m_\chi^2, \Lambda^2$. When combined with our assumption about the magnitude of the relative velocity, we keep only zeroth order terms $g_i(-M^2/\Lambda^2, \mathbf{v}_\perp^2) \simeq g_i(0,0) \equiv g_i$.

Next we select the relevant operators. We consider operators that are invariant under parity and time reversal and that are leading order in momentum and velocity. As a refresher; spin, momentum and velocity transforms under these symmetries as

$$P: \; i\mathbf{q} \to -i\mathbf{q}, \quad \mathbf{s} \to +\mathbf{s}, \quad \mathbf{v}_\perp \to -\mathbf{v}_\perp, \tag{6.2}$$
$$T: \; i\mathbf{q} \to +i\mathbf{q}, \quad \mathbf{s} \to -\mathbf{s}, \quad \mathbf{v}_\perp \to -\mathbf{v}_\perp. \tag{6.3}$$

With this we can build 6 operators

$$\mathcal{O}_1 = 1, \tag{6.4}$$
$$\mathcal{O}_2 = \mathbf{s}_1 \cdot \mathbf{s}_2, \tag{6.5}$$
$$\mathcal{O}_3 = -\frac{1}{\Lambda^2}(\mathbf{s}_1 \cdot \mathbf{q})(\mathbf{s}_2 \cdot \mathbf{q}), \tag{6.6}$$
$$\mathcal{O}_4 = (\mathbf{s}_1 \cdot \mathbf{v}_\perp)(\mathbf{s}_2 \cdot \mathbf{v}_\perp), \tag{6.7}$$
$$\mathcal{O}_{7,8} = -\frac{i}{\Lambda}\left[(\mathbf{s}_1 \pm \mathbf{s}_2) \cdot (\mathbf{q} \times \mathbf{v})\right]. \tag{6.8}$$

that respect both parity and time reversal. We here keep the subscript $7, 8$ instead of $5, 6$ to be consistent with [32] and to avoid confusion. Furthermore, we wish to restrict ourselves to operators generated by spin 1 particles or lower. This means that the operators should at most be quadratic in either $\mathbf{s}$ or $\mathbf{v}$ [42], and the operator $\mathcal{O}_4$ is therefore excluded. With the operators available we construct the amplitude (6.1) and Fourier transform with respect to $\mathbf{q}$ to obtain the long-range potential

$$V(\mathbf{r}, \mathbf{v}) = \frac{1}{4\pi r}\Bigg[\tilde{g}_1(r) + \tilde{g}_2(r)(\mathbf{s}_1 \cdot \mathbf{s}_2) + \frac{\tilde{g}_3(r)}{\Lambda^2 r^2}\left[3(\mathbf{s}_1 \cdot \hat{r})(\mathbf{s}_2 \cdot \hat{r}) - \mathbf{s}_1 \cdot \mathbf{s}_2\right] + \frac{\tilde{g}_{7,8}(r)}{\Lambda r}(\mathbf{s}_1 \pm \mathbf{s}_2) \cdot (\hat{r} \times \mathbf{v})\Bigg], \tag{6.9}$$

where we have factored terms by the dependence on r and the Fourier transform of the operators. The "new" couplings $\tilde{g}_i(r)$ are now combinations of the transform

of the "old" couplings g_i

$$\tilde{g}_1(r) = \int_0^\infty dM^2 \rho(M^2) e^{-Mr} \left[g_1 - g_1^{(1)} \frac{M^2}{\Lambda} \right], \tag{6.10}$$

$$\tilde{g}_2(r) = \int_0^\infty dM^2 \rho(M^2) e^{-Mr} \left[g_2 + \left(\frac{g_3}{3} - g_2^{(1)} \right) \frac{M^2}{\Lambda} \right], \tag{6.11}$$

$$\tilde{g}_3(r) = g_3 \int_0^\infty dM^2 \rho(M^2) e^{-Mr} \left[1 + Mr + \frac{1}{3}(Mr)^2 \right], \tag{6.12}$$

$$\tilde{g}_{7,8}(r) = g_{7,8} \int_0^\infty dM^2 \rho(M^2) e^{-Mr} \left[1 + Mr \right], \tag{6.13}$$

where $g_i^{(1)}$ are the next order terms in the expansion of $g_i(-M^2/\Lambda^2, \mathbf{v}_\perp) \to (-M^2/\Lambda^2)^n g_i^{(n)}/n!$.

We have further restrictions if we consider only spin half matter particles. A *CP* transformation corresponds to a conservation of total spin defined by the operator $\mathbf{S}^2 = (\mathbf{s}_1 + \mathbf{s}_2)^2$. For spin half particles this means a value of either 0 or 1 depending on whether the particles form a singlet or a triplet state. The conservation of total spin means that $\tilde{g}_8 = 0$, as the operator $(\mathbf{s}_1 - \mathbf{s}_2)$ changes the total spin. Using the conjugate momentum $\mathbf{p} = m_\chi \mathbf{v}/2$ we can write the potential in terms of more natural operator for a spin half system; $\mathbf{S}$ and $\mathbf{L} = \mathbf{r} \times \mathbf{p}$

$$V^{s_i=1/2} = \frac{1}{4\pi r} \Bigg[\left(\tilde{g}_1(r) - \frac{3}{4}\tilde{g}_2(r) \right) + \frac{1}{2}\tilde{g}_2(r)\mathbf{S}^2 + \frac{\tilde{g}_3(r)}{2\Lambda^2 r^2}[3(\mathbf{S}\cdot\hat{r})^2 - \mathbf{S}^2] + \frac{2\tilde{g}_7(r)}{m_\chi \Lambda r^2}\mathbf{S}\cdot\mathbf{L} \Bigg]. \tag{6.14}$$

In this operator form we can map out the potential for specific configurations of states. This potential does not generally conserve the orbital angular momentum and can therefore couple different l-modes together. A basis choice of conserved quantities must therefore exclude angular momentum, and we choose to use states of the total angular momentum J, total spin S and parity P. The l-mode(s) of each state is summarized in table (6.1).

Table 6.1: Table showing the associated l-mode(s) to each $|J, S, P\rangle$ state. Table 4 from [32]

J	S	P	l
0	0	-	0
0	1	+	1
1	0	+	1
1	1	+	1
1	1	-	0,2

Using these states we can find the effective potential for each combination of states $V = \langle \text{out}|V(r)|\text{in}\rangle$ of the type $|J, S, P\rangle$. Generally the in and out states can be different and $V(r)$ forms a matrix in the basis of these states. However, the leading order contribution comes from the diagonal elements. Using equation (6.14) as the potential bracketed by the total angular momentum states of particle configuration $|J, S, P\rangle$, we find these diagonal elements

$$|0,0,-\rangle \to V_1 = \left(\tilde{g}_1(r) - \frac{3}{4}\tilde{g}_2(r)\right)\frac{1}{4\pi r}, \tag{6.15}$$

$$|0,1,+\rangle \to V_2 = \left(\tilde{g}_1(r) + \frac{1}{4}\tilde{g}_2(r) - \frac{\tilde{g}_3(r)}{2\Lambda^2 r^2} - \frac{2\tilde{g}_7(r)}{m_\chi \Lambda r^2}\right)\frac{1}{4\pi r}, \tag{6.16}$$

$$|1,0,+\rangle \to V_3 = \left(\tilde{g}_1(r) - \frac{3}{4}\tilde{g}_2(r)\right)\frac{1}{4\pi r}, \tag{6.17}$$

$$|1,1,+\rangle \to V_4 = \left(\tilde{g}_1(r) + \frac{1}{4}\tilde{g}_2(r) + \frac{\tilde{g}_3(r)}{4\Lambda^2 r^2} - \frac{\tilde{g}_7(r)}{m_\chi \Lambda r^2}\right)\frac{1}{4\pi r}, \tag{6.18}$$

$$|1,1,-\rangle \to V_5 = \begin{pmatrix} \tilde{g}_1(r) + \frac{1}{4}\tilde{g}_2(r) & \frac{\tilde{g}_3(r)}{2\sqrt{2}\Lambda^2 r^2} \\ \frac{\tilde{g}_3(r)}{2\sqrt{2}\Lambda^2 r^2} & \tilde{g}_1(r) + \frac{1}{4}\tilde{g}_2(r) - \frac{\tilde{g}_3(r)}{4\Lambda^2 r^2} - \frac{3\tilde{g}_7(r)}{m_\chi \Lambda r^2} \end{pmatrix}\frac{1}{4\pi r}. \tag{6.19}$$

The last potential shows the coupling between a $l = 0$ and $l = 2$ modes. In the case of a scalar or vector mediator the factor $\tilde{g}_3 = \tilde{g}_7 = 0$ and this coupling between modes does not take place, while for all other mediators $\tilde{g}_3 \neq 0$. In this thesis we do not consider the potential V_5.

The interaction term in a Lagrangian can be written in a basis of the operators $\mathcal{O}_i$ of equations (6.4)-(6.8). For a pseudo-scalar interaction, $\mathcal{L} \supset i\lambda\bar{\chi}\gamma^5\chi\varphi$, the interaction term corresponds to the operator $\mathcal{O}_3$ only [1], meaning that g_3 is the

[1]Table 1 of [32] identifies which of the couplings g_i and operators $\mathcal{O}_i$ that corresponds to the interaction term for all mediator types.

only non-zero coupling constant. The coupling constant is

$$g_3 = \lambda^2 \frac{\Lambda^2}{m_\chi^2}, \tag{6.20}$$

where we have here explicitly accounted for the scaling dependence of the coupling constant. In the weakly coupled regime the density function becomes $\rho(M^2) = \delta(M^2 - m_\varphi)$. From eqs. (6.10)-(6.13) the surviving terms are

$$\tilde{g}_2(r) = \frac{\lambda^2 m_\varphi^2}{3m_\chi^2} e^{-m_\varphi r}, \tag{6.21}$$

$$\tilde{g}_3(r) = \frac{\lambda^2 \Lambda^2}{m_\chi^2} e^{-m_\varphi r} h(m_\varphi, r), \tag{6.22}$$

where $h(m_\varphi, r) = \left[1 + m_\varphi r + \frac{1}{3}(m_\varphi r)^2\right]$. Inserting this into the equations (6.15)-(6.18) we get

$$|0,0,-\rangle \to V_1 = -\frac{\lambda^2 m_\varphi^2}{4m_\chi^2} \frac{e^{-m_\varphi r}}{4\pi r}, \tag{6.23}$$

$$|0,1,+\rangle \to V_2 = \frac{1}{\mu r^2} + \left[\frac{\lambda^2 m_\varphi^2}{12 m_\chi^2} - \frac{\lambda^2 h(m_\varphi, r)}{2 m_\chi^2 r^2}\right] \frac{e^{-m_\varphi r}}{4\pi r}, \tag{6.24}$$

$$|1,0,+\rangle \to V_3 = \frac{1}{\mu r^2} - \frac{\lambda^2 m_\varphi^2}{4m_\chi^2} \frac{e^{-m_\varphi r}}{4\pi r}, \tag{6.25}$$

$$|1,1,+\rangle \to V_4 = \frac{1}{\mu r^2} + \left[\frac{\lambda^2 m_\varphi^2}{12 m_\chi^2} + \frac{\lambda^2 h(m_\varphi, r)}{4 m_\chi^2 r^2}\right] \frac{e^{-m_\varphi r}}{4\pi r}, \tag{6.26}$$

where we have added the centrifugal barrier term for the $l = 1$ orbital angular momentum modes with the reduced mass μ. Changing to the dimensionless parameters established for the Schrödinger equation in section 5.3 and assuming identical particles such that $\mu = m_\chi/2$ we derive the dimensionless potential $\mathcal{V} = \frac{2\mu}{\kappa^2} V$

$$|0,0,-\rangle \to \mathcal{V}_1 = -\frac{\alpha^2}{8\xi^2} \frac{e^{-x/\xi}}{x}, \tag{6.27}$$

$$|0,1,+\rangle \to \mathcal{V}_2 = \frac{2}{x^2} + \left[\frac{\alpha^2}{6\xi^2} - \frac{\alpha^2 h(\xi, x)}{4x^2}\right] \frac{e^{-x/\xi}}{x}, \tag{6.28}$$

$$|1,0,+\rangle \to \mathcal{V}_3 = \frac{2}{x^2} - \frac{\alpha^2}{8\xi^2} \frac{e^{-x/\xi}}{x}, \tag{6.29}$$

$$|1,1,+\rangle \to \mathcal{V}_4 = \frac{2}{x^2} + \left[\frac{\alpha^2}{6\xi^2} + \frac{\alpha^2 h(\xi, x)}{8x^2}\right] \frac{e^{-x/\xi}}{x}, \tag{6.30}$$

where $h(\xi, x) = 1 + x/\xi + \frac{1}{3}(x/\xi)^2$.

We see that potential $\mathcal{V}_4$ is strictly positive and will therefore be a repulsive potential. As such it will prevent bound state formation and will not lead to Sommerfeld enhancements. Potential $\mathcal{V}_3$ is a bit trickier to evaluate. A Yukawa potential does allow for bound state formation, and has been studied in this context [31]. The Yukawa term in $\mathcal{V}_3$ does however have a factor $\alpha^2/(6\xi^2)$ suppressing it. ξ involves the ratio of the reduced mass and the mediator mass. We have assumed that the mass of the matter particle to be much greater than the mediator mass in the derivation of this potential and as such $\xi \gg 1$ and the Yukawa term can effectively be ignored. This means that the potential (6.29) will not be very effective at forming bound states and we will not consider it in our further calculations. The same factor also suppresses the Yukawa term in both potential $\mathcal{V}_1$ and $\mathcal{V}_2$, however with no centrifugal term in $\mathcal{V}_1$ and with the $\sim 1/x^3$ term in potential $\mathcal{V}_2$, both potentials allow for bound state formation and Sommerfeld enhancement.

The $\sim 1/x^3$ term is a singular term and leads to unphysical predictions if not renormalized. A potential is defined as regular [43] if at $r = 0$ the potential goes as

$$\lim_{r\to 0} r^2 V(r) = 0, \tag{6.31}$$

singular if

$$\lim_{r\to 0} r^2 V(r) = \pm\infty, \tag{6.32}$$

and transitional if

$$\lim_{r\to 0} r^{2+\varepsilon}(r) = \begin{cases} 0 & \text{if } \varepsilon > 0 \\ \pm\infty & \text{if } \varepsilon < 0\,. \end{cases} \tag{6.33}$$

In quantum mechanics a singular potential leads to ones loss of the ability to determine to phase factor between two solutions, and unbounded systems. Landau and Lifshitz [44] has a simple example to illustrate the problem of unbounded energies for singular potentials. If we consider a particle confined to a small region r_0 around the origin. The uncertainty in position of that particle would be of order $\sim r_0$ meaning that through the uncertainty principle it has a momenta of order $\sim 1/r_0$. With a potential of the form g/r^m, the average energy is then approximately

$$E \sim 1/r_o^2 + g/r^m, \tag{6.34}$$

where g is either a negative or a positive number for respectively an attractive or repulsive potential. For $g < 0$ and $m > 2$ we see that the energy would go to $-\infty$ in the limit $r \to 0$, and the system is unbounded. If $m < 2$ then the system is bounded and if $g > 0$ then m can take arbitrary values. All the problems associated with singular potentials only occur for attractive potentials, and only

repulsive potentials do not require renormalization.

It has been shown that whether an effective potential is regular or singular is related to the renormalizability of the quantum field theory that produces it [45]. A non-renormalizable theory leads to a singular potential, a renormalizable theory to a transitional potential, and a superrenormalizable theory to a regular potential. To renormalize the effective potential we adopt the Wilsonian treatment of divergences. By integrating out the behavior at short distances we can expand the short range physics in terms of Dirac δ-functions. We regulate the potential by a short distance a and expand the behavior at $r < a$ in terms of a series of local operators to parameterize the unknown physics,

$$V(r) \to V(r)\theta(r-a) + c_0(a)\delta^3(r) + c_2(a)a^2\Delta^2\delta^3(r) + ... \tag{6.35}$$

We can then truncate the expansion at any order as long as the momenta of the exchanging particle q is smaller than the energy cutoff scale $\Lambda = a^{-1}$. The constants c_i cannot be derived from first principle and generally needs to be determined by experimental data. However, we are focused on the non-relativistic regime where long-range effects dominate. This means that we will truncate to first order and choose to regulate the potential with a square well

$$V_{\text{reg}}(r) = V(r)\theta(r - r_{\text{cut}}) + V_0\theta(r_{\text{cut}} - r), \tag{6.36}$$

where V_0 is the depth of the potential V at r_{cut} such that the potential is continuous. In principle we can calculate the short-range behavior, or use experimental data and determine the cutoff. A reasonable value for the energy scale will be the reduced mass μ of the two dark matter particles, as it is the scale were the non-relativistic approximation breaks down. We therefore set r_{cut} such that $V_0 = V(r_{\text{cut}}) = -\mu$. For the dimensionless potentials, $\mathcal{V}_1$ - $\mathcal{V}_4$, established in (6.27) - (6.30), we must also make the cutoff dimensionless. We do this as established in (5.60), by multiplying V_0 with the factor $2\mu/\kappa^2$ which means the dimensionless cutoff will be

$$\mathcal{V}_0 = -\frac{2}{\alpha^2}. \tag{6.37}$$

Only the contribution that arises from the effective potential (6.14) is regulated. The centrifugal barrier arises from the separation of variables and is non-singular, and unrelated to the UV physics. It is therefore not regulated by the cutoff.

This has implications of the potential $\mathcal{V}_2$ as its minima depends on the relative strengths of the $\sim -1/x^3$ and $\sim 1/x^2$ terms. If x_{cut} is large enough it may remove the minima needed for a bound state solution. We check this by numerically finding the x_{cut} value, and the minima, x_{min}, of $\mathcal{V}_2$ for a given value of α and ξ. What we find is that the ratio $x_{\text{cut}}/x_{\text{min}}$ is roughly constant as a function

of ξ, but changes in value with α as shown in table 6.2.

Table 6.2: The ratio $x_{\text{cut}}/x_{\text{min}}$ for a range of values for α and ξ. This ratio corresponds to the energy at which we would have to cut the singular potential such that a minima is available for bound state formation. A value of 2.5 would correspond to a cutoff at $V_0 = 2.5\mu$.

ξ	$\alpha = 1$	$\alpha = 0.5$	$\alpha = 0.1$
1	2.56959	4.19639	12.3758
5	2.66088	4.23138	12.3775
10	2.66515	4.23264	12.3776
20	2.66628	4.23296	12.3776
50	2.6666	4.23305	12.3776

Table 6.2 tells us that in order for a minima to be included we must set the cutoff at a higher energy. For the best case scenario, $\alpha = 1$, $\xi = 1$, this would mean a cut at $V_0 = 2.56959\mu$. This is in a region where the non-relativistic approximation looses validity and the assumptions made to find the effective potential breaks down. This means that the only potential of the four that allows for bound state formation and Sommerfeld enhancement is the potential $\mathcal{V}_1$.

The true upper limit to α is given by the perturbative limit, $\alpha = 4\pi$. This due to a $1/4\pi$ factor that scales the coupling α in a loop integral such that for $\alpha \leq 4\pi$ each loop will have a less than 1 factor that can be used for a perturbative expansion. While the value of α can be larger than 1, we have through this thesis equated α and v_{rel} in orders of power counting, to be consistent in the non-relativistic limit. This works well for a low value of α, but may add complications when becoming large in value. To have a minimum in the renormalized version of potential $\mathcal{V}_2$, the coupling must be $\alpha \sim \frac{3}{2}\pi$.

Chapter 7

Calculations and results

We consider an interaction Lagrangian

$$\begin{aligned}\mathcal{L} = &\bar{\chi}_1 i\not{\partial}\chi_1 + \bar{\chi}_2 i\not{\partial}\chi_2 + \frac{1}{2}\partial_\mu\varphi\partial^\mu\varphi - m_1\bar{\chi}_1\chi_1 - m_2\bar{\chi}_2\chi_2 - \frac{1}{2}m_\varphi^2\varphi^2 \\ &- g_1\varphi\bar{\chi}_1\gamma^5\chi_1 - g_2\varphi\bar{\chi}_2\gamma^5\chi_2. \end{aligned} \tag{7.1}$$

Unlike a scalar or vector, the effective potential generated by the pseudo-scalar mediator depends on the spin structure of the fermions to leading order. In equation (6.14) we see the general dependence on the spin structure that can occur in an effective potential in the non-relativistic regime. For a scalar or vector mediator only $\tilde{g}_1(r)$ and $\tilde{g}_2(r)$ are non-zero and the potential will have a component that is independent of the state of the particles. This means that to leading order the analysis done for scalar matter particles in [29] will hold for fermionic matter and in [31] this is used to calculate the bound state formation and annihilation cross-sections for massive scalar and vector mediators. A pseudo-scalar mediator potential does not have any component independent of the spin and will introduce complications. We will see this explicitly when calculating the amplitude of the hard process for bound state formation.

Annihilation is however a simpler problem to solve as the on-shell approximation and the partial wave expansion allows for zeroth order calculations of the hard process as it is independent of the spin structure. For the annihilation process the total angular state of the two-particle configuration only impacts the $\tilde{G}^{(4)}$ component in figure 5.3, and thereby its effect appears only in the Sommerfeld factor (5.51) in terms of the scattering solution to the Schrödinger equation.

For both annihilation and bound state formation the first step will be to solve the Schrödinger equation for the potentials $\mathcal{V}_1$ (6.27) and $\mathcal{V}_2$ (6.28) established in chapter 6.

7.1 Solutions to the Schrödinger equation

To solve the Schrödinger equation (5.60) for potential $\mathcal{V}_1$ (6.27) we must first find the boundary condition at $x \to 0$. The standard boundary condition for a Yukawa potential with a centrifugal term is

$$\lim_{x\to 0} \chi'(x) = (l+1) \lim_{x\to 0} \frac{\chi(x)}{x}, \tag{7.2}$$

which implies that the solution scales as x^{l+1} in this region. Potential $\mathcal{V}_1$ is of a similar form but with $l = 0$. While the boundary condition (7.2) is set for $l > 0$ it is valid in the limit $x \to 0$ and can be used for the $l = 0$ case.

The numerical method for solving the Schrödinger equation (5.60) is different for the bound state and the scattering state. For the scattering process we know what energy is and can solve the differential equation for a set of initial conditions, (7.2).

For the bound state solution we have to find the eigenenergy as well as the eigenstate. We accomplish this through the Mathematica function ParametricNDSolve. This function allows for solving a differential equation as a function of a set of variables $x, y, ...$ while leaving a set of parameters as input values. For solving the Schrödinger equation we set a unitless quantity a as the parameter replacing γ in (5.60), while solving over x. We can then run over different values of a and using an error function to determine the solution that is closest to an eigenstate, thereby also finding the corresponding eigenvalue. The error function

$$err = \frac{\int dx \left| \mathcal{D}\left(\psi(x)/\sqrt{N}\right) - \gamma^2 \left(\psi(x)/\sqrt{N}\right) \right|}{\int dx \left| \gamma^2 \left(\psi(x)/\sqrt{N}\right) \right|}, \tag{7.3}$$

where $\mathcal{D} = \frac{d^2}{dx^2} + \left(\frac{-l(l+1)}{x^2} - \frac{2\mu}{\kappa^2} V(x) \right)$ is the radial equation differential operator such that $\mathcal{D}\psi(x) = \gamma^2 \psi(x)$, and N is the normalization

$$N = \int dx |\psi(x)^2|. \tag{7.4}$$

The error function will then be zero for the exact eigenenergy $a = \gamma$, but will in general give a minima as a function of a. This will however be inefficient as the resolution wanted in the run over a values requires a large amount of computation time. To reduce the computation time we introduce an automated minima search.

This automated search is an approximation of taking a second derivative and testing whether it is positive, providing a fast minima search at the cost of accuracy. The search takes the difference between all the error function values and

determines if that difference is positive, zero, or negative and assigns that element the values 1, 0, -1 respectively. We then take the difference between all these values as well. If a point is a minimum then the previous and next value will be larger generating the values 1, -1 in the first step. In the next step the difference between them will give the value 2. So after taking the second difference we need only identify the elements of value 2 to find the minimas.

This allows us to run a sparse initial resolution in a values, then identify the minimas. We then adjust the resolution around these points and run again. We can then increase the desired final resolution by increasing the number of such runs that we make, allowing for a fine final resolution without an unnecessary amount of calculations. The method does rely on an initial grid that is fine enough to actually find the minimas initially.

While this method works very well for a standard Yukawa or Coulomb potential, for the potential V_1 it becomes ineffective. This is due to the very fine grid resolution needed for solving the boundary value problem, when the potential changes as rapidly as ours does here. The method described above is very accurate but time consuming. When we additionally need to increase the grid size significantly the time requirements increase as well. We then adopt an alternative method to find the wavefunctions.

With the condition at the endpoint, $\lim_{x\to\infty} \chi(x) = 0$, of a bound state solution and the initial conditions (7.2) we have an extra condition we can apply. Since initial value problems are often quicker to solve numerically, we can solve the differential equation with the conditions (7.2) then find for what values of a the solution is zero at the numerical endpoint. With the rapidly changing potential we have to be careful not to overshoot with the initial first derivative. This means that we have to use a first derivative that is small enough not to overshoot in the first step, but still large compared to the initial value at the startpoint.

Though fast, this method has the disadvantage that we cannot guaranty that we find the ground state solution. The method requires us to find the roots of the solution as a function of the variable a, of which there infinitely many. Using this method we find three bound state solutions for the parameter values $\alpha = 0.5$ and $\xi = 50$, shown in figure 7.1.

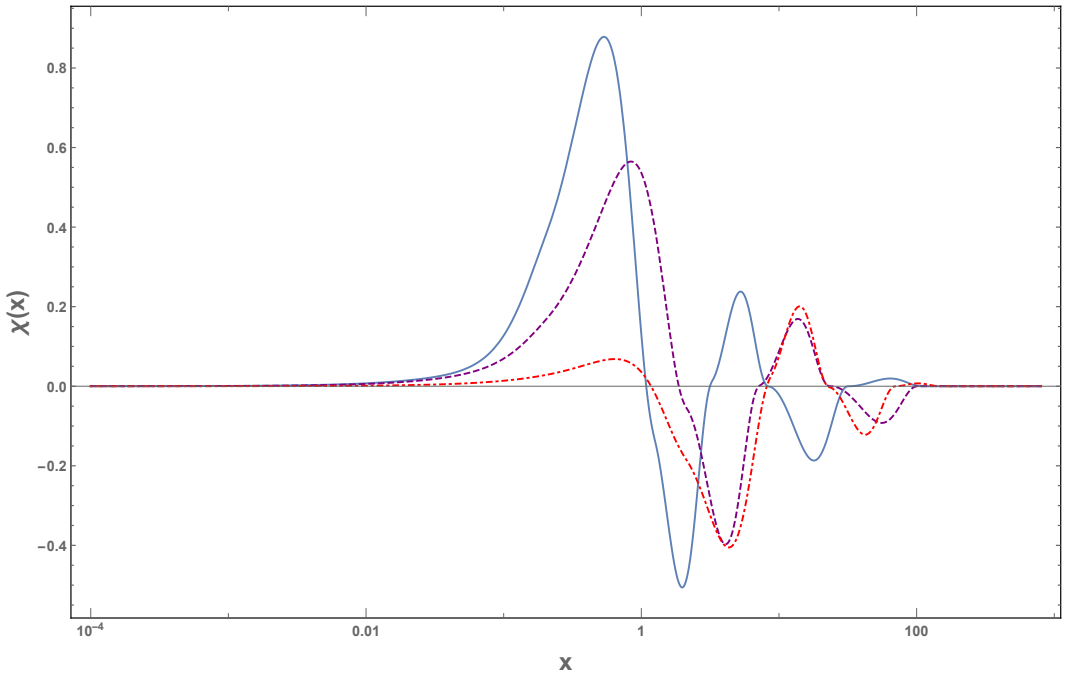

Figure 7.1: Plot of the wavefunctions for the potential (6.27) with $\alpha = 0.5$, $\xi = 50$ for all lines. The lines represents different energies; $a = 3.91987$ (Solid), $a = 2.75903$ (Dashed), $a = 0.807955$ (Dot dashed)

7.2 Annihilation

The annihilation process with ladder diagrams will have the form as seen in figure 7.2. The ladder contribution corresponds to the $\tilde{G}^{(4)}$ contribution from figure 5.3 and is bracketed by the $|J, S, P\rangle$ states give one of the potential $\mathcal{V}_1$ - $\mathcal{V}_4$ (6.27 - 6.30).

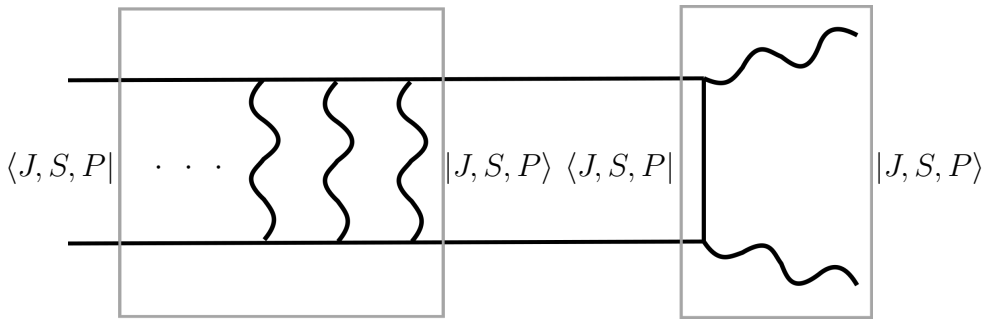

Figure 7.2: Annihilation of a particle-antiparticle pair into two force carrying particles with the Sommerfeld enhancement through the infinite ladder and the lowest order hard process for $2 \to 2$ annihilation.

The first box of figure 7.2 gives the contribution that corresponds to the Sommerfeld factor (5.51). The factor depends on the effective potential through the scattering solution to the Schrödinger equation and we will therefore in general have a separate factor for each of the potentials $\mathcal{V}_1$ - $\mathcal{V}_4$. Since only the potential $\mathcal{V}_1$ is attractive, it is the only one that can give a Sommerfeld enhancement factor.

The second part of figure 7.2 shows the $2 \to 2$ annihilation process bracketed by these same state. However, considering the expansion (5.45) of this annihilation process, the diagram is independent of the potential or the final state to leading order order. The constant a_l in (5.45) is a dimensionless quantity that needs to be estimated. For a $2 \to 2$ process, as in figure 7.2, there are two vertices that contribute with a g^2 factor times the multiplicity of the diagram. There are four ways of constructing the annihilation amplitude from symmetries of the diagram. This means that the constant should be $a_0 = 4g^2 = 16\pi\alpha$. From (5.48) we have that the cross-section for the annihilation of dark matter through a pseudo-scalar mediator in the non-relativistic regime will then be

$$(\sigma_{\text{ann}} v_{\text{rel}})_0 = \sigma_0 S_{0,\text{ann}} \tag{7.5}$$

where

$$\sigma_0 = \frac{4\pi\alpha^2}{m\mu} \tag{7.6}$$

from equation (5.50) and from (5.51) we get

$$S_{0,\text{ann}} = \left|\phi_{\mathbf{k}(\mathbf{r}=0)}\right|^2 = \lim_{x\to 0}\left[\frac{\chi_{|\mathbf{k}|,l=0}(x)}{x}\right]. \tag{7.7}$$

To find this value we take a closer look at the asymptotic behavior of the scattering state (5.64) and the condition (5.65). These conditions are true up to a normalization of the wavefunction. Iengo [27] shows that this normalization determines the enhancement by

$$S_{l,\text{ann}} = \left(\frac{1\cdot 3\cdots(2l+1)}{C}\right)^2, \tag{7.8}$$

contrasting (5.51) by a normalization C that is determined by the asymptotic limit of the solution

$$\varphi_l(y) \xrightarrow[y\to\infty]{} C\sin\left(y - \frac{l\pi}{2} + \delta_l\right), \tag{7.9}$$

with $y = \zeta x$. The scaling between the solutions is given by

$$C\varphi_l(y) = \chi_{|\mathbf{k}|,l}(y). \tag{7.10}$$

This means that when solving the radial Schrödinger equation (5.60), the solution will give an asymptotic such that the equation condition (5.65) will not be exactly equal to ζ^2 but be off by multiplicative constant C. We can then find this constant C, and thereby the Sommerfeld enhancement, by

$$C = \sqrt{\frac{\left|\chi_{|\mathbf{k}|,l}(x)\right|^2 + \left|\chi_{|\mathbf{k}|,l}(x - \pi\zeta/2)\right|^2}{\zeta^2}}. \tag{7.11}$$

In figure 7.3 we show the Sommerfeld enhancement as a function of ξ for a range of different values of ζ. The larger the value of ζ, the better the non-relativistic approximation becomes. We see that as ζ grows the change in enhancement tends to 1. As part of the assumptions made in deriving the pseudo-scalar potentials we required that $\xi \gg 1$, and for these values we see that the value of the Sommerfeld enhancement is very close to 1. Even for $\xi = 1$, the enhancement is only ≈ 1.03. This contrasts results for a vector mediator where the enhancement can range from a factor 10 to 1000 [31].

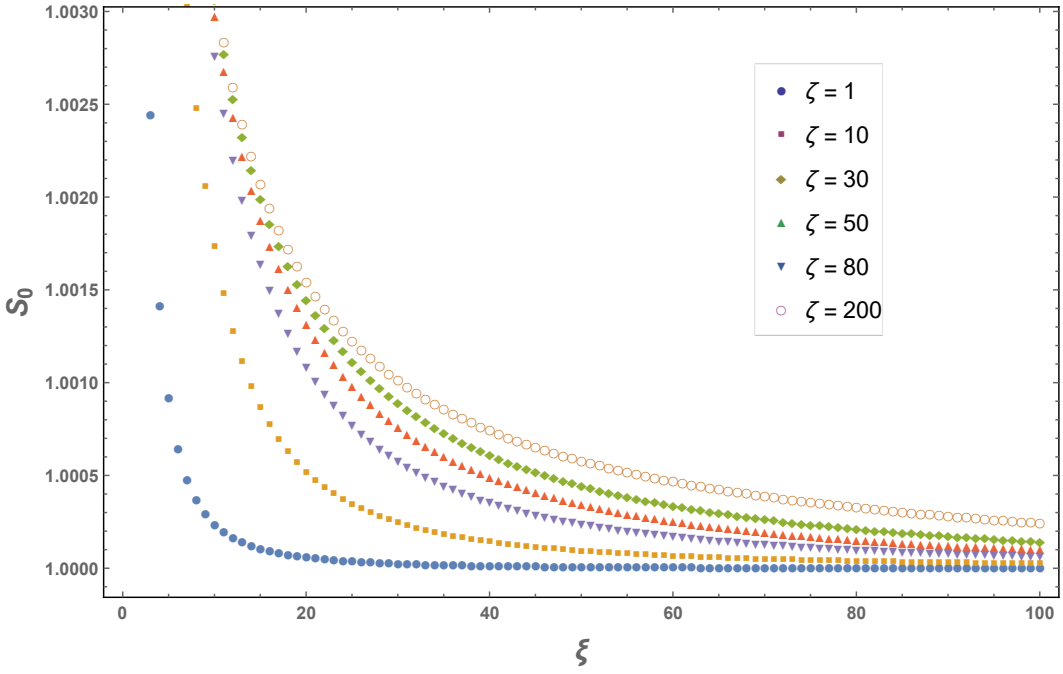

Figure 7.3: Plot of the Sommerfeld enhancement factor for the potential $\mathcal{V}_1$ (6.27) with $\alpha = 0.5$ as a function of $\xi = \mu\alpha/m_\varphi$. The different data sets represent values of; $\zeta = 1$ (Filled Circle), $\zeta = 10$ (Square), $\zeta = 30$ (Diamonds), $\zeta = 50$ (Triangle), $\zeta = 80$ (Upside down triangle), $\zeta = 200$ (Empty Circle)

We find that for the attractive potential $\mathcal{V}_1$ (6.27) there is a negligible enhancement. This means that we find no enhancement for the annihilation process in

the non-relativistic regime. It is known from contemporary sources that the enhancement for a Yukawa interaction is small but with the additional suppression as in the pseudo-scalar case, there is no enhancement at all. When we look at the potential V_1 (6.23) with dimensions

$$V(r) = -\frac{m_\varphi^2}{4m_\chi^2}\frac{\alpha e^{-m_\varphi r}}{r} \tag{7.12}$$

we see that the suppering factor $\frac{m_\varphi^2}{4m_\chi^2}$ effectively scales the coupling such that

$$V(r) = -\frac{\alpha' e^{-m_\varphi r}}{r} \tag{7.13}$$

with $\alpha' = \frac{m_\varphi^2}{4m_\chi^2}\,\alpha$ where $\alpha' \ll \alpha$. The lower the value of the coupling, the less of an effect there will be from Sommerfeld enhancement as the potential will go to 0 faster as $r \to \infty$.

We can conclude that there is a significantly different behavior for a pseudo-scalar mediator than for a scalar or vector in the non-relativistic limit. While the Sommerfeld effect has been studied previously for similar potentials, the bound state formation has not been studied for a pseudo-scalar mediator.

7.3 Bound state formation

For the bound state formation cross-section we must calculate the lowest order contribution from the hard scattering amplitude $\tilde{C}_{\varphi-\text{amp}}$. Figure 7.4 shows this lowest order contribution for two distinct dark matter particles. While we do most of the calculations with the idea of distinct particles, we are ultimately interested in a particle-antiparticle model, as we studied in chapter 6.

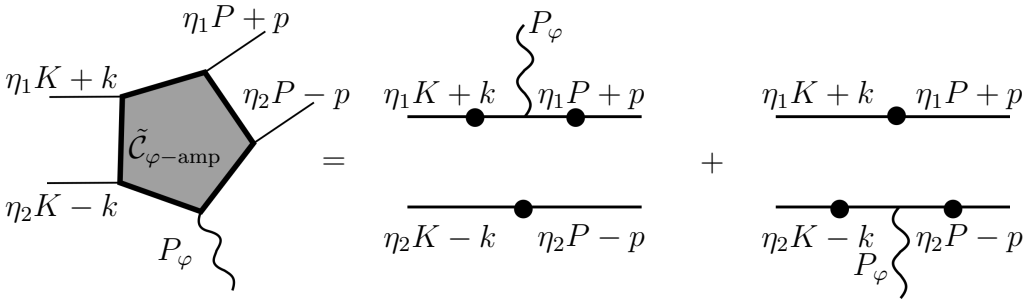

Figure 7.4: The lowest order contribution to the hard scattering process of dissipative bound state formation.

Figure 7.4 shows the lowest order contribution to the φ-amputated hard scattering process

$$\begin{aligned}&(2\pi)^4\delta^4(K-P-P_\varphi)i\mathcal{C}^{(5)}_{\varphi-\mathrm{amp}}(P_\varphi,p_1,p_2;q_1,q_2)=\\&-ig_1m_1\tilde{s}_1(p_1)\gamma_1^5\tilde{s}_1(q_1)(2\pi)^4\delta^4(P_\varphi+p_1-q_1)\tilde{s}_2(q_2)(2\pi)^4\delta^4(p_2-q_2)\\&-ig_2m_2\tilde{s}_2(p_2)\gamma_2^5\tilde{s}_2(q_2)(2\pi)^4\delta^4(P_\varphi+p_2-q_2)\tilde{s}_1(q_1)(2\pi)^4\delta^4(p_1-q_1).\end{aligned}\tag{7.14}$$

Equivalently

$$\begin{aligned}&\mathcal{C}^{(5)}_{\varphi-\mathrm{amp}}(P_\varphi,\eta_1P+p,\eta_2-p;\eta_1K+q,\eta_2K-q)=-\Big[g_1m_1\tilde{s}_1(\eta_1P+p)\gamma_1^5\\&\times(2\pi)^4\delta^4(q-p-\eta_2P_\varphi)+g_2m_2\tilde{s}_2(\eta_2-p)\gamma_2^5(2\pi)^4\delta^4(q-p-\eta_2P_\varphi)\Big]S(q;K).\end{aligned}\tag{7.15}$$

where we used the fact that $S(q;K)=\tilde{s}_1(\eta_1K+q)\tilde{s}_2(\eta_2K-q)=\tilde{s}_2(\eta_2K-q)\tilde{s}_1(\eta_1K+q)$. We define the two quantities

$$\Xi_1(\mathbf{p},\mathbf{q};K,P)\equiv\int\frac{dp^0}{2\pi}\tilde{s}_1(\eta_1P+p)\gamma_1^5\int\frac{dq^0}{2\pi}S(q;K)(2\pi)\delta(q^0-p^0-\eta_2P_\varphi^0),\tag{7.16}$$

$$\Xi_2(\mathbf{p},\mathbf{q};K,P)\equiv\int\frac{dp^0}{2\pi}\tilde{s}_2(\eta_1P+p)\gamma_2^5\int\frac{dq^0}{2\pi}S(q;K)(2\pi)\delta(q^0-p^0-\eta_2P_\varphi^0),\tag{7.17}$$

such that we may write

$$\begin{aligned}\mathcal{M}_{\mathrm{trans}}(\mathbf{q};\mathbf{p})=-S_0^{-1}(\mathbf{p};P)\Big[&g_1m_1\Xi_1(\mathbf{p},\mathbf{q};K,P)(2\pi)^3\delta^3(\mathbf{q}-\mathbf{p}-\eta_2\mathbf{P}_{\boldsymbol{\varphi}})\\&+g_2m_2\Xi_2(\mathbf{p},\mathbf{q};K,P)(2\pi)^3\delta^3(\mathbf{q}-\mathbf{p}-\eta_2\mathbf{P}_{\boldsymbol{\varphi}})\Big]S_{0,}^{-1}(\mathbf{q};K),\end{aligned}\tag{7.18}$$

using the definition (5.24).

By taking the Fourier transform of $\delta(q^0-p^0-\eta_2P_\varphi^0)$ we can write (7.16) as

$$\Xi_1(\mathbf{p},\mathbf{q};K,P)=\int dte^{-i\eta_2P_\varphi^0t}\int\frac{dp^0}{2\pi}\tilde{s}_1(\eta_1P+p)e^{-ip^0t}\gamma_1^5\int\frac{dq^0}{2\pi}S(q;K)e^{iq^0t}.\tag{7.19}$$

while $\int\frac{dq^0}{2\pi}S(q;K)e^{iq^0t}$ is known from equation (4.54), we must calculate $\int\frac{dp^0}{2\pi}\tilde{s}_1(\eta_1P+$

$p)e^{-ip^0t}$. Using the alternate form of the propagator (4.51) we get

$$\int \frac{dp^0}{2\pi}\left[\frac{\Lambda_1^+(\eta_1\mathbf{P}+\mathbf{p})}{\eta_1 P^0+p^0-E_1(\eta_1\mathbf{P}+\mathbf{p})+i\epsilon}+\frac{\Lambda_1^-(\eta_1\mathbf{P}+\mathbf{p})}{\eta_1 P^0+p^0+E_1(\eta_1\mathbf{P}+\mathbf{p})-i\epsilon}\right]\gamma_1^0 e^{-ip^0t}$$

$$=\begin{cases}\Lambda^+_{1,\mathbf{p}}\gamma_1^0 e^{i(\eta_1 P^0-E_{1,\mathbf{p}})t} & \text{for } t>0\\ \\ -\Lambda^-_{1,\mathbf{p}}\gamma_1^0 e^{i(\eta_1 P^0+E_{1,\mathbf{p}})t} & \text{for } t<0\quad ,\end{cases} \tag{7.20}$$

where we have introduced the short hand notation of $_{1,\mathbf{p}}$ to mean of particle type 1 with incoming relative momenta $\mathbf{p}$ as opposed to $_{2,\mathbf{q}}$ to mean particle type 2 with outgoing relative momenta $\mathbf{q}$. From equations (7.20) and (4.51) we see that the spinor structure of (7.16) will be of the form

$$\Lambda^\pm_{1,\mathbf{p}}\gamma_1^0\gamma_1^5\Lambda^\pm_{1,\mathbf{q}}\gamma_1^0\Lambda^\pm_{2,\mathbf{q}}\gamma_1^0=\left[\frac{(E_{1,\mathbf{p}}\pm\gamma_1^0\boldsymbol{\gamma}_1\cdot(\eta_1\mathbf{P}+\mathbf{p})\pm\gamma_1^0 m_1)\gamma_1^0}{2E_{1,\mathbf{p}}}\gamma_1^5\right.$$
$$\left.\times\frac{(E_{1,\mathbf{q}}\pm\gamma_1^0\boldsymbol{\gamma}_1\cdot(\eta_1\mathbf{K}+\mathbf{q})\pm\gamma_1^0 m_1)\gamma_1^0}{2E_{1,\mathbf{q}}}\frac{(E_{2,\mathbf{q}}\pm\gamma_2^0\boldsymbol{\gamma}_2\cdot(\eta_2\mathbf{K}-\mathbf{q})\pm\gamma_2^0 m_2)\gamma_2^0}{2E_{2,\mathbf{q}}}\right]. \tag{7.21}$$

The energies $E_{1,\mathbf{p}}$,$E_{1,\mathbf{q}}$, and $E_{2,\mathbf{q}}$ are to lowest order $E_{1,\mathbf{p}}\simeq m_1+\mathbf{p}^2/2m_1$. This means that

$$\frac{1}{E_{1,\mathbf{p}}}\simeq\frac{1}{m_1}\left(1-\frac{\mathbf{p}^2}{2m_1^2}\right), \tag{7.22}$$

where we have dropped the terms that goes as $\sim\mathbf{P}\cdot\mathbf{p}$ and $\sim\mathbf{P}^2$ from the expansion (3.9) as $\mathbf{P}^2$ corrections are of order v_{rel}^4, α^4, see equation (5.67), while $\mathbf{p}^2$ is of order v_{rel}^2. Therefore the 8 combinations

$$\begin{gathered}\gamma_1^0\gamma_1^5\gamma_1^0\gamma_2^0,\ \gamma_1^0\gamma_1^5\gamma_1^0 m_2,\ \gamma_1^0\gamma_1^5\gamma_2^0 m_1,\ \gamma_1^5\gamma_1^0\gamma_2^0 m_1,\\ \gamma_1^0\gamma_1^5 m_1 m_2,\ \gamma_1^5\gamma_1^0 m_1 m_2,\ m_1^2\gamma_1^5\gamma_2^0,\ \gamma_1^5 m_1^2 m_2,\end{gathered} \tag{7.23}$$

will give terms that are of lowest order in momentum when we have factorized out the γ^5 component. Using the commutation relation $\{\gamma_1^5,\gamma_1^0\}=0$ we can factor these terms such that the γ^5 comes first. Taking the sign of the terms from (7.21) we can organize the term as shown in table 7.1.

When discussing leading order terms, we must also consider the contribution from the exponential factors in (7.19). From table 7.1 we see that the combination of terms that give the lowest order contribution to (7.16) will be $\Lambda^-\Lambda^+\Lambda^+$. Equation (4.54) shows that closing in both upper and lower half-plane will give the required $\Lambda^+\Lambda^+$ but to get the Λ^- factor we must have $t<0$ from (7.20). For the combination of Λs we know that the integral will be

$$\int_{-\infty}^{0} dt e^{i(\eta_1 P^0+E_{1,\mathbf{p}}-\eta_1 K^0+E_{1,\mathbf{q}}-\eta_2 P_\varphi^0)t}. \tag{7.24}$$

Table 7.1: Table of the sign for the leading order terms for the expression (7.16) in momentum. The last column shows the sum of these leading order term in the non-relativistic limit. The parenthesis $(-)$ marks the sign of the term after the commutation of the γ matrices.

	$(-)\gamma_1^5\gamma_2^0$	$(-)\gamma_1^5 m_2$	$(-)\gamma_1^5\gamma_1^0\gamma_2^0 m_1$	$\gamma_1^5\gamma_1^0\gamma_2^0 m_1$	$(-)\gamma_1^5\gamma_1^0 m_1 m_2$
$\Lambda^+\Lambda^+\Lambda^+$	$-$	$-$	$-$	$+$	$-$
$\Lambda^+\Lambda^+\Lambda^-$	$-$	$+$	$-$	$+$	$+$
$\Lambda^+\Lambda^-\Lambda^+$	$-$	$-$	$+$	$+$	$+$
$\Lambda^-\Lambda^+\Lambda^+$	$-$	$-$	$-$	$-$	$-$
$\Lambda^+\Lambda^-\Lambda^-$	$-$	$+$	$+$	$+$	$-$
$\Lambda^-\Lambda^+\Lambda^-$	$-$	$+$	$-$	$-$	$+$
$\Lambda^-\Lambda^-\Lambda^+$	$-$	$-$	$+$	$-$	$+$
$\Lambda^-\Lambda^-\Lambda^-$	$-$	$+$	$+$	$-$	$-$
	$\gamma_1^5\gamma_1^0 m_1 m_2$	$\gamma_1^5\gamma_2^0 m_1^2$	$\gamma_1^5 m_1^2 m_2$	Non-rel	
$\Lambda^+\Lambda^+\Lambda^+$	$+$	$+$	$+$	0	
$\Lambda^+\Lambda^+\Lambda^-$	$-$	$+$	$-$	0	
$\Lambda^+\Lambda^-\Lambda^+$	$+$	$-$	$-$	0	
$\Lambda^-\Lambda^+\Lambda^+$	$-$	$-$	$-$	$-\gamma_1^5$	
$\Lambda^+\Lambda^-\Lambda^-$	$-$	$-$	$+$	0	
$\Lambda^-\Lambda^+\Lambda^-$	$+$	$-$	$+$	0	
$\Lambda^-\Lambda^-\Lambda^+$	$-$	$+$	$+$	0	
$\Lambda^-\Lambda^-\Lambda^-$	$+$	$+$	$-$	0	

We then use the equality $P_\varphi^0 = K^0 - P^0$ to get

$$\int_{-\infty}^{0} dt e^{i(P^0 - K^0 + E_{1,\mathbf{p}} + E_{1,\mathbf{q}})t} = \frac{-i}{P^0 - (K^0 - E_{1,\mathbf{p}} - E_{1,\mathbf{q}})}. \tag{7.25}$$

In equation (4.57) we used the fact that the combination of terms $P^0 - E_{1,\mathbf{p}} - E_{2,\mathbf{p}} \simeq \mathcal{E} - \frac{\mathbf{p}^2}{\mu}$. The expression 7.16 will have the conservation of three-momenta $\delta^3(\mathbf{q} - \mathbf{p} - \eta_2 \mathbf{P}_\varphi)$ imposed and as such $\mathbf{p} \simeq \mathbf{q}$ to lowest order in v_{rel}. This means that for identical particles

$$K^0 - E_{1,\mathbf{p}} - E_{1,\mathbf{q}} \simeq \mathcal{E} - \frac{\mathbf{q}^2}{\mu}, \tag{7.26}$$

and (7.25) goes as $\sim 1/m$ to leading order, and this is not the leading order we can get from the exponential. With the combination $++$ we get the exponential

$$\int_{0}^{\infty} dt e^{i(P^0 - E_{2,\mathbf{p}} - E_{1,\mathbf{q}})t} = \frac{i}{P^0 - E_{2,\mathbf{p}} - E_{1,\mathbf{q}}}, \tag{7.27}$$

which goes as $\sim \frac{1}{\mathbf{p}^2/m}$. Therefore first order terms of the combination $+++$ will give corrections to the same order as the zeroth order terms of $-++$[1]. Before we find the second order terms of $+++$ let us note the this process is second order in v_{rel}. This means that we expect the process to be suppressed at low velocities as in the non-relativistic regime and bound state formation may be subdominant to the annihilation process. This contrasts with the case of a scalar mediator for which, without the γ^5 component, the combination that gives leading order contribution is $+++$, and a leading order independent of v_{rel}.

The combination $+++$ gives to first order the terms

$$
\begin{aligned}
&\Lambda^+_{1,\mathbf{p}}\gamma^0_1\gamma^5_1\Lambda^+_{1,\mathbf{q}}\gamma^0_1\Lambda^+_{2,\mathbf{p}}\gamma^0_2 = \\
&\frac{1}{8}\Bigg[\gamma^5_1\gamma^0_2 - \frac{\gamma^5_1 m_2}{E_{2,\mathbf{q}}} - \frac{\gamma^5_1\gamma^0_1\gamma^0_2 m_1}{E_{1,\mathbf{q}}} + \frac{\gamma^5_1\gamma^0_1\gamma^0_2 m_1}{E_{1,\mathbf{p}}} - \frac{\gamma^5_1\gamma^0_1 m_1 m_2}{E_{1,\mathbf{q}}E_{2,\mathbf{q}}} + \frac{\gamma^5_1\gamma^0_1 m_1 m_2}{E_{1,\mathbf{p}}E_{2,\mathbf{q}}} \\
&+ \frac{\gamma^5_1\gamma^0_2 m_1^2}{E_{1,\mathbf{p}}E_{1,\mathbf{q}}} + \frac{\gamma^5_1 m_1^2 m_2}{E_{1,\mathbf{p}}E_{1,\mathbf{q}}E_{2,\mathbf{q}}} + \frac{\gamma^5_1\boldsymbol{\gamma}_2\cdot(\eta_2\mathbf{K}-\mathbf{q})}{E_{2,\mathbf{q}}} - \frac{\gamma^5_1\boldsymbol{\gamma}_1\cdot(\eta_1\mathbf{K}+\mathbf{q})\gamma^0_1\gamma^0_2}{E_{1,\mathbf{q}}} \\
&+ \frac{\gamma^5_1\boldsymbol{\gamma}_1\cdot(\eta_1\mathbf{P}+\mathbf{p})\gamma^0_1\gamma^0_2}{E_{1,\mathbf{p}}} - \frac{\gamma^5_1\boldsymbol{\gamma}_2\cdot(\eta_2\mathbf{K}-\mathbf{q})\gamma^0_1 m_1}{E_{1,\mathbf{q}}E_{2,\mathbf{q}}} - \frac{\gamma^5_1\boldsymbol{\gamma}_1\cdot(\eta_1\mathbf{K}+\mathbf{q})\gamma^0_2 m_1}{E_{1,\mathbf{p}}E_{1,\mathbf{q}}} \\
&+ \frac{\gamma^5_1\boldsymbol{\gamma}_1\cdot(\eta_1\mathbf{P}+\mathbf{p})\gamma^0_2 m_1}{E_{1,\mathbf{p}}E_{1,\mathbf{q}}} - \frac{\gamma^5_1\boldsymbol{\gamma}_1\cdot(\eta_1\mathbf{K}+\mathbf{q})\gamma^0_1 m_2}{E_{1,\mathbf{q}}E_{2,\mathbf{q}}} + \frac{\gamma^5_1\boldsymbol{\gamma}_1\cdot(\eta_1\mathbf{P}+\mathbf{p})\gamma^0_1 m_2}{E_{1,\mathbf{p}}E_{2,\mathbf{q}}} \\
&+ \frac{\gamma^5_1\boldsymbol{\gamma}_2\cdot(\eta_2\mathbf{K}-\mathbf{q})\gamma^0_1 m_1}{E_{1,\mathbf{p}}E_{2,\mathbf{q}}}\Bigg].
\end{aligned}
$$

In the non-relativistic limit the zeroth order terms cancel, and their corresponding second order terms originating from the expansion of (7.22), in the non-relativistic limit where $\gamma^0 \sim 1$. For the already first order terms we will only keep zeroth order contributions from (7.22). This means that the expansion becomes

$$
\begin{aligned}
&\Lambda^+_{1,\mathbf{p}}\gamma^0_1\gamma^5_1\Lambda^+_{1,\mathbf{q}}\gamma^0_1\Lambda^+_{2,\mathbf{p}}\gamma^0_2 = \frac{\gamma^5_1}{8}\Bigg[\frac{\boldsymbol{\gamma}_2\cdot(\eta_2\mathbf{K}-\mathbf{q})}{m_2} \\
&- \frac{\boldsymbol{\gamma}_1\cdot(\eta_1\mathbf{K}+\mathbf{q})\gamma^0_1\gamma^0_2}{m_1} + \frac{\boldsymbol{\gamma}_1\cdot(\eta_1\mathbf{P}+\mathbf{p})\gamma^0_1\gamma^0_2}{m_1} - \frac{\boldsymbol{\gamma}_2\cdot(\eta_2\mathbf{K}-\mathbf{q})\gamma^0_1}{m_2} - \frac{\boldsymbol{\gamma}_1\cdot(\eta_1\mathbf{K}+\mathbf{q})\gamma^0_2}{m_1} \\
&+ \frac{\boldsymbol{\gamma}_1\cdot(\eta_1\mathbf{P}+\mathbf{p})\gamma^0_2}{m_1} - \frac{\boldsymbol{\gamma}_1\cdot(\eta_1\mathbf{K}+\mathbf{q})\gamma^0_1}{m_1} + \frac{\boldsymbol{\gamma}_1\cdot(\eta_1\mathbf{P}+\mathbf{p})\gamma^0_1}{m_1} + \frac{\boldsymbol{\gamma}_2\cdot(\eta_2\mathbf{K}-\mathbf{q})\gamma^0_1}{m_2}\Bigg].
\end{aligned}
$$

[1]Note that any combination of last two factors other than $++$ will give a similar higher order contribution from both (4.54) and from the resulting exponentials, giving no leading order contributions.

Ξ_1 will then be

$$\Xi_1(\mathbf{p},\mathbf{q};K,P) \simeq \frac{\Lambda^-_{1,\mathbf{p}}\gamma^0_1\gamma^5_1\Lambda^+_{1,\mathbf{q}}\gamma^0_1\Lambda^+_{2,\mathbf{p}}\gamma^0_2}{K^0-E_{1,\mathbf{q}}-E_{2,\mathbf{q}}} \quad \frac{1}{P^0-(K^0-E_{1,\mathbf{p}}-E_{1,\mathbf{q}})}$$

$$-\frac{\Lambda^+_{1,\mathbf{p}}\gamma^0_1\gamma^5_1\Lambda^+_{1,\mathbf{q}}\gamma^0_1\Lambda^+_{2,\mathbf{p}}\gamma^0_2}{K^0-E_{1,\mathbf{q}}-E_{2,\mathbf{q}}} \quad \frac{1}{P^0-E_{2,\mathbf{p}}-E_{1,\mathbf{q}}}. \tag{7.28}$$

For Ξ_2, the possible combinations of Λs are given by $\Lambda^\pm_{2,\mathbf{p}}\gamma^0_2\gamma^5_2\Lambda^\pm_{2,\mathbf{q}}\gamma^0_2\Lambda^\pm_{1,\mathbf{q}}\gamma^0_1$. This leads to the same conclusion as that for Ξ_1 shown in table 7.1 with the interchange of the subscripts $1 \leftrightarrow 2$. As such it is still the combination $-++$ that gives one contribution and $+++$ the other. From the corresponding exponential factors we get

$$\Xi_2(\mathbf{p},\mathbf{q};K,P) \simeq -\frac{\Lambda^-_{2,\mathbf{p}}\gamma^0_2\gamma^5_2\Lambda^+_{2,\mathbf{q}}\gamma^0_2\Lambda^+_{1,\mathbf{p}}\gamma^0_1}{K^0-E_{1,\mathbf{q}}-E_{2,\mathbf{q}}} \quad \frac{1}{(K^0-E_{1,\mathbf{p}}-E_{1,\mathbf{q}})-P^0}$$

$$-\frac{\Lambda^+_{2,\mathbf{p}}\gamma^0_2\gamma^5_2\Lambda^+_{2,\mathbf{q}}\gamma^0_2\Lambda^+_{1,\mathbf{p}}\gamma^0_1}{K^0-E_{1,\mathbf{q}}-E_{2,\mathbf{q}}} \quad \frac{1}{P^0-E_{2,\mathbf{p}}-E_{1,\mathbf{q}}}. \tag{7.29}$$

From the above analysis we have determined the momentum and spinor configuration of the diagram $C^{(4)}_{\varphi-\text{amp}}$ of the transition amplitude (5.24). Since we additionally know the momentum dependence of S_0^{-1} in the non-relativistic limit from (4.57), we find that

$$M_{\text{trans}} \sim \mathbf{p} \text{ for } v_{\text{rel}} \to 0. \tag{7.30}$$

This means that the process will be suppressed compared to a scalar mediator.

From chapter 6 we know that the effective potential depends on the two-particle state of the incoming and outgoing particles. Symbolically this means that

$$\begin{aligned}&\langle J,S,P|\,\tilde{G}^{(4)}\mathcal{A}^{(5)}\tilde{G}^{(4)}\,|J''',S''',P'''\rangle = \langle J,S,P|\,\tilde{G}^{(4)}\\ &\times\sum_{J',S'}|J',S',P'\rangle\,\langle J',S',P'|\,\mathcal{A}^{(5)}\sum_{J'',S''}|J'',S'',P''\rangle\,\langle J'',S'',P''|\,\tilde{G}^{(4)}\,|J''',S''',P'''\rangle\,,\end{aligned} \tag{7.31}$$

where in the second step we inserted a completeness relation. The combination $\langle J,S,P|\,\tilde{G}^{(4)}\,|J,S,P\rangle$ gives the solution to the Schrödinger equation corresponding to the effective potential the state $|J,S,P\rangle$ generates. This gives the $\tilde{\psi}$ and

$\tilde{\phi}$ functions in the amplitude (5.23) while

$$\langle J', S', P'| \mathcal{A}^{(5)} |J'', S'', P''\rangle \Rightarrow \langle J', S', P'| \mathcal{M}_{\text{trans}} |J'', S'', P''\rangle . \tag{7.32}$$

In chapter 6 we show that the only state that give an attractive potential and/or has a minima to allow bound state solutions is $|0, 0, -\rangle$. This means that the final $\langle J, S, P| \tilde{G}^{(4)} |J, S, P\rangle$ factor must be with $|0, 0, -\rangle$ to a bound state to form. While the initial $\langle J, S, P| \tilde{G}^{(4)} |J, S, P\rangle$ factor can be with a different state, only $|0, 0, -\rangle$ give a Sommerfeld enhancement, the others giving a suppression due to the repulsive potentials. Therefore we must use the state $|0, 0, -\rangle$ for both initial and final states

$$\begin{aligned}\langle 0, 0, -| \tilde{G}^{(4)} \mathcal{M}_{\text{trans}} \tilde{G}^{(4)} |0, 0, -\rangle = \langle 0, 0, -| \tilde{G}^{(4)} |0, 0, -\rangle \\ \times \langle 0, 0, -| \mathcal{M}_{\text{trans}} |0, 0, -\rangle \langle 0, 0, -| \tilde{G}^{(4)} |0, 0, -\rangle .\end{aligned} \tag{7.33}$$

The process $\mathcal{U} \to \mathcal{B}\varphi$ of $\mathcal{M}_{\text{trans}}$ conserves CP and total angular momentum J. The initial state $\mathcal{U}$ is entirely described by $|0, 0, -\rangle$, while for the final state, only the fermion bound state has the quantum numbers of $|0, 0, -\rangle$. The initial state has the conserved quantum numbers $J^{CP} = 0^-$. The final state will have CP

$$CP(\mathcal{B}\varphi) = CP_{\mathcal{B}}\ CP_{\varphi}\ (-1)^{l_{\mathcal{B}\varphi}}, \tag{7.34}$$

where $l_{\mathcal{B}\varphi}$ is the angular momentum of the two-particle state of $\mathcal{B}$ and φ. The bound state has $CP_{\mathcal{B}} = (-1)^{l+S+1}$ while the pseudo-scalar has $CP_{\varphi} = -1$. Since the bound state has $l = 0$ and $S = 0$, the angular momentum $l_{\mathcal{B}\varphi}$ must be a odd number. Only the bound state contributes to the total spin of the final state

$$S(\mathcal{B}\varphi) = J_{\mathcal{B}} = 0, \tag{7.35}$$

while the total angular momentum can take the values

$$J(\mathcal{B}\varphi) = 0 \text{ or } 1. \tag{7.36}$$

For $J(\mathcal{B}\varphi) = 1$, the angular momentum must be $l_{\mathcal{B}\varphi} = 1$ and CP is conserved. However, J is a conserved quantity and the initial state has $J = 0$. This implies that $l_{\mathcal{B}\varphi} = 0$ which means that CP conservation is violated and the process $\langle 0, 0, -| \mathcal{M}_{\text{trans}} |0, 0, -\rangle$ is not allowed.

The result is that for the potentials considered in this thesis, bound state formation is suppressed by a Sommerfeld suppression from using an alternative $|J, S, P\rangle$ for the initial state, or from the amplitude $\mathcal{M}_{\text{trans}}$ not being zeroth order in momentum. This suggests that bound state formation is subdominant to annihilation. Together with the enhancement of annihilation processes being negligible, this suggests a significantly different phenomenology then that for a scalar of vector mediator.

Chapter 8

Conclusions

In this thesis we take the procedure of Petraki *et al.* to derive the equations for cross-sections for fermions in the non-relativistic regime. This has not been done previously in the level of detail of this thesis, and is original work. We find that the difference between the fermionic case and the scalar case is contained in terms of the 1PI kernel $\tilde{W}$, and the hard scattering amplitude $\mathcal{C}_{\varphi-\text{amp}}$ of the bound state formation process. It is this 1PI kernel $\tilde{W}$ that generates the effective potential for a given mediator.

Applying this method to the potential mediated by a pseudo-scalar we find a dependence on the total angular momentum of the two-particle configuration of the incoming and outgoing dark matter particles. For two dark matter particles there are five states that give effective potentials V_1 - V_5 (6.15 - 6.19). Of these we consider the four potentials V_1 - V_4 (6.23 - 6.26) in this thesis, for which only the two potentials V_1 and V_2 have the possibility of forming a bound state solution. Potential V_1 is strictly negative and therefore attractive. The other potential, V_2 scales as $\sim 1/x^3$ and is singular: this potential needs to be renormalized. We do this by regulating the potential with a cutoff x_{cut}, where for $x \leq x_{\text{cut}}$ we approximate the potential with a square well. We find that the interplay between the cutoff and the centrifugal barrier moves the local minima that is needed for a bound state solution to the non-relativistic regime, thereby making the potential strictly positive and repulsive. This means that only the potential V_1 will give either a Sommerfeld enhancement or bound state formation.

We calculate the Sommerfeld factor for potential V_1, and the enhancement is found to be negligible. This is a significant difference from what we see with scalar or vector mediators. There have been other studies on the Sommerfeld enhancement for a pseudo-scalar. Bedague *et al.* [46] study the enhancement from a pseudo-scalar arising from Goldstone boson. They calculate the Sommerfeld effect for an S-wave ($l = 0$) annihilation process, but they assume a potential of the form $\sim 1/x^3$ which they regulate with a square well within a cutoff. We

see in this thesis that the S-wave process does not have a singular component of the form used by Bedague *et al.*, and the P-wave ($l = 1$) process that does will not give any enhancement. The negligible enhancement can be seen from the suppression factor that scales the potential V_1. This factor effectively scales the coupling α to α' where $\alpha' = m_\varphi^2/4m_\chi^2\,\alpha \ll \alpha$. This scales the potential such that it goes to 0 faster as $x \to \infty$ than a non-scaled Yukawa potential, and the long-range effects that become important in the non-relativistic regime get suppressed.

For the bound state formation process we find the lowest order contribution to the hard scattering process, figure 7.4. We calculate what the diagram gives in the non-relativistic limit. With a pseudo-scalar mediator we find that there is no zeroth order contribution in momentum, and that the amplitude for this process will scale as $\sim |\mathbf{p}|$. We know that only one of the potentials can give a Sommerfeld enhancement or bound state solution. This means that the initial and final state of the particle pair is given by $|J, S, P\rangle = |0, 0, -\rangle$, where J is the total angular momentum, S is the total spin, and P is the parity. Since we consider a CP conserving theory this means that the conserved quantity in the process is J^{CP}. The pseudo-scalar is a CP odd particle which means the initial two-particle state cannot be equal to the final two-particle state while conserving CP. Since the final state must be $|0, 0, -\rangle$ for a bound state solution to exist, the initial state must have a repulsive potential that gives a Sommerfeld suppression factor. While the Sommerfeld suppression should be as negligible as the enhancement, no enhancement means the process is sub-dominant.

We conclude that the BSF and Sommerfeld enhancement is negligible for a pseudo-scalar mediator for the possible states studied in this thesis. This suggests that a pseudo-scalar mediator cannot be used to be consistent with bounds for the different velocity regimes shown in figure 2.4.

8.1 Outlook and discussion

The primary concern of this thesis is to explore the physics of a pseudo-scalar mediator when considering annihilation and bound state formation. A further analysis of the allowed parameter space is not considered but can be interesting to look into. We have consistently used $\alpha = 0.5$ throughout the calculations done, irregardless of whether this gives a cross-section which satisfies the unitarity limit (5.42) for all our parameter values. For scalar or vector mediators the potential dependence on α is absorbed into the dimensionless variable ξ such that the potential is a function of variables $V = V(x, \xi)$. And while both σ_{BSF} and σ_{ann} depend on α, their ratio does not. As such they do not need to specify a value for α in their analysis, as it is implicit included in the variable ξ. For a pseudo-scalar mediator the potentials, V_1 and V_2, that occur do depend on α

explicitly and its value needs to be set independent of ξ. By making use of the unitarity limit (5.42) one can find a limit on our parameter space by further analysis.

If α could take the value $3/2\pi$ then a local minimum exist in the non-relativistic regime. Such a coupling, though large, is still in principle in the perturbative regime. This would mean that there is another final state that allows for a bound state solution and bound state formation may no longer be suppressed by CP conservation. One of the key assumptions used in this thesis is that the Bohr momentum, $\mu\alpha$, for a bound state is of the same order as the relative momentum μv_{rel} in order power counting. Whether this equating of terms looses validity when the value of α becomes to large is difficult to ascertain. What we can more easily find is the upper limit of α is through the unitarity limit (5.42) to determine if such high values are even allowed.

This could be tested by using an α that is high enough to give the two potential, potentials for bound state solutions, and calculate the annihilation and bound state formation cross-sections. Whether these cross-sections satisfy the unitarity limit will still be dependent of the mass of the mediator m_φ, and as such a numerical study would have to be implemented to find the upper bound on α.

There is an additional difficulty in calculating the bound state formation cross-section. The process in figure 7.4 has a final state mediating particle. This means that the emitted pseudo-scalar will be off-shell. Therefore the z-direction chosen for the initial singlet or triplet state will not be oriented in the same direction as the final singlet or triplet state. With this taken into consideration one needs to use the expansions of convolution integrals presented appendix B of [31] to find bound state formation cross-section.

Finally one can go further by studying the potential (6.19). The corresponding state $|1,1,-\rangle$ can have both $l = 0$ and $l = 2$ modes and the potential will couple these states together. This means that the different l-mode wavefunctions that solve the Schrödinger equation with this potential couples together as well. Solving a set of coupled differential equations is an often studied problem. Here a further complication arises from the need to renormalize the potential, the resulting interplay between terms, and finding when/if the resulting potential has a minima to allow bound state formation. Looking at this potential

$$|1,1,-\rangle \to V = \begin{pmatrix} \tilde{g}_1(r) + \frac{1}{4}\tilde{g}_2(r) & \frac{\tilde{g}_3(r)}{2\sqrt{2}\Lambda^2 r^2} \\ \frac{\tilde{g}_3(r)}{2\sqrt{2}\Lambda^2 r^2} & \tilde{g}_1(r) + \frac{1}{4}\tilde{g}_2(r) - \frac{\tilde{g}_3(r)}{4\Lambda^2 r^2} - \frac{3\tilde{g}_7(r)}{m_\chi \Lambda r^2} \end{pmatrix} \frac{1}{4\pi r},$$

we see that only the bottom right component has the possibility of being attractive, and having a minima. This would mean that the state with $l = 2$ can have

a bound state solution, while the $l = 0$ state cannot. However, these states are coupled and one cannot be solved without the other. Additionally one would have to consider what it would mean for the cross-sections, and how to add the contributions from the different modes. This problem is more involved and it is unclear whether bound state formation exists or not. Further study would be needed.

Bound state formation of dark matter particles have a rich phenomenology and can be realized in nature. While being an active and popular field of study, more work on this front is needed. This thesis is aimed at providing a detailed look at the theory behind bound state formation for fermions, and making a contribution in this direction by concentrating on the not-so-well studied pseudo-scalar potentials. We find that the Sommerfeld enhancement is negligible for annihilation and that the bound state formation is subdominant to the annihilation process mediated by a pseudo-scalar. These results are important for future studies of bound state formation phenomenology and model building for dark matter.

Bibliography

[1] F. Zwicky. Die Rotverschiebung von extragalaktischen Nebeln. *Helvetica Physica Acta*, 6:110–127, 1933.

[2] Vera C. Rubin and W. Kent Ford, Jr. Rotation of the Andromeda Nebula from a Spectroscopic Survey of Emission Regions. *The Astrophysical Journal*, 159:379, February 1970.

[3] Planck Collaboration. *Planck* 2015 results: XIII. Cosmological parameters. *Astronomy & Astrophysics*, 594:A13, October 2016.

[4] Planck Collaboration. *Planck* 2015 results: I. Overview of products and scientific results. *Astronomy & Astrophysics*, 594:A1, October 2016.

[5] Alexandre Refregier. Weak Gravitational Lensing by Large-Scale Structure. *Annual Review of Astronomy and Astrophysics*, 41(1):645–668, September 2003.

[6] J. Anthony Tyson, Greg P. Kochanski, and Ian P. Dell'Antonio. Detailed Mass Map of CL 0024+1654 from Strong Lensing. *The Astrophysical Journal*, 498(2):L107–L110, May 1998.

[7] Aaron D. Lewis, David A. Buote, and John T. Stocke. *Chandra* Observations of A2029: The Dark Matter Profile Down to below 0.01 $r_{\rm vir}$ in an Unusually Relaxed Cluster. *The Astrophysical Journal*, 586(1):135–142, March 2003.

[8] Brian D. Fields, Paolo Molaro, and Subir Sarkar. Big-Bang Nucleosynthesis. *Chinese Physics C*, 38(9):090001, August 2014. arXiv: 1412.1408.

[9] Douglas Clowe, Marua Brada, Anthony H. Gonzalez, Maxim Markevitch, Scott W. Randall, Christine Jones, and Dennis Zaritsky. A Direct Empirical Proof of the Existence of Dark Matter. *The Astrophysical Journal*, 648(2):L109–L113, September 2006.

[10] Jonathan L. Feng. Dark Matter Candidates from Particle Physics and Methods of Detection. *Annual Review of Astronomy and Astrophysics*, 48(1):495–545, August 2010.

[11] David H. Weinberg, James S. Bullock, Fabio Governato, Rachel Kuzio de Naray, and Annika H. G. Peter. Cold dark matter: controversies on small scales. *Proceedings of the National Academy of Sciences*, 112(40):12249–12255, October 2015. arXiv: 1306.0913.

[12] David Merritt, AlisterW. Graham, Ben Moore, Jrg Diemand, and Bala Terzi. Empirical Models for Dark Matter Halos. I. Nonparametric Construction of Density Profiles and Comparison with Parametric Models. *The Astronomical Journal*, 132(6):2685–2700, January 2006.

[13] J. F. Navarro, V. R. Eke, and C. S. Frenk. The cores of dwarf galaxy haloes. *Monthly Notices of the Royal Astronomical Society*, 283(3):L72–L78, December 1996.

[14] Andrew A. de Laix, Robert J. Scherrer, and Robert K. Schaefer. Constraints on Self-Interacting Dark Matter. *The Astrophysical Journal*, 452:495, October 1995. arXiv: astro-ph/9502087.

[15] Abraham Loeb and Neal Weiner. Cores in Dwarf Galaxies from Dark Matter with a Yukawa Potential. *Physical Review Letters*, 106(17), April 2011. arXiv: 1011.6374.

[16] Mark Vogelsberger, Jesus Zavala, and Abraham Loeb. Subhaloes in Self-Interacting Galactic Dark Matter Haloes. *Monthly Notices of the Royal Astronomical Society*, 423(4):3740–3752, July 2012. arXiv: 1201.5892.

[17] Miguel Rocha, Annika H. G. Peter, James S. Bullock, Manoj Kaplinghat, Shea Garrison-Kimmel, Jose Onorbe, and Leonidas A. Moustakas. Cosmological Simulations with Self-Interacting Dark Matter I: Constant Density Cores and Substructure. *Monthly Notices of the Royal Astronomical Society*, 430(1):81–104, March 2013. arXiv: 1208.3025.

[18] Annika H. G. Peter, Miguel Rocha, James S. Bullock, and Manoj Kaplinghat. Cosmological Simulations with Self-Interacting Dark Matter II: Halo Shapes vs. Observations. *Monthly Notices of the Royal Astronomical Society*, 430(1):105–120, March 2013. arXiv: 1208.3026.

[19] Felix Kahlhoefer, Kai Schmidt-Hoberg, Janis Kummer, and Subir Sarkar. On the interpretation of dark matter self-interactions in Abell 3827. *Mon.Not.Roy.Astron.Soc.*, 452:L54–L58, September 2015.

[20] Jan Conrad. Indirect Detection of WIMP Dark Matter: a compact review. *arXiv:1411.1925 [astro-ph, physics:hep-ex, physics:hep-ph]*, November 2014. arXiv: 1411.1925.

[21] Teresa Marrodan Undagoitia and Ludwig Rauch. Dark matter direct-detection experiments. *Journal of Physics G: Nuclear and Particle Physics*, 43(1):013001, January 2016. arXiv: 1509.08767.

[22] Scott W. Randall, Maxim Markevitch, Douglas Clowe, Anthony H. Gonzalez, and Marusa Brada. Constraints on the SelfInteraction Cross Section of Dark Matter from Numerical Simulations of the Merging Galaxy Cluster 1e 065756. *The Astrophysical Journal*, 679(2):1173–1180, June 2008.

[23] A. Sommerfeld. ber die Beugung und Bremsung der Elektronen. *Annalen der Physik*, 403(3):257–330, January 1931.

[24] John March-Russell and Stephen M. West. WIMPonium and boost factors for indirect dark matter detection. *Physics Letters B*, 676(4-5):133–139, June 2009.

[25] William Shepherd, Tim M. P. Tait, and Gabrijela Zaharijas. Bound states of weakly interacting dark matter. *Physical Review D*, 79(5), March 2009.

[26] Benedict von Harling and Kalliopi Petraki. Bound-state formation for thermal relic dark matter and unitarity. *Journal of Cosmology and Astroparticle Physics*, 2014(12):033–033, December 2014. arXiv: 1407.7874.

[27] R. Iengo. Sommerfeld enhancement: general results from field theory diagrams. *Journal of High Energy Physics*, 2009(05):024–024, May 2009. arXiv: 0902.0688.

[28] S. Cassel. Sommerfeld factor for arbitrary partial wave processes. *Journal of Physics G: Nuclear and Particle Physics*, 37(10):105009, October 2010. arXiv: 0903.5307.

[29] Kalliopi Petraki, Marieke Postma, and Michael Wiechers. Dark-matter bound states from Feynman diagrams. 2015(6), June 2015. arXiv: 1505.00109.

[30] E. E. Salpeter and H. A. Bethe. A Relativistic Equation for Bound-State Problems. 84(6):1232–1242, December 1951.

[31] Kalliopi Petraki, Marieke Postma, and Jordy de Vries. Radiative bound-state-formation cross-sections for dark matter interacting via a Yukawa potential. *arXiv:1611.01394 [hep-ph]*, November 2016. arXiv: 1611.01394.

[32] Brando Bellazzini, Mathieu Cliche, and Philip Tanedo. The Effective Theory of Self-Interacting Dark Matter. *Physical Review D*, 88(8), October 2013. arXiv: 1307.1129.

[33] M. Milgrom. A modification of the Newtonian dynamics as a possible alternative to the hidden mass hypothesis. *The Astrophysical Journal*, 270:365–370, July 1983.

[34] Torsten Bringmann, Felix Kahlhoefer, Kai Schmidt-Hoberg, and Parampreet Walia. Strong constraints on self-interacting dark matter with light mediators. *arXiv:1612.00845 [hep-ph]*, December 2016. arXiv: 1612.00845.

[35] Marco Cirelli, Paolo Panci, Kalliopi Petraki, Filippo Sala, and Marco Taoso. Dark Matter's secret liaisons: phenomenology of a dark U(1) sector with bound states. *arXiv:1612.07295 [astro-ph, physics:hep-ph]*, December 2016. arXiv: 1612.07295.

[36] Paul Hoyer. Bound states from QED to QCD. February 2014. arXiv: 1402.5005.

[37] Michael Edward Peskin and Daniel V. Schroeder. *An Introduction To Quantum Field Theory*. Westview Press, October 1995.

[38] Noboru Nakanishi. A General Survey of the Theory of the Bethe-Salpeter Equation. *Progress of Theoretical Physics Supplement*, 43:1–81, January 1969.

[39] Claude Itzykson and Jean-Bernard Zuber. *Quantum Field Theory*. Courier Corporation, September 2012.

[40] Z. K. Silagadze. Wick-Cutkosky model: an introduction. *arXiv:hep-ph/9803307*, March 1998. arXiv: hep-ph/9803307.

[41] Kim Griest and Marc Kamionkowski. Unitarity Limits on the Mass and Radius of Dark Matter Particles. *Phys.Rev.Lett.*, 64:615, 1990.

[42] A. Liam Fitzpatrick, Wick Haxton, Emanuel Katz, Nicholas Lubbers, and Yiming Xu. The Effective Field Theory of Dark Matter Direct Detection. *Journal of Cosmology and Astroparticle Physics*, 2013(02):004–004, February 2013. arXiv: 1203.3542.

[43] WILLIAM M. FRANK, DAVID J. LAND, and RICHARD M. SPECTOR. Singular Potentials. *Reviews of Modern Physics*, 43(1):36–98, January 1971.

[44] L.D. Landau and E.M. Lifshitz. *Quantum Mechanics : Non-relativistic Theory*. Pergamon, second edition edition, 1965.

[45] A. Bastai, L. Bertocchi, S. Fubini, G. Furlan, and M. Tonin. On the treatment of singular bethe-salpeter equations. *Il Nuovo Cimento*, 30(6):1512–1531, December 1963.

[46] Paulo F. Bedaque, Michael I. Buchoff, and Rashmish K. Mishra. Sommerfeld enhancement from Goldstone pseudo-scalar exchange. *Journal of High Energy Physics*, 2009(11):046–046, November 2009. arXiv: 0907.0235.